PHYSICAL REVIEW B **87**, 235120 (2013)

Anyonic quantum spin chains: Spin-1 generalizations and topological stability

C. Gils,[1,2] E. Ardonne,[3,4] S. Trebst,[5,6] D. A. Huse,[7] A. W. W. Ludwig,[8] M. Troyer,[1] and Z. Wang[6]

[1]*Theoretische Physik, Eidgenössische Technische Hochschule Zürich, 8093 Zürich, Switzerland*

[2]*Department of Mathematics and Statistics, University of Saskatchewan, Saskatoon, Canada S7N 5E6*

[3]*Nordita, Royal Institute of Technology and Stockholm University, Roslagstullsbacken 23, SE-106 91 Stockholm, Sweden*

[4]*Department of Physics, Stockholm University, AlbaNova University Center, SE-106 91 Stockholm, Sweden*

[5]*Institute for Theoretical Physics, University of Cologne, 50937 Cologne, Germany*

[6]*Microsoft Research, Station Q, University of California, Santa Barbara, California 93106, USA*

[7]*Physics Department, Princeton University, Princeton, New Jersey 08544, USA*

[8]*Physics Department, University of California, Santa Barbara, California 93106, USA*

(Received 20 March 2013; published 17 June 2013)

There are many interesting parallels between systems of interacting non-Abelian anyons and quantum magnetism occurring in ordinary SU(2) quantum magnets. Here we consider theories of so-called $\mathrm{su}(2)_k$ anyons, well-known deformations of SU(2), in which only the first $k+1$ angular momenta of SU(2) occur. In this paper, we discuss in particular anyonic generalizations of ordinary SU(2) spin chains with an emphasis on anyonic spin $S=1$ chains. We find that the overall phase diagrams for these anyonic spin-1 chains closely mirror the phase diagram of the ordinary bilinear-biquadratic spin-1 chain including anyonic generalizations of the Haldane phase, the AKLT construction, and supersymmetric quantum critical points. A novel feature of the anyonic spin-1 chains is an additional topological symmetry that protects the gapless phases. Distinctions further arise in the form of an even/odd effect in the deformation parameter k when considering $\mathrm{su}(2)_k$ anyonic theories with $k \geqslant 5$, as well as for the special case of the $\mathrm{su}(2)_4$ theory for which the spin-1 representation plays a special role. We also address anyonic generalizations of spin-$\frac{1}{2}$ chains with a focus on the topological protection provided for their gapless ground states. Finally, we put our results into the context of earlier generalizations of SU(2) quantum spin chains, in particular so-called (fused) Temperley-Lieb chains.

DOI: 10.1103/PhysRevB.87.235120 PACS number(s): 05.30.Pr, 03.65.Vf, 03.67.Lx

I. INTRODUCTION

Ever since the early days of condensed-matter physics, quantum magnets have played an integral role in shaping our understanding of interacting quantum many-body systems. Following the experimental discovery of the high-temperature superconductors whose undoped parent compounds typically are antiferromagnets, the study of quantum magnets has further intensified, yielding a plethora of deeper insights. Early on, quantum spin chains—typically one-dimensional arrangements of SU(2) spins—have become prototypical systems that proved to be fruitful ground for analytical descriptions and quasiexact numerical analysis.[1] One seminal result was the exact solution of the antiferromagnetic spin-$\frac{1}{2}$ Heisenberg chain via the Bethe ansatz and its description in terms of conformal field theory. Another crucial contribution was Haldane's realization[2] that the antiferromagnetic spin-1 Heisenberg chain forms a gapped state with characteristic zero-energy edge states for open boundary conditions, a principle observation that holds true for all half-integer and integer spin chains. More recently, it has been found that the gapped Haldane phase of the spin-1 chain is an example of a symmetry protected topological phase[3,4] making it a one-dimensional cousin of topological insulator states in two and three dimensions,[5] which have attracted much recent interest.

Over the years, a plethora of physical systems that connect to the elementary physics of quantum spin chains have been identified, including transition metal oxides,[6] Au quantum wires on semiconducting surfaces,[7] or ultracold atoms in optical lattices.[8] Recently, it has been realized that certain "deformations" of quantum spins can be used to describe some of the more peculiar topological properties of exotic quasiparticles, so-called non-Abelian anyons, that arise in certain topologically ordered systems, including certain fractional quantum Hall states,[9] $p_x + ip_y$ superconductors,[10] heterostructures of topological insulators and superconductors,[11] heterostructures of spin-orbit coupled semiconductors and superconductors,[12] and possibly certain Iridates,[13] which may effectively realize the Kitaev honeycomb model.[14] To be more specific, the deformations of quantum spins are representations of the anyon theories called $\mathrm{su}(2)_k$, which can be described as theory of ordinary SU(2) quantum spins that is deformed in such a way that only the first $k+1$ (generalized) angular momenta,

$$j = 0, \frac{1}{2}, 1, \ldots, \frac{k}{2},$$

can occur. These generalized angular momenta capture the non-Abelian properties of the anyonic quasiparticles present in the $\mathrm{su}(2)_k$ theory. For instance, the non-Abelian nature of the so-called Majorana fermion is captured by the generalized angular momentum 1/2 of the $\mathrm{su}(2)_2$ theory. The same holds for so-called Ising anyons, while Fibonacci anyons can be represented by the generalized angular momentum 1 of the $\mathrm{su}(2)_3$ theory. Similar to the coupling of two ordinary spins, a pair of generalized angular momenta can be combined (or "fused") into a new set of joint quantum numbers. For instance, for $k \geqslant 2$, two generalized angular momenta $1/2$ can be combined to form either a state with generalized angular momentum 0 or a state with generalized angular momentum

1, which is written as

$$1/2 \times 1/2 = 0 + 1, \tag{1}$$

reminiscent of two ordinary spin-$\frac{1}{2}$'s forming either a singlet or a triplet state. Similarly, two generalized angular momenta 1 can be combined into

$$1 \times 1 = 0 + 1 + 2 \tag{2}$$

for deformation parameters $k \geqslant 4$. For lower values of k, the rules differ because the number of representations is limited by k. In particular, for $k = 3$, one finds $1 \times 1 = 0 + 1$, while for $k = 2$, one has $1 \times 1 = 0$. Finally, for $k = 1$, the general momentum 1 is not allowed. For the anyonic theories, the above equations are often referred to as fusion rules.

The many-body physics of a set of interacting non-Abelian anyons can be captured by a Hamiltonian that is formed by pairwise interactions which assign energies to the different outcomes in the above fusion rules. Such an approach is a straightforward generalization of the conventional Heisenberg model, whose pairwise interaction term $J\vec{S}_i \cdot \vec{S}_j$ is simply a projector onto the singlet state, which is energetically favored for antiferromagnetic couplings ($J < 0$) or penalized for ferromagnetic couplings ($J > 0$).

The first step in this direction was taken by some of us for anyonic spin-$\frac{1}{2}$ chains in Ref. 15 and later generalized to spin-1 chains in Ref. 16 by the current group of authors. The careful analysis of the ground states of these one-dimensional systems has resulted in a number of insights. First, anyonic spin-$\frac{1}{2}$ chains typically form gapless ground states which can be described in terms of conformal field theory.[15] These gapless states turn out to be protected by a topological symmetry inherent to the anyon chains that renders them stable against local perturbations.[15,17] Moreover, these gapless states can, in fact, be interpreted as edge states that reveal the true ground state of a two-dimensional set of anyons, a novel topological liquid that is separated by the original topological liquids (of which the anyons are excitations) by an edge.[16] This picture has been verified by a careful analysis of ladder systems, in which multiple chains are coupled.[18]

Going beyond spin-$\frac{1}{2}$ chains, we began to study the physics of anyonic spin-1 chains with first results being reported in a preceding (much more condensed) paper.[16] In the paper at hand, we provide an in-depth discussion of these anyonic spin-1 chains. We find that many of the distinctive features of ordinary SU(2) spin-$\frac{1}{2}$ and spin-1 chains also hold for their anyonic cousins. For instance, anyonic spin-1 chains exhibit a gapped topological phase for antiferromagnetic couplings, the anyonic generalization of the Haldane phase. Exploring the phase diagram of chains of pairwise interacting spin-1 anyons, we find a striking resemblance of the anyonic phase diagram to the one of the ordinary bilinear-biquadratic spin-1 chain. In particular, we find multiple gapless phases (and phase transitions) in addition to the gapped Haldane phase. For the former, a similar topological protection mechanism and edge-state interpretation holds as for the gapless phases of the anyonic spin-$\frac{1}{2}$ chains.[16]

The focus of this paper is to provide an exhaustive description of the phase diagram(s) of the anyonic spin-1 chains. Our exploration of these systems has led to a large amount of results as the phase diagrams turned out to be much richer than initially anticipated. In particular, we find two families of phase diagrams depending on whether the deformation parameter k of the su(2)$_k$ anyonic theories is odd or even. Moreover, we obtain a distinct phase diagram for $k = 4$, a result that can be explained by the special role played by the generalized angular momentum 1 in the su(2)$_4$ theory.

In order to guide the reader through these various results we have taken some care to structure the paper as follows. We start with an introduction to the anyonic su(2)$_k$ theories and a description of the anyonic generalization of the Heisenberg model in Sec. II. The following sections then give a detailed exposé of our results, devoting Sec. III to the discussion of anyonic spin-1 chains with odd deformation parameters $k \geqslant 5$, followed by a discussion of the case of even deformation parameters $k \geqslant 6$ in Sec. IV. In Sec. V we turn to the case of $k = 4$ for which the spin-1 representation plays a special role and a rich phase diagram is obtained. We then turn to anyonic spin-$\frac{1}{2}$ chains and discuss their physics, in particular their topological stability in Sec. VI. We end with a broader discussion of our results, in particular in light of other deformations of conventional spin chains such as continuous su(2)$_q$ deformations or so-called (fused) Temperley-Lieb spin chains. The main part of the paper is followed by appendixes that provide the technical details of our calculations.

II. THE ANYONIC QUANTUM SPIN-CHAIN HAMILTONIANS

In light of the recent interest in topological phases of matter, it is of great importance to gain an understanding of topological models in their simplest incarnation, and we will thus study one-dimensional chains of interacting non-Abelian anyons. In this section, we briefly explain the models by drawing parallels with ordinary one-dimensional spin chains. Moreover, we explain why the "topological" nature of these models goes beyond the fact that they are constructed from "topological" particles, namely, non-Abelian anyons.

One of the prototypical one-dimensional spin-chain models is the Heisenberg model, in which SU(2) spins interact via a "spin-spin" interaction of the type $\vec{S}_i \cdot \vec{S}_j$, where the labels i and j denote the locations of the interacting spins. Often, one restricts the interaction to nearest-neighbor or next-nearest-neighbor pairs of spins. For the description of the anyonic quantum spin chains, it will be beneficial to think of this interaction in terms of the total spin of the two interacting spins. In this paper, we consider only nearest-neighbor interactions.

As a first example, we look at conventional SU(2) spin-$\frac{1}{2}$ and consider the total spin $\vec{S}_T = (\vec{S}_i + \vec{S}_{i+1})$ of two interacting spins $\vec{S}_i$ and $\vec{S}_{i+1}$, whose magnitude is characterized by the eigenvalue of $(\vec{S}_T)^2 = (\vec{S}_i + \vec{S}_{i+1})^2$. Because the total spin $\vec{S}_T$ can be either 0 or 1, with $\vec{S}_T^2$ eigenvalues 0 and 2, we can write

$$(\vec{S}_i + \vec{S}_{i+1})^2 = 0P_i^{(0)} + 2P_i^{(1)}, \tag{3}$$

where the projection operator $P_i^{(s)}$ projects onto the total spin s channel of the two spins $\vec{S}_i$ and $\vec{S}_{i+1}$. Evaluating the left-hand side, one obtains

$$\vec{S}_i \cdot \vec{S}_{i+1} = P_i^{(1)} - \tfrac{3}{4}\mathbb{I}_i = -P_i^{(0)} + \tfrac{1}{4}\mathbb{I}_i, \tag{4}$$

where in the last step we used that we can rewrite the identity operator as $\mathbb{I}_i = P_i^{(0)} + P_i^{(1)}$, which holds in the case of spin-$\frac{1}{2}$. We conclude that the Heisenberg interaction assigns energy to two interacting spins, depending on their combined spin, and the Heisenberg Hamiltonian can be written in terms of projectors as

$$H = J \sum_i P_i^{(0)}, \tag{5}$$

where $J = -1$ corresponds to an antiferromagnetic coupling, and $J = 1$ to the ferromagnetic version.

For spin-1, one can similarly write the bilinear and biquadratic terms $\vec{S}_i \cdot \vec{S}_{i+1}$ and $(\vec{S}_i \cdot \vec{S}_{i+1})^2$, respectively, in terms of the projection operators $P_i^{(1)}$ and $P_i^{(2)}$. In particular, the relations

$$\begin{aligned} (\vec{S}_i + \vec{S}_{i+1})^2 &= 2P_i^{(1)} + 6P_i^{(2)}, \\ (\vec{S}_i + \vec{S}_{i+1})^4 &= 4P_i^{(1)} + 36P_i^{(2)}, \end{aligned} \tag{6}$$

can be rewritten as

$$\begin{aligned} (\vec{S}_i \cdot \vec{S}_{i+1}) &= P_i^{(1)} + 3P_i^{(2)} - 2\mathbb{I}_i, \\ (\vec{S}_i \cdot \vec{S}_{i+1})^2 &= -3P_i^{(1)} - 3P_i^{(2)} + 4\mathbb{I}_i. \end{aligned} \tag{7}$$

Consequently, the bilinear-biquadratic spin-1 Hamiltonian,

$$H_{\mathrm{bb}} = \sum_i \cos(\theta_{\mathrm{bb}})(\vec{S}_i \cdot \vec{S}_{i+1}) + \sin(\theta_{\mathrm{bb}})(\vec{S}_i \cdot \vec{S}_{i+1})^2, \tag{8}$$

can be expressed in terms of the projectors $P_i^{(1)}$ and $P_i^{(2)}$ as follows:

$$\begin{aligned} H_{\mathrm{bb}} &= \sum_i J_2 P_i^{(2)} + J_1 P_i^{(1)} \\ &= \sum_i \cos\theta_{2,1} P_i^{(2)} - \sin\theta_{2,1} P_i^{(1)}. \end{aligned} \tag{9}$$

Here, the relation between the two angles $\theta_{2,1}$ and θ_{bb} is given by

$$\tan\theta_{2,1} = \frac{\tan\theta_{\mathrm{bb}} - 1/3}{1 - \tan\theta_{\mathrm{bb}}}, \quad \tan\theta_{\mathrm{bb}} = \frac{\tan\theta_{2,1} + 1/3}{1 + \tan\theta_{2,1}}. \tag{10}$$

We now shift our attention to anyonic degrees of freedom. Details about anyon models, in particular those of type $\mathrm{su}(2)_k$, can be found in Appendix A. A general introduction can be found, e.g., in Refs. 14, 19, and 20. Here, we only introduce those concepts that are necessary for defining the chain Hamiltonians. The Hamiltonians for the anyon chains that we consider in this paper are of the form of Eq. (9). The projectors $P_i^{(j)}$ in that equation have, however, a different meaning for anyons (as compared to ordinary spins), which are defined in Eq. (12) below.

Anyons are labeled by generalized angular momenta, or—in the language of anyons models—"topological charges." These generalized angular momenta correspond to quantum numbers, just as in the case of ordinary spin degrees of freedom. The notion of combined spin, or tensor product of spins, corresponds to the notion of "fusion" in the language of anyons, and can in general result in more than one type of anyon. The possible outcomes are called "fusion channels." The generalization of the Heisenberg interaction for spins to the anyonic case is to assign an energy to two interacting anyons based on their fusion channel. How this is done in practice, will be described in more detail below and in Appendix C.

The class of anyons considered in this paper is derived from SU(2) where spin-S ranges from $S = 0, 1/2, 1, 3/2, \ldots$. In contrast, $\mathrm{su}(2)_k$ anyons contain only a subset of generalized angular momenta, namely,

$$j = 0, \frac{1}{2}, 1, \ldots, \frac{k}{2}.$$

The truncation, characterized by the "level" k, has two important consequences which we will describe in the following.

The first consequence concerns the fusion rules of the anyons. The tensor product of two SU(2) spins S_1 and S_2 decomposes as

$$S_1 \otimes S_2 = |S_1 - S_2| \oplus \cdots \oplus (S_1 + S_2).$$

The process of taking tensor products is associative, and the same is true for the fusion rules. Because of the truncation in the $\mathrm{su}(2)_k$ theory, the SU(2) tensor product rule has to be modified. It turns out that there is only one way of doing this, consistent with the requirement that the fusion rules are associative. In particular, the fusion rules of $\mathrm{su}(2)_k$ anyons read

$$\begin{aligned} j_1 \times j_2 = |j_1 - j_2| + (|j_1 - j_2| + 1) + \cdots \\ + \min(j_1 + j_2, k - j_1 - j_2). \end{aligned} \tag{11}$$

The second important consequence of the truncation follows from the fusion rules. The dimension of the Hilbert space of a number N of ordinary SU(2) spin-$\frac{1}{2}$'s is equal to 2^N, and the spins can add up to a maximum spin of $N/2$. In contrast, the dimension of the Hilbert space of a number N of $j = 1/2$ anyons in the $\mathrm{su}(2)_k$ theory is smaller than 2^N. In Appendix A, it is shown that the dimension of the Hilbert space for N $j = 1/2$ anyons grows as $d_{1/2}^N$, asymptotically for large N, where $d_{1/2} = 2\cos(\frac{\pi}{k+2})$ is the so-called *quantum dimension* of the $j = 1/2$ anyon. For $1 < k < \infty$, this implies that the effective number of degrees of freedom for each anyon is irrational. This is less mysterious than it sounds: All this is saying is that one cannot think of the Hilbert space of N anyons as a tensor product of N one-anyon Hilbert spaces.

Because the Hilbert space does not have a tensor product structure, an alternative description of the state space and the Hamiltonian acting on it is needed. We describe here how this can be done, but leave the details for the appendixes, where we also give an explicit description of the Hamiltonians studied in this paper.

The Hilbert space of a chain of anyons can be described in terms of a so-called "fusion tree." In Fig. 1, the fusion tree for a chain of "spin-1" anyons is displayed. The lines in the fusion tree carry a label indicating the type of anyon the line corresponds to. The lines coming from above correspond to the spin-1 anyons which constitute the chain. The horizontal lines,

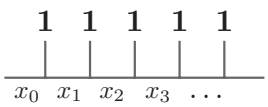

FIG. 1. The anyonic spin-1 chain.

FIG. 2. (Color online) The basis transformation for the anyonic spin-1 chain.

labeled by x_i, are the actual degrees of freedom. The possible "values" of the x_i are the same as those of the anyons present in the anyon model, namely, $x_i = 0, 1/2, \ldots, k/2$, in the case of su(2)$_k$ anyons. The x_i cannot be chosen arbitrarily, but may only take values such that the fusion rules are obeyed at the trivalent points. For example, the anyon type x_1 has to appear in the fusion product of $x_0 \times 1$, the anyon type x_2 appears in the fusion product $x_1 \times 1$, and so on. Each labeling of the fusion tree that is consistent with the fusion rules corresponds to a (orthonormal) state in the Hilbert space, and these states span this space.

Typically, we use periodic boundary conditions $x_L = x_0$, which implies that x_0 has to appear in the fusion product $x_{L-1} \times 1$, where L denotes the number of sites of the chain. States in the Hilbert space are written as $|x_0, x_1, \ldots, x_{L-1}\rangle$.

The Hamiltonian assigns an energy based on the fusion channel of two neighboring anyons in the chain. However, in the above-discussed representation of the Hilbert space (see Fig. 1), the fusion channel of two neighboring anyons is not explicit. To remedy this problem, we employ a local basis transformation which changes the order in which the anyons are fused. This is permissible because of the associativity of the fusion rules. For ordinary SU(2) spins, this basis transformation is described in terms of the Wigner $6j$ symbols. In the case of anyons, this basis transformation is described by what are known as the F symbols. A detailed discussion of the F symbols, as well as explicit representations for su(2)$_k$ anyons, can be found in Appendix B.

The basis transformation is depicted in Fig. 2. On the left-hand side, x_1 is fused with a spin-1 anyon, resulting in x_2, which is subsequently fused with the next spin-1 anyon, resulting in anyon type x_3. After the basis transformation, one first fuses the two spin-1 anyons, resulting in $\tilde{x}_2$, which is fused with x_1, resulting in the anyon type x_3. Both bases are equivalent; however, in the second basis, the fusion channel of the two spin-1 anyons is explicit, namely, $\tilde{x}_2$. Thus, after performing this basis transformation, one can assign the appropriate energy based on the value of $\tilde{x}_2$. Subsequently, one transforms back to the original basis. The operator projecting onto the anyon j channel of two neighboring anyons i and $i+1$ is thus given by

$$P_i^{(j)} = F_i^{-1} \Pi_i^{(j)} F_i, \tag{12}$$

where F_i is shorthand for the local basis transformation depicted in Fig. 2. The operator $\Pi_i^{(j)}$ projects onto the fusion channel $\tilde{x}_i = j$; i.e., the fusion of two anyons into an anyon of type j is penalized with energy $E = 1$, while the other possible fusion channels are assigned $E = 0$. For explicit matrix representations of $P_i^{(j)}$ we refer to Appendix C.

It is important to realize that the form of the projector (12) is universal and applicable to anyonic chains composed of arbitrary types of anyons. Changing to a different anyon model will merely result in a different structure of the Hilbert space and different F symbols.

A. Topological symmetry

In this section, we present a detailed discussion of the "topological symmetry operator." The Hamiltonians considered in this paper commute with the topological symmetry operator, and the associated symmetry plays a crucial role in the analysis of the anyonic chain models.

In panel (a) of Fig. 3, a chain of type-j anyons with periodic boundary conditions is displayed (in this particular case, $L = 3$). For each type of anyon l, there exists a topological operator Y_l. The action of this operator Y_l on the state $|x_0, x_1, \ldots, x_{L-1}\rangle$ [panel (a) of Fig. 3] for $L = 3$ can be described as follows. First, an additional anyon of type l is created inside the spine of the fusion tree, as displayed in panel (b) of Fig. 3. This additional spin-l anyon is "merged" with the fusion diagram by applying an F matrix, namely, $(F_l^{x_0,x_0,l})_0^{x_0'}$, resulting in the state

$$\sum_{x_0'} \left(F_l^{x_0,x_0,l}\right)_0^{x_0'} |x_0', x_1, \ldots, x_{L-1}\rangle,$$

as depicted in panel (c) of Fig. 3. Next, one "moves" the additional spin-l anyon around the ring, by applying additional

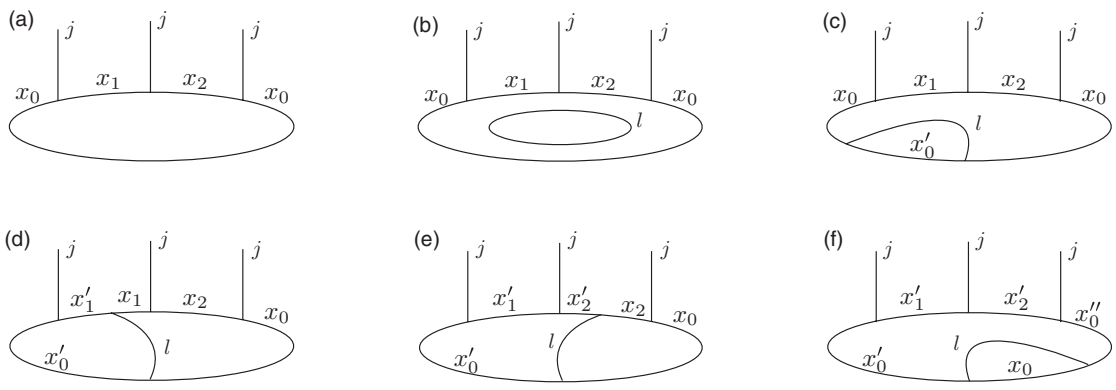

FIG. 3. Various stages in the calculation of the topological symmetry operator.

F matrices. After the first step, one obtains the state

$$\sum_{x_0',x_1'} \left(F_l^{x_0,x_0,l}\right)_0^{x_0'} \left(F_{x_0'}^{j,x_1,l}\right)_{x_0}^{x_1'} |x_0',x_1',\ldots,x_{L-1}\rangle,$$

as illustrated in panel (d) of Fig. 3. Another move of this sort gives

$$\sum_{x_0',x_1',x_2'} \left(F_l^{x_0,x_0,l}\right)_0^{x_0'} \left(F_{x_0'}^{j,x_1,l}\right)_{x_0}^{x_1'} \left(F_{x_1'}^{j,x_2,l}\right)_{x_1}^{x_2'} |x_0',x_1',\ldots,x_{L-1}\rangle,$$

as shown in panel (e) of Fig. 3. Finally, after L steps, one has come full circle, giving rise to the states

$$\sum_{x_0',x_1',\ldots,x_L'} \left(F_l^{x_0,x_0,l}\right)_0^{x_0'} \prod_{i=0}^{L-1} \left(F_{x_i'}^{j,x_{i+1},l}\right)_{x_i}^{x_{i+1}'} |x_0',x_1',\ldots,x_{L-1}'\rangle,$$

as depicted in panel (f) of Fig. 3, for $L = 3$. From the general properties of anyon models (see, e.g., Refs. 14 and 19), we find that $x_0'' = x_0'$ (the overall topological quantum number of an isolated set of anyons cannot change). We can now remove the additional spin-l anyon in the same way as we added it, thereby finishing the operation of acting with Y_l on the state $|x_0,x_1,\ldots,x_{L-1}\rangle$. Thus, we obtain the expression

$$Y_l|x_0,x_1,\ldots,x_{L-1}\rangle = \sum_{x_0',x_1',\ldots,x_{L-1}'} \prod_{i=0}^{L-1} \left(F_{x_i'}^{j,x_{i+1},l}\right)_{x_i}^{x_{i+1}'} \times |x_0',x_1',\ldots,x_{L-1}'\rangle. \quad (13)$$

We can now state the matrix elements of the topological operator Y_l in the fusion tree basis:

$$\langle x_0',x_1',\ldots,x_{L-1}'|Y_l|x_0,x_1,\ldots,x_{L-1}\rangle = \prod_{i=0}^{L-1} \left(F_{x_{i+1}'}^{j,x_i,l}\right)_{x_{i+1}}^{x_i'}. \quad (14)$$

The above definition of the topological operator does not depend on whether the additional spin-l anyon is encircled by the anyon chain [as in panels (b)–(f) of Fig. 3] or whether the additional spin-l anyon encircles the entire anyon chain. When using the latter description of the topological operator, one can think of the additional spin-l anyon as going around the "fusion product" of all the spin-j anyons constituting the anyonic chain, or better, encircling the flux through the chain. This flux i through the chain is related to the additional spin-l anyon via the modular S matrix, as depicted in Fig. 4. For a derivation of this relation, see, e.g., Refs. 14 and 19, and the explicit form of S in the case of su(2)$_k$ anyons is given in Appendix A.

The definition of the topological operator contains elements of the F matrices only. This is also true for the anyonic spin Hamiltonians we consider in this paper. It follows

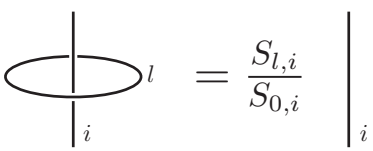

FIG. 4. Relation between the flux i through the chain and the additional spin-l anyon.

that the operators Y_l commute with the Hamiltonian and that a topological quantum number can be assigned to all the eigenstates. This has far-reaching consequences for the stability of the critical phases. Excited states which are relevant in the renormalization group sense (i.e., have energy smaller than 2) may lie in a different topological sector than the ground state and thus do not drive the system into a different phase. In addition, we see that the operators Y_l play an important role in the zero-energy ground states at the AKLT point in the Haldane-gapped phase of the spin-1 models.

III. ANYONIC SU(2)$_k$ SPIN-1 CHAINS: ODD $k \geqslant 5$

A. Introduction

We start our discussion of anyonic quantum spin chains with the anyonic version of the ordinary SU(2) spin-1 Heisenberg chain, which has long been appreciated as one of the paradigmatic spin chain models. For antiferromagnetic couplings the spin-1 chain is well known to form a gapped phase, in distinction from the gapless spin-$\frac{1}{2}$ Heisenberg chain.[2]

In the following sections, we discuss in detail the anyonic su(2)$_k$ deformations of the ordinary SU(2) spin-1 chain. We see that much of the seminal features of the SU(2) spin-1 chain carry over to these anyonic deformations with a number of new subtleties arising. One is a dependence of the observed phases and phase diagrams on the deformation parameter k. In particular, we find an even/odd effect in k for $k \geqslant 5$ and a distinctive behavior for $k = 4$. We have therefore split our discussion of the anyonic spin-1 chains into three different sections. We address anyonic spin-1 chains with *odd* $k \geqslant 5$ in the remainder of this section, in which we also give a brief recount of the phase diagram of the ordinary SU(2) spin-1 chain. The subsequent section is devoted to the case of $k \geqslant 6$ with k being *even*. Finally, an entire section is devoted to a detailed account of the physics for the special case of $k = 4$.

B. The ordinary SU(2) Heisenberg spin-1 chain

Before addressing the physics of the anyonic spin chains we briefly recapitulate the phase diagram of the ordinary SU(2) spin-1 Heisenberg chain. While the latter is typically discussed as a circle phase diagram in terms of bilinear and biquadratic spin exchange, we recast the phase diagram in terms of the projector representation in Eq. (9), the generic representation of anyonic spin chains. Figure 5 shows the phase diagram in the projector representation of Eq. (9). It contains four different phases, of which two are gapped phases and two are gapless phases. The well known Haldane phase[2] extends in the parameter regime $-\arctan(2/3) < \theta_{2,1} < \pi/2$ and includes the so-called Affleck-Kennedy-Lieb-Tasaki (AKLT) point[21] at $\theta_{2,1} = 0$ (in which only the projector $P^{(2)}$ is present in the Hamiltonian), at which the exact form of the ground-state wave function in terms of a valence bond solid state can be obtained. The conventional (gapped) Heisenberg chain (bilinear in spin-1 operators) with antiferromagnetic coupling corresponds to $\theta_{2,1} = -\arctan(1/3)$. The second gapped phase is a (spontaneously) dimerized phase[22] that occurs in the parameter regime $-\pi/2 < \theta_{2,1} < -\arctan(2/3)$. The phase transition at $\theta_{2,1} = -\arctan(2/3)$ between the two gapped phases is described by the su(2)$_2$ conformal field theory with

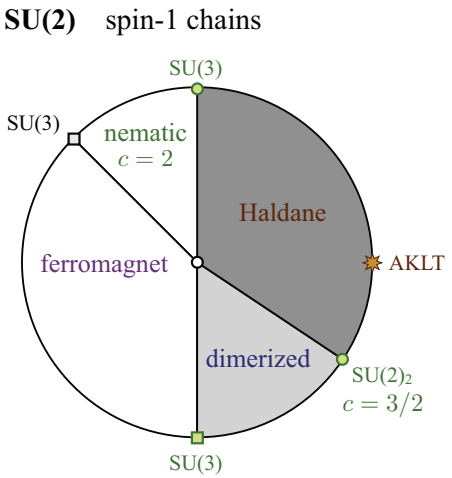

FIG. 5. (Color online) Phase diagrams of the ordinary SU(2) spin-1 chain in a projector representation (9) with $J_1 = -\sin(\theta_{2,1})$ and $J_2 = \cos(\theta_{2,1})$.

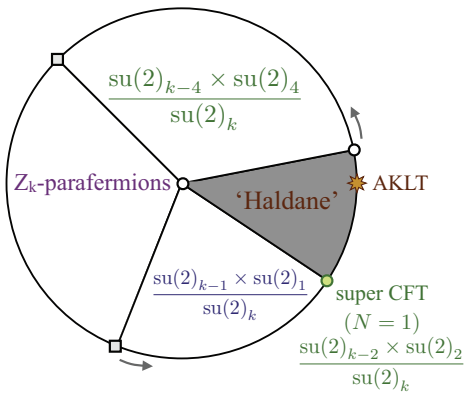

FIG. 6. (Color online) Phase diagrams of the anyonic $su(2)_k$ spin-1 chain with odd k in a projector representation (9), where $J_1 = -\sin(\theta_{2,1})$ and $J_2 = \cos(\theta_{2,1})$. With increasing (odd) index $k \geqslant 5$ the phase boundaries move as indicated by the arrows.

central charge $c = 3/2$, which happens to possess $N = 1$ supersymmetry, a result that can be obtained by means of a (nested) Bethe ansatz.[23]

At the other end of the Haldane gapped phase, $\theta_{2,1} = \pi/2$, there is a phase transition to gapless phase that extends over the range $\pi/2 < \theta_{2,1} < 3\pi/4$. This critical phase can be described by a conformal field theory with central charge $c = 2$. There are characteristic quadrupolar (nematic) spin correlations[24] in this phase, as well as a three-sublattice structure[25] resulting in soft modes at momenta $K = 0, 2\pi/3, 4\pi/3$. At the transition from the gapped Haldane phase to this critical nematic phase at $\theta_{2,1} = \pi/2$, the system has enhanced SU(3) symmetry. This point in the phase diagram of the spin-1 SU(2) chain represents actually the SU(3) chain with a fundamental representation at each site, which is known to be described by the $SU(3)_1$ conformal field theory. (This chain is again exactly solvable by a Bethe ansatz.[26,27])

Finally, there is a gapless ferromagnetic phase, extending over the parameter range $3\pi/4 < \theta_{2,1} < 3\pi/2$. The phase transitions from this phase to both the adjacent dimerized phase and the nematic phase are first order. In the vicinity of the transition between the dimerized and ferromagnetic phase, early analytical work[28] suggested the possibility of an intermediate nematic phase, which, however has later been found to not materialize.[24,29,30]

C. Phase diagram of the anyonic spin-1 chains: Overview

In this section, we provide an overview of the phase diagram of the anyonic spin-1 chains for odd $k \geqslant 5$. This phase diagram bears great resemblance to the corresponding phase diagram of the SU(2) spin-1 Heisenberg chain (Fig. 5). The generic phase diagram for the $su(2)_k$ spin-1 chain is given in Fig. 6. In Figs. 7 and 8, we display the phase diagrams for $k = 5$ and $k = 7$, respectively, as well as the characteristic spectra of the four different phases and the $(N = 1)$ supersymmetric critical point which separates the Haldane gapped phase and the phase which is called the "Z_2 sublattice phase" [this is the phase intervening between the Haldane phase and the Z_k-parafermion phase, and it encompasses the angles $\theta_{2,1} \lesssim -0.19\pi \approx -\arctan(2/3)$].

The spin-1 anyonic spin chain is gapped in a finite region around $\theta_{2,1} = 0$. This gapped phase is the anyonic analog of the Haldane gapped phase, and the point $\theta_{2,1} = 0$ is equivalent to the AKLT point. At this point, the Hamiltonian penalizes the fusion of two neighboring anyons in the spin-2 channel. The ground states with periodic boundary conditions can be found exactly at this point, for all k, and the ground-state degeneracy is $(k + 1)/2$.

For $\theta_{2,1} < 0$, there is a phase transition at $\theta_{2,1} \approx -0.19\pi$ into an extended critical region. The position of this phase transition did not show any appreciable dependence on the value of k (remember that $k \geqslant 5$ throughout this section). This gapless region occurs where the ordinary SU(2) spin-1 chain is in the gapped dimerized phase. This difference in behavior is the most remarkable distinction between the ordinary SU(2) spin-1 chain and the anyonic spin-1 chains.

The critical point at $\theta_{2,1} \approx -0.19\pi \approx -\arctan(2/3)$, separating the Haldane phase and the extended critical region, is described in terms of an $N = 1$ supersymmetric minimal conformal model.

For angles $\theta_{2,1} > 0$, there is a phase transition from the Haldane phase into another extended critical region which bears some resemblance to the extended nematic region in case of the ordinary spin-1 chain. In particular, this phase has a Z_3 sublattice structure. The location of the phase transition does depend on k, and moves towards $\theta_{2,1} = \pi/2$ with increasing k.

Finally, there is an extended critical region in the vicinity of $\theta_{2,1} = \pi$, the point where the fusion of two neighboring anyons into the spin-2 channel is favored. This critical phase is the anyonic analog of the ferromagnetic phase of the ordinary spin-1 chain, and the critical behavior is described by the Z_k parafermion conformal field theory.

The phase transitions from the ferromagnetic phase to the neighboring extended critical regions are first order. The phase transition into the anyonic version of the nematic phase occurs

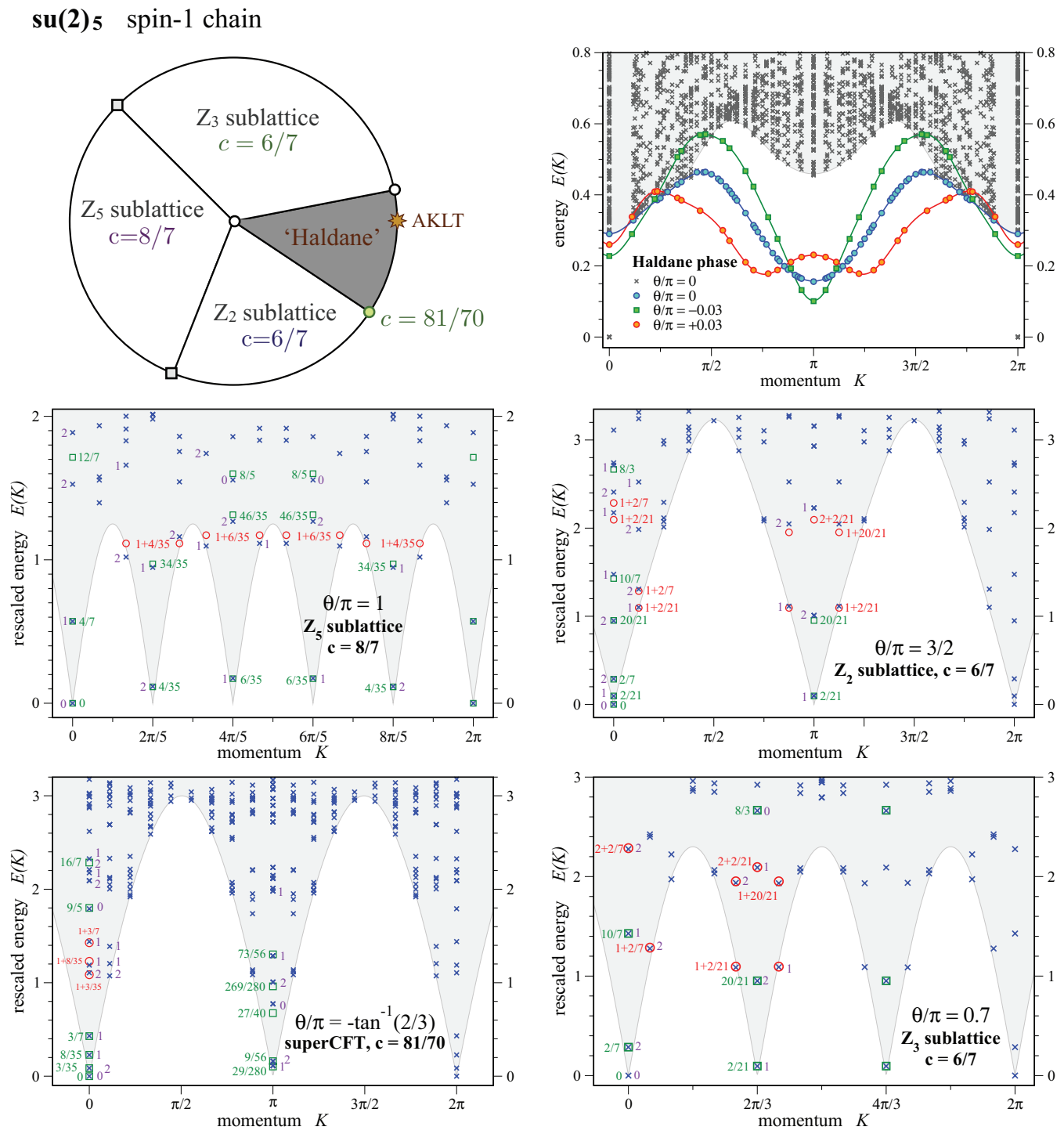

FIG. 7. (Color online) The su(2)$_5$ spin-1 chain. The energy spectra for the various phases of the phase diagram are shown in the top left panel. For the critical phases/points the energy spectra have been rescaled to match the CFT prediction given in Eq. (15). Green squares indicate the location of the primary fields; red circles indicate the descendant fields. The energies predicted by CFT are given in green (red) for primary (descendant) fields. The topological symmetry sector is indicated by the violet index. Data shown are for system sizes $L = 18$ and $L = 15$, respectively.

at $\theta_{2,1} = 3\pi/4$, independent of the value of k. The location of the other phase transition depends on k, and moves towards $\theta_{2,1} = 3\pi/2$ for increasing k.

Below, we discuss in detail each of the phases mentioned above. We focus on the topological properties and the similarities to the ordinary SU(2) spin-1 chain.

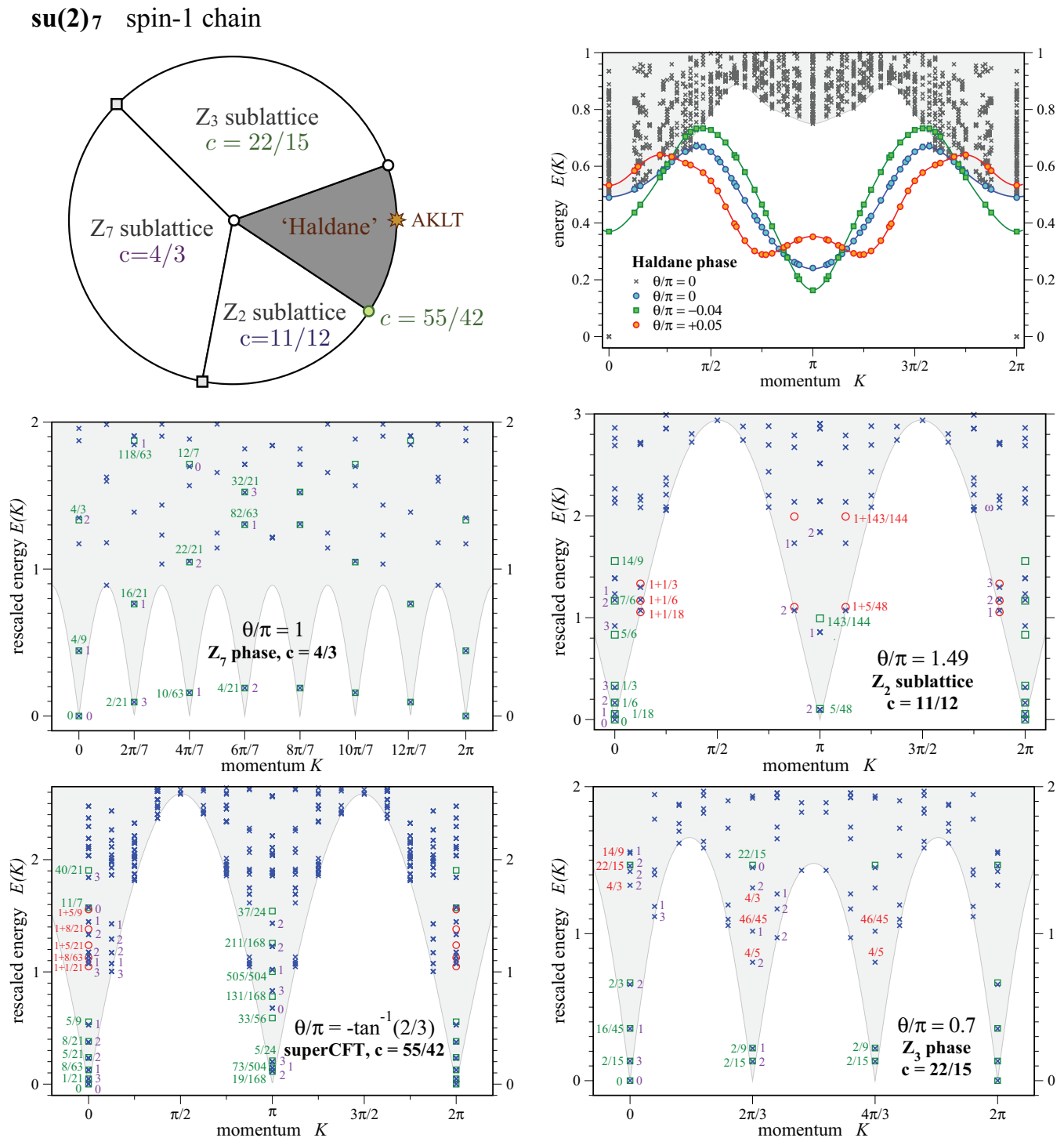

FIG. 8. (Color online) The su(2)$_7$ spin-1 chain. The energy spectra for the various phases of the phase diagram are shown in the top left panel. For the critical phases/points the energy spectra have been rescaled to match the CFT prediction given in Eq. (15). Green squares indicate the location of the primary fields, red circles indicate the descendant fields. The energies predicted by CFT are given in green (red) for primary (descendant) fields. The topological symmetry sector is indicated by the violet index. Data shown are for system sizes $L = 16$ and $L = 14$, respectively.

D. Critical phases

We investigate the phase diagram of our model numerically using exact diagonalization. In our analysis, we follow a standard procedure to determine the conformal field theory describing the behavior of the extended critical regions and the critical points: The numerically obtained spectrum is first shifted (by some constant offset) such that the ground state has zero energy. The spectrum is then rescaled such that the

TABLE I. Critical theories in the $su(2)_k$ spin-1 chains for $k \geqslant 5$.

Gapless theory	Coset description	Central charge			
		k	$k=5$	$k=7$	SU(2) ($k\to\infty$)
Z_k phase	$su(2)_k/u(1)_{2k}$	$c=2\frac{k-1}{k+2}$	$c=8/7$	$c=4/3$	$c=2$
Z_2 phase	$su(2)_{k-1}\times su(2)_1/su(2)_k$	$c=1-\frac{6}{(k+1)(k+2)}$	$c=6/7$	$c=11/12$	$c=1$
Z_3 phase	$su(2)_{k-4}\times su(2)_4/su(2)_k$	$c=2-\frac{24}{(k-2)(k+2)}$	$c=6/7$	$c=22/15$	$c=2$
Superconformal point	$su(2)_{k-2}\times su(2)_2/su(2)_k$	$c=\frac{3}{2}-\frac{12}{k(k+2)}$	$c=81/70$	$c=55/42$	$c=3/2$

energy of the lowest lying excitation matches the energy of the lowest lying excitation of the conformal field theory (CFT) describing the phase. The so-obtained energy spectrum is finally compared to the energy spectra of candidate CFTs. The CFT (if any) which matches the numerically obtained energy levels is the one describing the system at the angle θ. We note that the list of candidate CFTs is limited: If the chain is critical, each energy level in the spectrum corresponds to a field in the applicable CFT. These fields satisfy fusion rules which have to be compatible with the fusion rules of the underlying $su(2)_k$ theory. This constraint restricts the candidate CFTs that could describe the criticality of anyonic quantum chains.

The eigenenergies in a system of finite size described by a CFT take the form[31]

$$E = E_1 L + \frac{2\pi v}{L}\left(-\frac{c}{12} + h + \bar{h}\right), \tag{15}$$

where the velocity v is an overall scale factor and c is the central charge of the CFT. The scaling dimensions $h+\bar{h}$ take the form $h = h^0 + n$, $\bar{h} = \bar{h}^0 + \bar{n}$, with n and $\bar{n}$ non-negative integers, and h^0 and $\bar{h}^0$ are the holomorphic and antiholomorphic conformal weights of the primary fields in the given CFT. The momenta K (in units $2\pi/L$) are such that $K = h - \bar{h} + K_0$ or $K = h - \bar{h} + K_0 + L/2$, where K_0 is a constant shift of the momentum that determines at which momentum the primary field occurs. This shift can be determined from the numerics and is not fixed by conformal symmetry. Thus, different microscopic realizations of the same CFTs can give rise to different values for K_0. In Table I, we give the CFTs describing the various different critical behavior observed in the anyonic quantum chains.

As explained in Sec. II, the anyonic spin chains have a topological symmetry; all the states in the spectrum can therefore be assigned a topological quantum number. The possible eigenvalues of the topological symmetry operator, also denoted as topological quantum numbers, are in one-to-one correspondence with the types of anyons which appear in the particular anyon theory considered.

1. Z_k-parafermion phase

We begin the discussion of the phase diagram given in Fig. 6 with the Z_k-parafermion phase, which corresponds to the gapless ferromagnetic phase in the SU(2) spin-1 chain. In the anyonic spin-1 chains, this phase contains the point $\theta_{2,1} = \pi$, where it is favorable for two neighboring anyons to be in the spin-2 channel. One of the phase boundaries of this phase is located at $\theta_{2,1} = 3\pi/4$. The location of the other phase boundary depends on k: With increasing k, it moves towards the location of the phase boundary in the SU(2) spin-1 chain (at angle $\theta_{2,1} = 3\pi/2$).

The spectra at angle $\theta_{2,1} = \pi$ for $k=5$ and $k=7$ are displayed in the middle panel of Figs. 7 and 8, respectively. The energy spectra were rescaled such that the energy of the lowest excitation matches the energy predicted by the Z_k parafermion CFT.[32] Some details of this CFT are reviewed in Appendix E 4. In the figures, we indicate the locations of the energies of the states corresponding to the primary fields by green squares, while blue crosses correspond the numerically obtained energy levels. We find good agreement between numerically obtained energy spectra and the Z_k parafermion CFTs for both the $su(2)_5$ and the $su(2)_7$ anyon models. For $su(2)_5$, we also indicate the location of a few descendant fields that match the numerical prediction. Generally, the identification of descendant fields is more difficult due to finite size effects.

The fields of the Z_k parafermion theory carry two labels (l,m) that take the values $l = 0,1,\ldots,(k-1)$, and $m = 0,2,\ldots,2(k-1)$. The momentum and topological quantum number of the fields is determined by the labels m and l, respectively. The topological quantum number simply is given by l. For the momentum, the following relation holds: $K = \frac{2m\pi}{k}$.

We find that there are no *relevant* primary fields which have the same set of quantum numbers as the identity field. This implies that there are no relevant operators that can be added to the Hamiltonian to drive a phase transition if both translational and topological symmetry are left unbroken. This phase is an example of a critical phase whose criticality is protected by the topological symmetry.

2. Z_2 phase: (A,D) modular invariant of coset $su(2)_{k-1}\times su(2)_1/su(2)_k$

Upon increasing $\theta_{2,1}$, one encounters a first-order transition from the Z_k parafermion phase into a different extended critical phase that has a Z_2 sublattice symmetry. We identified the CFTs describing these critical phases for $k=5$ and $k=7$ as Virasoro conformal minimal models, with central charge $c = 1 - \frac{6}{(k+1)(k+2)}$. However, the field content describing the criticality is not the "usual" minimal model—the diagonal (A,A) modular invariant—but the so-called (A,D) modular invariant which contains a different number of fields. Details of these different modular invariants can be found in Refs. 33–35. For our purposes, it suffices to notice that some of the primary fields in the (A,A) invariant do not appear in the (A,D) invariant while others appear twice. The details of this CFT are summarized in Table VII in Appendix E 1. The scaling dimensions of the fields are given in Eq. (E1).

Again, it is possible to identify the topological sectors and the momenta at which the various fields occur from the labels of the fields. As discussed in Appendix E 1, the fields can be labeled by (r,s), where s takes the values $s = 1,3,\ldots,k$. The topological sector is determined by $(s-1)/2$, while the momenta are fixed by the r label. In particular, for $k = 5$, the fields with labels $r = 1,5$ occur at $K = 0$, while the fields with label $r = 3$ occur both at $K = 0,\pi$. For $k = 7$, the fields with $r = 1,3,5,7$ occur at $K = 0$, while the fields at $r = 4$ are doubly degenerate and occur $K = \pi$.

3. Z_3 phase: Coset $su(2)_{k-4} \times su(2)_4/su(2)_k$

At $\theta_{2,1} = 3\pi/4$, there is a first-order transition between the Z_k "ferromagnetic" phase and a critical region of criticality that exhibits a Z_3 sublattice symmetry. We determined that the CFT describing the Z_3 critical region is a series of coset models with S_3 symmetry, namely, $\frac{\mathrm{su}(2)_4\times\mathrm{su}(2)_{k-4}}{\mathrm{su}(2)_k}$. In Appendix E 3, we list some details of these coset models, in particular, the scaling dimensions of the primary fields (a detailed analysis can be found in Refs. 36 and 37). The primary fields are labeled by two integers (r,s). As was the case for the Z_2 critical phase, only a subset of the fields appear in the spectrum, namely those with $r+s$ even. In addition, the label s has to be odd, and it determines the topological quantum number via $(s-1)/2$. The location of the second end point of this Z_3 critical region (i.e., the transition to the Haldane gapped phase) is found to vary with k.

In Figs. 7 and 8, we display representative energy spectra for this phase (angle $\theta_{2,1} = 0.7\pi$). In these spectra, we indicate the topological sectors of some of the low-lying fields and give the scaling dimensions of the primary fields.

4. Superconformal critical point

The transition between the Z_2 phase and the Haldane gapped phase occurs at the angle $\theta_{2,1} \approx -0.19\pi$, which shows little dependence on the level k. The critical point itself is described by a $N = 1$ superconformal minimal model,[38] $\frac{\mathrm{su}(2)_2\times\mathrm{su}(2)_{k-2}}{\mathrm{su}(2)_k}$. Details on this theory can be found in Appendix E 2. In the limit of $k \to \infty$, this theory approaches the $\mathrm{su}(2)_2$ theory, which describes the critical point in the SU(2) spin-1 bilinear-biquadratic spin chain.

In the spectra for $k = 5$ and $k = 7$ of the anyonic spin-1 chain at this critical point, we indicate the scaling dimensions and topological sectors of the primary fields which are labeled by (r,s). As in the other coset models (excluding the Z_k parafermion theory), the label s is associated with the $\mathrm{su}(2)_k$ denominator of the coset and hence labels the topological sector. The momentum at which the primary fields appear is determined by $K = (r+s \bmod 2)\pi$.

The superconformal critical point separates the Haldane gapped phase from the Z_2 sublattice critical region. Therefore, we expect that there will be a relevant perturbation which drives the phase transition between these two different phases and that this perturbation does not break any symmetries. A relevant perturbation is a field which has the same quantum numbers as the ground state and whose scaling dimension is smaller than two. Such a field indeed exists: It carries the labels $(r,s) = (3,1)$ and has scaling dimension $1 + \frac{4}{k}$; i.e., it is a relevant field for all k. We note that at $K = \pi$, there also is a relevant field with labels $(r,s) = (2,1)$ which has scaling dimension $\frac{3}{8} + \frac{3}{2k}$. As a consequence, a gap is expected to develop if a perturbation which staggers the chain is added to the system.

5. Stability of the critical phases

We recapitulate that in all three extended critical phases there is no relevant field in the same symmetry sector as the ground state, which is a requirement for the phases to be stable. This notion of topological stability is explained in more detail in the Sec. VI dealing with the anyonic spin-$\frac{1}{2}$ chains, where we show in detail that the critical behavior of those chains is protected by the topological symmetry.

As explained above, there is a relevant operator with the same quantum numbers as the ground state at the superconformal point. This operator drives the transition from the superconformal point to the Haldane gapped phase on one side of the phase diagram and the extended critical region with Z_2 sublattice symmetry on the other side.

E. The gapped Haldane phase

In addition to the gapless phases that were discussed in detail in the previous section, the spin-1 anyonic chains also exhibit a gapped phase, as can be seen in Fig. 6. The properties of this gapped phase are strikingly similar to the properties of the Haldane phase in the ordinary bilinear-biquadratic spin-1 chain. For instance, the point $\theta_{2,1} = 0$ allows for a straightforward generalization of the AKLT point of the ordinary SU(2) model. At this AKLT point, the degenerate ground states can be constructed explicitly (see Sec. III E3). In Sec. III E4, we discuss the ground states of the open chain and find the degeneracy of the anyonic spin-1 chain can be understood in a similar way as the degeneracy of the SU(2) model at the AKLT point. Before we deal with the ground states at the AKLT point, we first discuss the energy spectrum and the phase boundaries of the Haldane phase.

1. Energy spectrum

The energy spectrum in the gapped phase is shown in Figs. 7 and 8 for coupling parameter $\theta = 0$. It can be seen that there exists a quasiparticle band whose qualitative shape is identical to the magnon band of triplet excitations of the ordinary AKLT point. The complete spectrum is shown at angle $\theta_{2,1} = 0$: The ground states occur at momentum $K = 0$, and there exists a quasiparticle band (shown in blue) and a continuum of scattering states (shown in gray). The quasiparticle band is also displayed for coupling parameters $\theta_{2,1}$ close to $\theta_{2,1} = 0$ (in red for $\theta_{2,1} > 0$, in green for $\theta_{2,1} < 0$). It can be seen that when approaching the critical phase with Z_3 sublattice symmetry—i.e., for increasing $\theta > 0$—the minimum of the quasiparticle band moves away from $K = \pi$ towards $K = 2\pi/3$ and $K = 4\pi/3$. When decreasing the angle $\theta_{2,1} < 0$, the quasiparticle band remains at momentum $K = \pi$, which is consistent with the Z_2 sublattice symmetry of the superconformal critical point. From a finite-size scaling analysis of the energy spectra, we confirm that the gapped phase does, indeed, extend over a finite range of coupling parameters θ. Figures 7 and 8 show that the size of the energy gap (at $\theta_{2,1} = 0$) increases from $\Delta E(k = 5) \approx 0.16$ to $\Delta E(k = 7) \approx 0.24$.

This behavior suggests that the qualitative shape of the energy spectra at the AKLT point is preserved for all k with the energy gap at $\theta_{2,1} = 0$ approaching $\Delta E(k \to \infty) \approx 0.41$.[39]

2. *Phase boundaries*

The Haldane phase and the $\mathrm{su}(2)_{k-1} \times \mathrm{su}(2)_1/\mathrm{su}(2)_k$ critical phase are separated by a superconformal critical point, which is located at coupling parameter $\theta_{2,1} \approx -0.19\pi$ for both $k = 5$ and $k = 7$. This is very close to the position of the phase transition where the Haldane gapped phase gives way for a different phase in the ordinary SU(2) spin-1 chain (see the phase diagram in Fig. 6), namely, $\theta_{2,1} = -\arctan(2/3)$.

The position of the phase boundary at the other end of the gapped phase clearly depends on the level k. Comparing the position of this point for $k = 5$ and $k = 7$ suggests that it moves towards $\theta_{2,1} = \pi/2$ for increasing k. This scenario is consistent with the ordinary model, as can be seen by comparing the phase diagrams of the anyonic and ordinary SU(2) spin-1 chain (Figs. 6 and 5, respectively).

3. *Ground states in the periodic chain (anyonic equivalent of AKLT point)*

In the ordinary SU(2) spin-1 chain, there exists a point within the Haldane gapped phase—the so-called AKLT[21] point—where the ground state can be obtained exactly. At the AKLT point, the Hamiltonian penalizes two neighboring spins that are in the spin-2 channel. To construct the ground state, it is helpful to think of the spin-1's as composed of two spin-$\frac{1}{2}$'s which are projected onto the spin-1 channel. In the ground state, each of these spin-$\frac{1}{2}$'s forms a singlet with a spin-$\frac{1}{2}$ particle that is associated with a neighboring spin-1, as depicted in Fig. 9. In this situation two neighboring spin-1's will never combine into an overall spin-2 and, therefore, the state has zero energy. It can be shown that for periodic boundary conditions this ground state is nondegenerate.[21]

At the corresponding point (angle $\theta_{2,1} = 0$) in the phase diagram of the anyonic chains, the Hamiltonian [Eqs. (9) and (12)] penalizes two neighboring anyons to fuse in the spin-2 channel. As for the ordinary SU(2) quantum spin model, the ground state can be obtained exactly at this point. In contrast to the SU(2) case, there exists a topological symmetry which dictates that the ground state is degenerate even in the case of periodic boundary conditions (we will deal with the open chain in the next section). One of these degenerate ground states is easily found, while the others can be obtained by making use of the topological symmetry operator (see Sec. II for details).

We present the simplest case of $k = 5$ here and give the results for arbitrary k in Appendix D. We start by constructing one zero-energy ground state. For $k = 5$, the allowed spins are

FIG. 9. (Color online) The AKLT construction of the valence-bond-solid state on a finite chain of spin-1 degrees of freedom. Each solid circle represents a spin-$\frac{1}{2}$ variable, each dotted ellipse corresponds to a spin-1 particle, and and each line connecting two spin-$\frac{1}{2}$ variables symbolizes a singlet bond.

0,1,2, and the fusion rules read

$$0\times 0 = 0 \qquad 0\times 1 = 1 \qquad 0\times 2 = 2$$
$$1\times 1 = 0+1+2 \qquad 1\times 2 = 1+2$$
$$2\times 2 = 0+1.$$

In particular, the fusion rule $2 \times 1 = 1 + 2$ implies that in the labeling of the Hilbert space, the assignment $(x_{i-1},x_i,x_{i+1}) = (2,2,2)$ is allowed. In addition, $(x_{i-1},x_i,x_{i+1}) = (2,1,2)$ is allowed as well. Fixing $x_{i-1} = x_{i+1} = 2$, one finds that the allowed values of $\tilde{x}_i$ in the transformed basis are $\tilde{x}_i = 0,1$, because 0 and 1 are the two possible fusion outcomes of $2 \times 2 = 0 + 1$. Because at the AKLT point, only the value $\tilde{x}_i = 2$ is penalized, it follows that the state $|v_0\rangle = |2,2,\ldots,2\rangle$ is a zero-energy ground state (recall that that Hamiltonian is a positive sum of projectors).

By employing the topological symmetry operators Y_l, with $l = 1,2$, we can construct other zero-energy ground states. The operators Y_l commute with the Hamiltonian; thus, the states $|v_1\rangle = Y_1|v_0\rangle$ and $|v_2\rangle = Y_2|v_0\rangle$ also have zero energy. It turns out that $|v_0\rangle$ is neither an eigenstate of Y_1 nor an eigenstate of Y_2. As a result, the number of ground states is three, which is in accordance with the number of particle types in the model. We note that Y_0 is the identity operator.

The explicit form of the states $|v_1\rangle$ and $|v_2\rangle$ is easily written. First of all, the only basis states with nonzero coefficient in $|v_1\rangle$ have $x_i = 1,2$ for all i. Similarly, the only basis states with nonzero coefficient in $|v_2\rangle$ have $x_i = 0,1$ for all i. To specify the coefficients, we introduce the notation $\#l$, which denotes the number of i's such that $x_i = l$. In addition, $\#(l,m)$ denotes the number of i's such that $x_i = l$ and $x_{i+1} = m$, where we use periodic boundary conditions, $x_L = x_0$.

Then we have

$$|v_1\rangle = \sum_{x_i\in\{1,2\}} f_1(\{x_i\})\,|x_0,x_1,\ldots,x_{L-1}\rangle$$
$$f_1(\{x_i\}) = (-1)^{\#2} d_1^{-L} d_2^{L/2} d_1^{3^{\frac{\#(2,1)}{2}}} d_2^{-\frac{\#(2,1)+\#(2,2)}{2}}, \tag{16}$$

as well as

$$|v_2\rangle = \sum_{x_i\in\{0,1\}} f_2(\{x_i\})\,|x_0,x_1,\ldots,x_{L-1}\rangle\,,$$
$$f_2(\{x_i\}) = (-1)^{\#1} d_1^{-L/2} d_2^{L/2} d_1^{\frac{\#1}{2}} d_2^{-\#1}. \tag{17}$$

Here, d_1 and d_2 are the quantum dimensions of particles with spin-1 and -2 respectively, and are given by $d_1 = 1 + 2\sin(3\pi/14)$ and $d_2 = 2\cos(\pi/7)$, respectively.

We labeled the ground states at the AKLT point by $|v_l\rangle$ with $l = 0,1,2$ for a good reason. In Sec. II, we explained that the topological symmetry operators Y_l effectively "add" or fuse a particle of type l to the fusion chain. At the AKLT point, this notion becomes very explicit. The states $|v_l\rangle$ are thought of as states of the chain in the l sector. In particular, $|v_0\rangle$ corresponds to the identity sector. Adding a particle of type l, i.e., acting with the operator Y_l, gives rise to a state in sector l, or $|v_l\rangle = Y_l|v_0\rangle$. Moreover, if one acts with Y_l on the state $|v_j\rangle$, one obtains a combination of states, which is given by the fusion rules. In particular, $Y_1|v_1\rangle = |v_0\rangle + |v_1\rangle + |v_2\rangle$, $Y_1|v_2\rangle = |v_1\rangle + |v_2\rangle$, and $Y_2|v_2\rangle = |v_0\rangle + |v_1\rangle$. Thus, loosely speaking, the ground states of the periodic anyonic spin-1 chain at the AKLT point form a representation of the fusion

algebra $\mathrm{su}(2)_k$. Because the modular S matrix diagonalizes the fusion rules, one can easily write down combinations of the ground states which are also eigenstates of the operators Y_l, namely, $|\psi_{\mathrm{AKLT,i}}\rangle = \sum_{j=0}^{2} S_{i,j}|v_j\rangle$, where $S_{i,j}$ is the modular S matrix for (the integer sector of) $\mathrm{su}(2)_5$, and the sum is over integer values.

For the explicit form of the AKLT ground states in the general case $\mathrm{su}(2)_k$, we refer to Appendix D.

4. *Ground states in the open chain (anyonic equivalent of AKLT point)*

Before describing the structure of the ground states of the open anyonic chains at the AKLT point, we briefly review the physics of the valence bond solid ground state at the AKLT point ($\theta_{2,1} = 0$ in phase diagram Fig. 6) of the ordinary bilinear-biquadratic spin-1 Heisenberg chain.[1,21] The Hamiltonian at $\theta = 0$ consists only of the projector onto a total spin-2 of two nearest-neighbor spins with a positive sign. Thus, in the ground state, a total spin-2 of two nearest-neighbor spins is suppressed. In the usual tensor product basis of local (site) states, the valence bond solid ground state is given by

$$|\Psi_{ab}\rangle = \varepsilon^{b_1 a_2}\varepsilon^{b_2 a_3}\cdots\varepsilon^{b_{L-1}a_L}\left|\psi_{ab_1}\right\rangle \otimes \left|\psi_{a_2 b_2}\right\rangle \otimes \cdots \otimes \left|\psi_{a_L b}\right\rangle, \tag{18}$$

where the summation over repeated upper and lower indices is assumed. The local spin-1 state $|\psi_{ab}\rangle$ is represented as the symmetric part of the tensor product of two spin-$\frac{1}{2}$ variables,

$$|\psi_{ab}\rangle = \frac{1}{\sqrt{2}}(|\psi_a\rangle \otimes |\psi_b\rangle + |\psi_b\rangle \otimes |\psi_a\rangle), \tag{19}$$

where ψ_a denotes one of the two eigenstates of the S^z spin-$\frac{1}{2}$ operator, which we label by $a = 1,2$. The antisymmetric tensor ε^{ab} enforces a singlet bond of the spin-$\frac{1}{2}$ variables a_{l+1} and b_l. Therefore, the total spin of the two nearest-neighbor spin-1 variables, consisting of four spin-$\frac{1}{2}$ variables which are labeled by a_l, b_l, a_{l+1}, b_{l+1}, can only assume the values 0 or 1. For a chain with open boundary conditions (see Fig. 9) the first and the last spin-$\frac{1}{2}$ variables indexed by a_1 and b_L do not form a singlet bond. These two spin-$\frac{1}{2}$ variables can add up to a total spin 0 or a total spin 1, giving rise to a fourfold degeneracy for the spin-1 bilinear-biquadratic chain at the AKLT point with open boundary conditions.

With the results above in mind, we now consider the fusion basis of the anyonic spin-1 chain, as shown in Fig. 1. We consider a chain of length L with open boundary conditions in the sense that variables x_0 and x_{L+1} form the ends of the chain. In analogy with the above discussion, we assume that variables x_0 and x_{L+1} can add up to a total spin of $x_0 \times x_{L+1}$ of 0 or 1 in the zero-energy ground states.

For a given choice of x_0 and x_{L+1}, we expect that there are no zero-energy ground states if $|x_{L+1} - x_0| > 1$ because the fusion product $x_0 \times x_{L+1}$ does not contain 0 nor 1 in this case. We expect one ground state to be present if $x_0 \times x_{L+1}$ contains 0 or 1, but not both. Finally, if both 0 and 1 appear in the fusion product $x_0 \times x_{L+1}$, we expect two zero-energy ground states. There is no S_z quantum number in anyonic spin chains associated with the "spins," and the state with total spin-1 (or better, topological charge 1) is thus not degenerate.

The analysis of the previous section is helpful in understanding the above-discussed results. We found that the ground states of the periodic chain have a particular form; namely, the only basis-states which have nonzero coefficients in these states are such that all the x_i take at most two values that have to differ by one. Thus, there is a ground state with all the $x_i \in \{0,1\}$, one ground state with the $x_i \in \{1,2\}$, etc. In addition, the state with all $x_i = (k-1)/2$ is also a zero-energy ground state.

The ground states of the open chain must be such that the bulk part of these states does not give an energy contribution. Thus, for a particular choice of boundary conditions x_0 and x_{L+1}, one can construct one ground state if $|x_0 - x_{L+1}| = 1$, because there is exactly one corresponding zero-energy ground state with periodic boundary conditions. For $x_0 = x_{L+1} = 0$, there is also one zero-energy ground state, while for $x_0 = x_{L+1} > 0$, there are two zero-energy ground states. For $|x_0 - x_{L+1}| > 1$, one finds that there are no zero-energy ground states. All of this is in accordance with the considerations above.

We computed the ground-state degeneracies for all possible choices of fixed boundary occupations (x_0, x_{L+1}) for both the $k = 5$ and the $k = 7$ model and find that the above-described picture is indeed the appropriate one. At the AKLT point $\theta_{2,1} = 0$, the ground-state energy is independent of the system size. In the Haldane gapped phase away from the AKLT point, the ground-state degeneracy is not exact and finite size effects occur. In Fig. 10, we show the lowest energies $\Delta E_i(x_0,x_{L+1}) = E_i(x_0,x_{L+1}) - E_0(x_0,x_{L+1})$, $i \geqslant 1$, of the $\mathrm{su}(2)_5$ spin-1 chain at coupling parameter $\theta_{2,1} = -0.01\pi$. The energy $E_0(x_0,x_{L+1})$ is the lowest energy of the open chain with fixed boundary occupations x_0 and x_{L+1}, and it is not necessarily a ground-state energy. By this we mean that the state is not a perturbation of a zero-energy ground state at $\theta_{2,1} = 0$. For the boundary condition $x_0 = 0$, $x_{L+1} = 2$, the

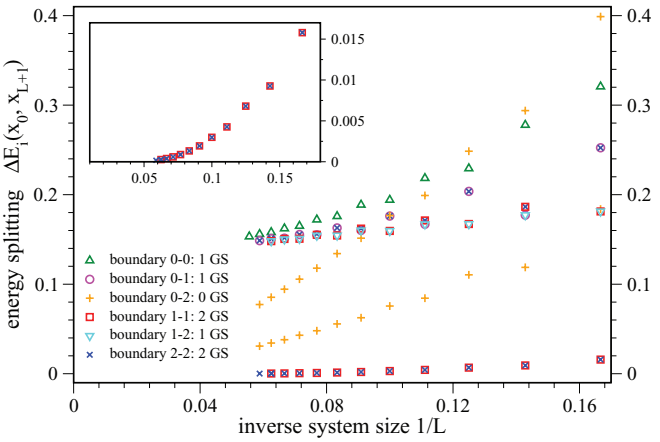

FIG. 10. (Color online) The eigenenergies $\Delta E_i(x_0,x_{L+1}) := E_i(x_0,x_{L+1}) - E_0(x_0,x_{L+1})$ $(i \geqslant 1)$ of the $\mathrm{su}(2)_5$ anyonic spin-1 chain with fixed boundaries x_0 and x_{L+1} as a function of $1/L$ at $\theta_{2,1} = -0.01\pi$. The legend at the lower left side indicates the values of x_0 and x_{L+1}. The energy $E_0(x_0,x_{L+1})$ is the lowest energy and not necessarily a "ground-state energy." For $x_0 = x_{L+1} = 1$ and for $x_0 = x_{L+1} = 2$, there are two almost degenerate zero-energy states, and $\Delta E_1(x_0,x_{L+1})$ corresponds to the finite-size splitting of the two ground states that decay exponentially with system size (see the inset).

lowest energy $E_0(0,2)$ is not a ground state (in the above sense) since both $\Delta E_1(0,2)$ and $\Delta E_2(0,2)$ approach zero in the limit $1/L \to 0$, as demonstrated in Fig. 10. For the boundary condition $x_0 = 1$, $x_{L+1} = 1$, as well as $x_0 = 2$, $x_{L+1} = 2$, the ground state is twofold degenerate, and the splitting of the two ground-state energies at finite system size L decays exponentially in $1/L$, as illustrated in the inset of Fig. 10. Again, this is in agreement with the above discussion because $1 \times 1 = 0 + 1 + 2$ and $2 \times 2 = 0 + 1$ [for $\mathrm{su}(2)_5$]; i.e., both fusion products allow for a total spin 0 and a total spin 1. For all remaining possible boundary conditions, there is one ground state, as can be seen from Fig. 10, where $\Delta E_1(x_0, x_{L+1})$ approaches a finite energy in the limit $1/L \to 0$. We also verified this scheme for the $\mathrm{su}(2)_7$ model and for different values of $\theta_{2,1}$ in the gapped phase.

IV. ANYONIC SU(2)$_k$ SPIN-1 CHAINS: EVEN $k \geqslant 6$

In the previous section, we discussed in detail the odd-k anyonic spin-1 chains. We found that the phase diagram of these models (see Fig. 5), bears great resemblance to the phase diagram of the SU(2) spin-1 chain (see Fig. 6). We observed one striking difference between the ordinary and the anyonic spin-1 chains, namely, the absence of a (gapped) "dimerized" phase in the case of the anyonic spin-1 chains. In this section, we present our result for the even-k anyonic spin-1 chains. For even k, the phase diagram is very similar to the case of odd k with the exception of an additional gapped phase which resembles the dimerized phase of the SU(2) spin-1 chain.

In this section, we focus on the case $k = 6$; however, our analysis for $k = 8$ indicates that the case $k = 6$ is generic for k even. The generic structure of the phase diagram for even $k \geqslant 6$ is analogous to the generic structure of the phase diagram for odd $k \geqslant 5$. We note that the case $k = 4$ is special and is considered in detail in the following section.

The fact that the phase diagrams for k even and odd differ is a very interesting feature of our model. As far as we are aware, this is the first time that a dependence on the parity of the level k has been observed. As we point out in the discussion, Koo and Saleur[40] considered a closely related loop model which contains a continuous parameter that plays the role of the discrete level k. The model considered by Koo and Saleur does not show any sign of the "even-odd" effect we observe. It would be very interesting to understand the differences and similarities of these two models in greater detail.

The phase diagram of the $k = 6$ anyonic spin-1 chain is presented in Fig. 11. We discuss the similarities and differences of this phase diagram to the phase diagram of the case $k = 5$ (Fig. 6). The locations of the phase boundaries in Fig. 11 correspond to the case $k = 6$. As was the case for k odd, we observe that some of the phase boundaries change upon increasing the value of (even) k. The direction of the movement of the phase boundaries is indicated by the arrows in the phase diagram.

Comparing the phase diagrams for odd and even k in Figs. 6 and 11, we first note that large parts of the phase diagram have a similar structure. At angle $\theta_{2,1} = 0$, we encounter a gapped Haldane phase, precisely as in the case of odd k. At angle $\theta_{2,1} \approx -0.19\pi$, there is a phase transition that is described by a $N = 1$ supersymmetric minimal model from the Haldane phase into

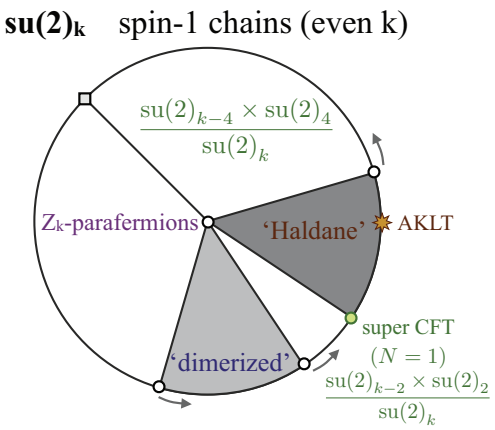

FIG. 11. (Color online) Phase diagram of the even-k anyonic $\mathrm{su}(2)_k$ spin-1 chain in a projector representation (9), where $J_1 = -\sin(\theta_{2,1})$ and $J_2 = \cos(\theta_{2,1})$. The locations of the phase boundaries correspond to the case $k = 6$. Some of the phase boundaries move with increasing (even) k; the arrows indicate the direction of the change.

an extended critical region (we comment on the latter critical region below). At the other end of the gapped Haldane phase, there is a phase transition at angle $\theta_{2,1} \approx 0.09\pi$ (for $k = 6$) to a critical region that exhibits a Z_3 sublattice symmetry and is described by the coset $\mathrm{su}(2)_4 \times \mathrm{su}(2)_{k-4}/\mathrm{su}(2)_k$ (we note that the corresponding critical region for odd k is described by the same CFT). This critical region extends all the way to $\theta_{2,1} = 3\pi/4$ at which point there is a first-order transition to a critical region with Z_k sublattice symmetry. So far, the phase diagram for even k has the same structure and phases as the one for odd k.

The phase diagrams for odd k versus even k begin to diverge at the angle where, for k odd, the critical region with Z_k sublattice symmetry transitions to a critical phase with Z_2 sublattice symmetry. While the former (Z_k) critical phase also appears for k even, the latter (Z_2 critical phase) does not; rather, there is a phase transition at $\theta_{2,1} \approx 1.41\pi$ (for $k = 6$) to a gapped phase. This gapped phase is characterized by broken translational invariance, as signified by a zero-energy ground state at $K = \pi$ present at the angle $\theta_{2,1} = 3\pi/2$. In addition, there are $(k + 2)/2$ degenerate ground states at momentum $K = 0$ with topological quantum numbers $(0, 1, 2, \ldots, k/2)$. The zero-energy ground state at $K = \pi$ is in topological symmetry sector $k/4$. Clearly, the nature of this "dimerized" gapped phase differs from the Haldane gapped phase.

Between the dimerized gapped phase and the Haldane gapped phase, we find an extended critical region. Due to the rather small extent of this critical region and the fact that we could not study large enough systems (the dimension of the Hilbert space increases with k), we have not been able to determine which CFT describes this extended critical region.

It is interesting to note that the structure of the phase diagram for even k bears closer resemblance to the phase diagram of the SU(2) bilinear-biquadratic spin-1 chain (see Fig. 5) than to the phase diagram for odd-k anyonic spin-1 chains. In particular, both the phase diagrams of the ordinary SU(2) spin-1 chain and the even-k anyonic spin-1 chain exhibit dimerized phases in the area surrounding the angle

$\theta_{2,1} = 3\pi/2$. It appears that for increasing even k, the phase diagram of the anyonic chain gravitates towards the phase diagram of the SU(2) chain. Our results for the $k = 8$ anyonic chain are consistent with this picture.

The phase diagram for the $k = 6$ anyonic spin-1 chain displays a unique feature; namely, its structure is symmetric in the line through the points $\theta_{2,1} = 3\pi/4, 7\pi/4$. The underlying reason is that the fusion rules of the $\mathrm{su}(2)_k$ theory are symmetric under the exchange $j \leftrightarrow k/2 - j$, where the labels j take the values $j = 0, 1/2, \ldots, k/2$. In the case of $k = 6$, this symmetry exchanges anyon spins $1 \leftrightarrow 2$. The location of the symmetry points follow from our parametrization of the Hamiltonian, as given in Eq. (9). We point out that this symmetry relates only the *sets of energy eigenvalues*, but not the possible degeneracy of the levels or their angular momenta.

For example, the energy levels levels at the point $\theta_{2,1} = \pi$—where the system is described by the Z_6 parafermion theory—are identical to those at angle $\theta_{2,1} = \pi/2$. At the latter point, the system is described by the coset $\mathrm{su}(2)_2 \times \mathrm{su}(2)_4/\mathrm{su}(2)_6$, which for $k = 6$ corresponds to the Z_6 parafermions. We note that the momenta of the states are not identical.

Similarly, the energies of the levels in the dimerized gapped phase are the same as the energies of the levels in the Haldane phase, even though the nature of these gapped phases is very different. We return to this issue below. Finally, we note that the phase transition from the dimerized phase to the critical region between the dimerized phase and the Haldane phase is given by an $N = 1$ supersymmetric model. As far as we can tell from our numerics, this is only true for the case $k = 6$. For $k = 8$ and higher, we have not been able to determine the CFT describing this phase transition.

V. ANYONIC $\mathrm{SU}(2)_k$ SPIN-1 CHAINS: $k = 4$

Having discussed the anyonic spin-1 models for odd $k \geqslant 5$ and even $k \geqslant 6$, we finally turn our attention to the remaining case $k = 4$. We pointed out in the Introduction that the phase diagram for $k = 4$ has a different structure than the phase diagrams for other values of k. The underlying reason is that the spin-1 particle is special in this case. The symmetry of the fusion rules under the exchange $j \leftrightarrow k/2 - j$ implies that $j = 1$ is mapped onto itself for $k = 4$. In addition, $k = 4$ is the lowest k for which a general fusion rule $1 \times 1 = 0 + 1 + 2$ applies. We refer to the discussion in Sec. VII for more details.

A. Hilbert space and Hamiltonian

The basis of the $\mathrm{su}(2)_4$ spin-1 chain is depicted in Fig. 1. Each labeling $\{x_i\}_{i=0,\ldots,L-1} \in \{0, \frac{1}{2}, 1, \frac{3}{2}, 2\}$ that satisfies the fusion rules at the vertices corresponds to a different basis state. In fact, the Hilbert space of the $\mathrm{su}(2)_4$ spin-1 chain splits into two independent sectors: The fusion rules impose that the local basis elements are either all integer valued or all half-integer valued. We use the following terminology:

(1) integer sector (IS), $\{x_i\}_{i=0,\ldots,L-1} \in \{0, 1, 2\}$;
(2) half-integer sector (HIS), $\{x_i\}_{i=0,\ldots,L-1} \in \{\frac{1}{2}, \frac{3}{2}\}$.

We only consider periodic boundary conditions for the $\mathrm{su}(2)_4$ chain, i.e., $x_L = x_0$.

We find that the differences in behavior between the IS and HIS $\mathrm{su}(2)_4$ spin-1 chains are rather subtle. We first describe the behavior of the model in the IS sector, followed by a discussion of the HIS sector.

As a first minor difference, we note that the number of states in the HIS is given by $2^L + \delta_{L,0}$, where L is the length of the chain. In the IS sector, however, the number of states is $2^L + 1$ when $L > 0$ is even and $2^L - 1$ when L is odd. The additional state in the even-L IS occurs at momentum $K = \pi$, while the additional state in the odd-L HIS occurs at momentum $K = 0$. Those are the only differences; the remaining 2^L $(2^L - 1)$ states where L even (odd) have the same momenta in the IS and HISs.

As we did for $k \geqslant 5$, we represent the Hamiltonian of the $\mathrm{su}(2)_4$ spin-1 chain in terms of the projectors onto the 1 and 2 channels with couplings J_1 and J_2, respectively. These couplings are parametrized by an angle $\theta_{2,1}$, where $J_2 = \cos\theta_{2,1}$ and $J_1 = -\sin\theta_{2,1}$. Explicitly, the Hamiltonians read

$$H_{\mathrm{IS}}^{(k=4)} = \sum_i \cos\theta_{2,1} P_{i,\mathrm{IS}}^{(2)} - \sin\theta_{2,1} P_{i,\mathrm{IS}}^{(1)}, \tag{20}$$

$$H_{\mathrm{HIS}}^{(k=4)} = \sum_i \cos\theta_{2,1} P_{i,\mathrm{HIS}}^{(2)} - \sin\theta_{2,1} P_{i,\mathrm{HIS}}^{(1)}\,. \tag{21}$$

The explicit form of the projectors are given in Appendix C 3 a.

B. Phase diagram in the integer Hilbert space sector (IS)

The phase diagram of the IS $\mathrm{su}(2)_4$ spin-1 chain [Hamiltonian given in Eq. (20)] is shown in the leftmost panel of Fig. 12. The phase diagram consists of two extended gapped phases which are separated by two extended gapless regions. The two phase transitions between the gapped phase with a Z_3-sublattice structure and the two gapless regions are first order. However, the phase transitions into the gapped phase with a Z_2-sublattice structure are continuous.

The critical behavior of the gapless regions is described by the Z_2 orbifold theory of the u(1)-compactified boson with central charge $c = 1$. Interestingly, the compactification radius varies continuously as a function of $\theta_{2,1}$ in the gapless regions. We found it difficult to determine the range of compactification radii which are realized in the model. The reason is that the finite size data make it difficult to determine the location of the transition between the gapped phase with the Z_2-sublattice structure and the critical regions. We devote Sec. V D to the issue of the location of these phase boundaries, dealing with the IS and the HIS at the same time.

1. *Gapped phases (IS)*

Gapped phase $\theta_{2,1} = \pi/2$. The gapped phase containing the point $\theta_{2,1} = \pi/2$ extends from $\theta_{2,1} = 0$ to $\theta_{2,1} = 3\pi/4$. These phase boundaries are easy to locate because the transitions to the gapless regions are first-order transitions, as we show in Sec. V D.

This gapped phase has a Z_3 sublattice symmetry, which results in a threefold degenerate ground state for system sizes that are a multiple of 3. These ground states occur at momenta $K = 0, 2\pi/3, 4\pi/3$ and their exact form can be established throughout the whole gapped phase.

At angle $\theta_{2,1} = \pi/2$, the Hamiltonian can be solved exactly. At this point, the Hamiltonian reduces to the equal sum of two projectors, namely, onto the spin-0 and spin-2

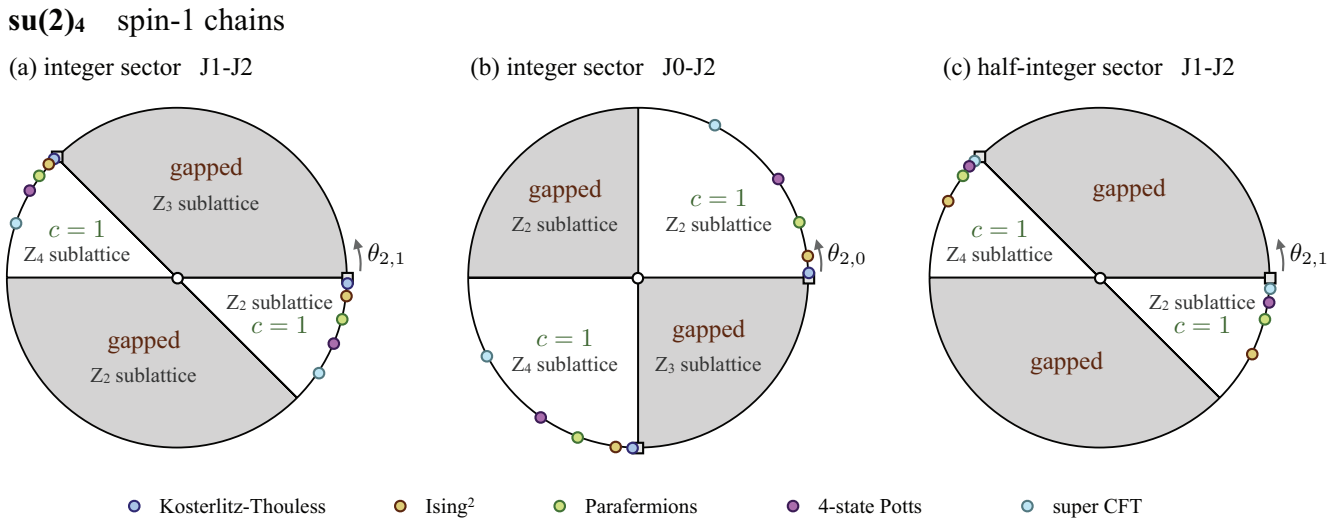

FIG. 12. (Color online) Phase diagrams of the su(2)$_4$ spin-1 chain in the integer sector and half-integer sector and different projector representations. The colored circles indicate special points in the $c = 1$ gapless phase that can be matched to the labeled CFTs.

channels (in addition, there is also a constant term $-L$). Throughout the region $0 \leqslant \theta_{2,1} \leqslant 3\pi/4$, the Hamiltonian is a sum of two projectors with positive coefficients (for a matrix representation of the Hamiltonian, see Appendix C 3). The three degenerate ground states are built from the basis state of the form $|11a_1\,11a_2\,11a_3,\ldots,11a_{L/3}\rangle$ and its two translations, where the a_i represent the states $|a\rangle_{3i} = (|0\rangle - |2\rangle)/\sqrt{2}$ at position $3i$. These three states can easily be combined to form three-momentum eigenstates. These ground states have energy $-L$ and are eigenstates of the two projectors with eigenvalue 0. The latter explains that these ground states persist throughout the whole gapped phase.

Gapped phase $\theta_{2,1} = 3\pi/2$. In the gapped phase surrounding the point $\theta_{2,1} = 3\pi/2$, the spectrum exhibits a Z_2 sublattice symmetry and a cosine-shaped quasiparticle dispersion. For even-L system sizes, the ground state is threefold degenerate, with the ground states occurring at momenta $K = 0,0,\pi$. Two of the three ground states at angle $\theta_{2,1} = 3\pi/2$ consist of states of the form $|1b_1\,1b_2\,1b_3,\ldots,1b_{L/2}\rangle$ and its translation by one site, where $|b\rangle_{2i} = (|0\rangle + |2\rangle)/\sqrt{2}$ at site $2i$. These two states can be combined to form the two ground states at momenta $K = 0,\pi$. The state $|111\ldots1\rangle$ is the third ground state and has momentum $K = 0$. For odd system sizes, this state is the only ground state of the system.

2. Gapless phases (IS)

The critical behavior of the su(2)$_4$ spin-1 chain is particularly interesting. We find that the critical behavior depends continuously on the angle describing the interaction. At particular values of the angle $\theta_{2,1}$, the behavior matches particular CFTs with central charge $c = 1$. In particular, these CFTs are the Z_2 orbifolds of a boson compactified on a circle of radius $R = \sqrt{2p}$. For the p integer, these are rational CFTs,[41,42] described in detail in the Appendix E 5. In this section, we limit the discussion to the most prominent features of these theories. In Sec. V D, we point out the particular orbifold theories that are realized in the su(2)$_4$ spin-1 chain.

To identify the critical theories describing the critical behavior as a function of the angle, we employ the standard technique of first shifting the spectrum such that the ground state has zero energy, followed by a rescaling of the energy to elucidate the conformal nature of the spectrum.

By means of this procedure, we identified several of the $c = 1$ orbifold theories. These theories "share" several operators that appear in the spectrum throughout the critical region. These operators are the ground state with $h_0 = \bar{h}_0 = 0$, two twist fields $\sigma_{1,2}$ with scaling dimension $h_\sigma + \bar{h}_\sigma = 1/8$, two twist fields $\tau_{1,2}$ with scaling dimension $h_\tau + \bar{h}_\tau = 9/8$, a field Θ with scaling dimension 2, and, finally, two fields $\Phi_{1,2}$ with scaling dimension $p/2$. For $p = 1$, the fields just described exhaust the full list, but in general, there are $p - 1$ additional fields ϕ_λ with scaling dimension $\frac{\lambda^2}{4p}$. These fields, as well as the associated momenta and topological symmetry sectors, are given in Table II. We checked that the assignments of the topological symmetry sectors are compatible with the fusion rules of the orbifold CFTs (for details, see Appendix E 5). For various values of p, the orbifold theories are also known under specific names, such as the Kosterlitz-Thouless theory ($p = 1$), the theory of two decoupled Ising models ($p = 2$), the Z_4 parafermion CFT ($p = 3$), the four-state Potts model ($p = 4$), and the superconformal minimal model with $c = 1$ ($p = 6$).

We identified several of the $c = 1$ Z_2 orbifold theories, including the ones with $p = 1,2,3,4,5,6$. On the left side of Fig. 13, we show the energy spectra associated with the $p = 1$ and $p = 3$ orbifold theories in the Z_2 critical region. On the right side of Fig. 13, we display the energy spectra associated with the $p = 2$ and $p = 6$ orbifold theories in the Z_4 critical region.

In Table III, we list the locations of some of the critical points as extracted from the numerical data. The procedure we followed to obtain these locations is described in more detail in Sec. V D. The location $\theta \approx -0.20\pi$ of case $p = 6$—the superconformal theories—is very close to the location of the superconformal point for the su(2)$_k$ spin-1 chains with $k \geqslant 5$, namely, $\theta_{2,1} \approx -0.19\pi$.

TABLE II. The scaling dimensions $(h+\bar{h})$ of the operators of the Z_2 orbifold of the compactified boson on a circle of radius $R=\sqrt{2p}$ for some integer p. The following abbreviations are used: sCFT, the (minimal) superconformal CFT with central charge $c=1$; Potts, 4-state Potts CFT; pCFT, Z_4 parafermion CFT; $(\text{Ising})^2$, square of the Ising CFT; KT, Kosterlitz-Thouless theory, equivalent to the compactified boson theory $u(1)_8$. We also list the numerically observed topological quantum numbers (Y symmetry: $y_0=y_2=2$, $y_{1/2}=y_{3/2}=0$, $y_1=-1$) and momentum quantum numbers K at which the fields appear in the various critical regions. The symmetry sectors of the fields with scaling dimensions $p/2$ depend on p. This is a consequence of the fact that the field with scaling dimension $(p-1)^2/2p$ at radius p corresponds to the field with dimension $p/2$ at radius $p-1$.

									IS	IS	HIS	HIS
p	1	2	3	4	6			Y	Z_2	Z_4	Z_2	Z_4
$h+\bar{h}$	KT	$(\text{Ising})^2$	pCFT	Potts	sCFT	9	10	Top.	K	K	K	K
0	0	0	0	0	0	0	0	y_0	0	0	0	0
$\frac{1}{8}$	$\frac{1}{8}$	$\frac{1}{8}$	$\frac{1}{8}$	$\frac{1}{8}$	$\frac{1}{8}$	$\frac{1}{8}$	$\frac{1}{8}$	$y_{1/2}$	0	$\frac{\pi}{2}$	0	$\frac{\pi}{2}$
$\frac{1}{8}$	$\frac{1}{8}$	$\frac{1}{8}$	$\frac{1}{8}$	$\frac{1}{8}$	$\frac{1}{8}$	$\frac{1}{8}$	$\frac{1}{8}$	$y_{1/2}$	π	$\frac{3\pi}{2}$	π	$\frac{3\pi}{2}$
$\frac{9}{8}$	$\frac{9}{8}$	$\frac{9}{8}$	$\frac{9}{8}$	$\frac{9}{8}$	$\frac{9}{8}$	$\frac{9}{8}$	$\frac{9}{8}$	$y_{1/2}$	0	$\frac{\pi}{2}$	0	$\frac{\pi}{2}$
$\frac{9}{8}$	$\frac{9}{8}$	$\frac{9}{8}$	$\frac{9}{8}$	$\frac{9}{8}$	$\frac{9}{8}$	$\frac{9}{8}$	$\frac{9}{8}$	$y_{1/2}$	π	$\frac{3\pi}{2}$	π	$\frac{3\pi}{2}$
2	2	2	2	2	2	2	2	y_0	0	0	0	0
$\frac{1}{2p}$		$\frac{1}{4}$	$\frac{1}{6}$	$\frac{1}{8}$	$\frac{1}{12}$	$\frac{1}{18}$	$\frac{1}{20}$	y_1	π	π	0	π
$\frac{4}{2p}$			$\frac{2}{3}$	$\frac{1}{2}$	$\frac{1}{3}$	$\frac{2}{9}$	$\frac{1}{5}$	y_1	0	0	0	0
$\frac{9}{2p}$				$\frac{9}{8}$	$\frac{3}{4}$	$\frac{1}{2}$	$\frac{9}{20}$	y_0	π	π	0	π
$\frac{16}{2p}$					$\frac{4}{3}$	$\frac{8}{9}$	$\frac{4}{5}$	y_1	0	0	0	0
$\frac{25}{2p}$					$\frac{25}{12}$	$\frac{25}{18}$	$\frac{5}{4}$	y_1	π	π	0	π
$\frac{36}{2p}$						2	$\frac{9}{5}$	y_0	0	0	0	0
$\frac{p}{2}$	$\frac{1}{2}$	1	$\frac{3}{2}$	2	3	9/2	5	y_0,y_1	0	0	0	π
$\frac{p}{2}$	$\frac{1}{2}$	1	$\frac{3}{2}$	2	3	9/2	5	y_0,y_1	$0,\pi$	π	π	$0,\pi$

The location of the superconformal point in the Z_4 critical region is $\theta_{2,1}\approx 0.92\pi$. In general, the relation between critical angle in the Z_2 critical region (which we for now denote by θ_2; similarly, θ_4 denotes the angle in the Z_4 critical region) is

$$\theta_4=\pi-\tan^{-1}(1+\tan\theta_2),\quad \theta_2=-\tan^{-1}(1+\tan\theta_4). \tag{22}$$

The spectra in Fig. 13 illustrate the different sublattice symmetry for the two gapless regions. In these spectra, we also indicate the topological symmetry sectors of some of the low-lying states. In the case of $su(2)_4$, the topological symmetry operator Y has three distinct eigenvalues, which are given by $y_0=y_2=2$, $y_{1/2}=y_{3/2}=0$, and $y_1=-1$. We thus use the labels $y=0,1/2,1$ for these sectors.

The presence of the different critical models with the same central charge $c=1$ indicates the presence of a marginal operator that drives the "transition" between the different critical theories and that gives rise to continuously varying critical exponents. Indeed, all the orbifold models share a marginal operator Θ with scaling dimension 2 whose topological symmetry coincides with that of the ground state. It is this operator which is responsible for the critical region with continuously changing exponents. It proved difficult to locate the phase transition between the critical regions and the gapped phase around $\theta_{2,1}=3\pi/2$. One reason might be that the transition to the gapped phase is also driven by a marginal operator, which allows for large finite size effects that thwart the localization of these critical points.

C. Phase diagram in the half-integer Hilbert space sector (HIS)

The behavior of the $su(2)_4$ spin-1 chain in the HIS mimics very closely that of the IS. The phase diagram is presented in the rightmost panel in Fig. 12. The phase boundaries are located at the same positions, but the details of the observed phases differ slightly. In the following discussion of the HIS $su(2)_4$ spin-1 chain, we emphasize the differences between the two sectors.

1. Gapped phases (HIS)

As noted above, there are some differences in the dimensions of the Hilbert spaces in the IS and the HIS, respectively. As a consequence, the IS and HIS models have different sublattice structures in the gapped phases. Namely, in the HIS, the ground state occurs at momentum $K=0$, and it is nondegenerate. All other features of the gapped phases in the HIS are very similar to those observed in the IS.

Gapped phase $\theta_{2,1}=\pi/2$. In gapped phase that surrounds the angle $\theta_{2,1}$, the ground state is nondegenerate and occurs at momentum $K=0$ (there is no sublattice structure). The model can be solved at angle $\theta_{2,1}=\pi/2$: The ground state can be expressed as follows:

$$|GS\rangle=\sum_{x_i=1/2,3/2}(-1)^{\#(3/2,3/2)}|x_0,x_2,\ldots,x_{L-1}\rangle.$$

Here, $\#(3/2,3/2)$ denotes the number of times the sequence $(x_i,x_{i+1})=(3/2,3/2)$ occurs in the state $|x_0,x_2,\ldots,x_{L-1}\rangle$ (note that periodic boundary conditions impose $x_L=x_0$). As

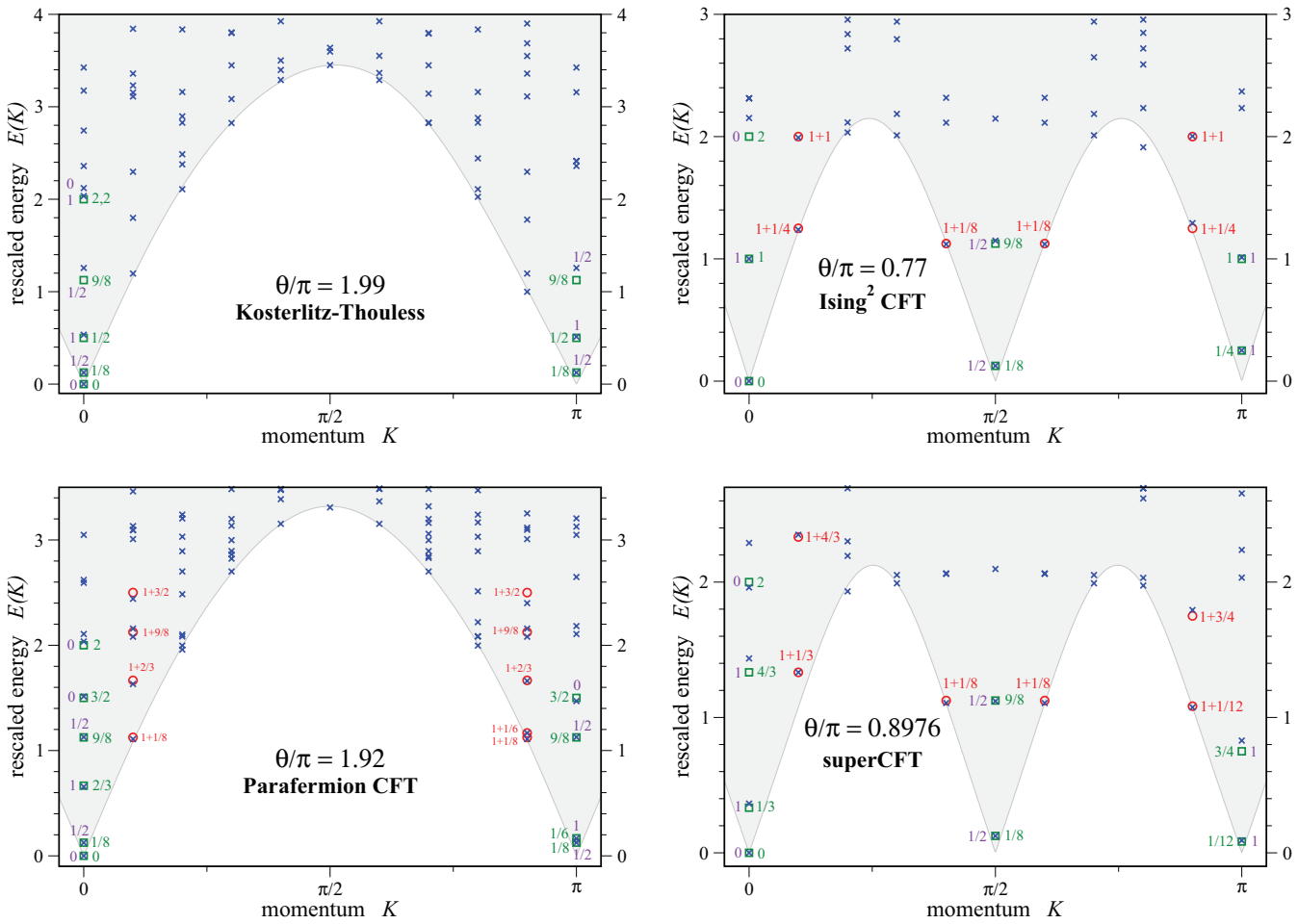

FIG. 13. (Color online) The su(2)$_4$ chain: IS. Energy spectra at various in the gapless phases of the phase diagram in Fig. 12(a). The energy spectra have been rescaled to match the CFT prediction given in Eq. (15). Green squares indicate the location of the primary fields; red circles indicate the descendant fields. The topological symmetry sector is indicated by the violet index. Data shown are for system size $L = 20$.

was the case for the ground state(s) at $\theta_{2,1} = \pi/2$ in the IS, this state is, in fact, the ground state throughout the whole gapped phase, i.e., for angle $0 \leqslant \theta_{2,1} \leqslant 3\pi/4$.

TABLE III. The approximate locations of some of the critical theories of the su(2)$_4$ spin-1 chain (20) in the integer sector (IS) are listed for both the Z_2 and the Z_4 critical regions. The angles without asterisks are obtained directly from exact diagonalization for $L = 20$; i.e., we matched the momentum-resolved spectrum to the CFT. The angles with an asterisk were obtained by using the relations between the angles θ_2 and θ_4, as explained in the text. We only list those values of p for which we could match the CFT description beyond any doubt.

p	Theory	Z_4	Z_2
1	Kosterlitz-Thouless	$0.755\pi^*$	-0.01π
2	Ising^2	0.77π	-0.04π
3	Parafermion	0.80π	-0.08π
4	4-state Potts	0.83π	-0.13π
5		0.88π	-0.17π
6	superCFT	0.92π	-0.20π
7		0.96π	$-0.23\pi^*$
8		0.98π	$-0.24\pi^*$

Gapped phase $\theta_{2,1} = 3\pi/2$. In the gapped phase that surrounds the angle $\theta_{2,1} = 3\pi/2$, the ground state is nondegenerate and occurs at momentum $K = 0$ (there is no sublattice symmetry). At $\theta_{2,1} = 3\pi/2$, the ground state is given by

$$|GS\rangle = \sum_{x_i=1/2,3/2} (-1)^{\#(1/2,3/2)} |x_0, x_2, \ldots, x_{L-1}\rangle.$$

All basis states contribute to the ground state. The sign of a term is given by the number of times the sequence $(x_i, x_{i+1}) = (1/2, 3/2)$ occurs in the basis state $|x_0, x_2, \ldots, x_{L-1}\rangle$ (periodic boundary conditions are assumed).

2. *Gapless phases (HIS)*

As in the IS, the phase diagram in the HIS has two extended regions where the model is critical. The criticality is again described by Z_2 orbifold models. We identified the orbifold models with parameters $p = 2, \ldots, 9$. Some of the critical angles are given in Table IV. In Fig. 14, we give the spectrum of associated with the $p = 2$ orbifold theory in the Z_4 critical region (left panel), and the $p = 3$ orbifold theory in the Z_2 critical region (right panel).

The difference between the two gapless regions in the HIS lies in the momentum quantum numbers, as indicated in

TABLE IV. The approximate locations of some of the critical theories of the su(2)$_4$ spin-1 chain in the HIS [Eq. (21)] for both the Z_2 and the Z_4 critical regions. The angles without asterisk are obtained directly from exact diagonalization for $L = 20$ by matching the momentum-resolved spectrum to the CFT. The angles with asterisks were obtained by using the relations between the angles θ_2 and θ_4, as given in Eq. (22). We only list those values of p for which we were able to match the CFT description beyond any doubt.

p	Theory	Z_4	Z_2
2	Ising^2	0.852π	-0.148π
3	Parafermion	0.795π	-0.078π
4	4-state Potts	0.774π	-0.046π
5		0.766π	-0.030π
6	superCFT	0.761π	-0.020π
7		$0.758\pi^*$	-0.015π
8		$0.756\pi^*$	-0.011π

Table II. The topological symmetry sectors in the HIS coincide with those found in the IS (see Table II). While this is to be expected for topological quantum numbers, it nevertheless shows that our results are consistent.

A major distinction between the IS and the HIS phase diagram of the su(2)$_4$ spin-1 chain is the order of the orbifold theories. By comparing the leftmost and the rightmost panels of Fig. 12, it can be seen that in the IS, the orbifold theories appear in ascending p order when moving away from the first-order transition points, while in the HIS, the orbifold theories appear in descending p order when moving away from gapped phase I. We exploit this result in locating the position of the critical end point of one of the the gapped phases (see following section).

D. The location of the phase boundaries

To locate the boundaries of the gapped and critical regions of the su(2)$_4$ spin-1 chain, we consider the ground-state energy as a function of the interaction angle θ. The analysis is most easily carried out by using an alternative parametrization of the Hamiltonian. Two spin-1 anyons can fuse into either a spin-0, a spin-1, or a spin-2 anyon; therefore we can write the Hamiltonian in terms of projectors onto the spin-2 and spin-0 channels, instead of the spin-2 and spin-1 channels, as we did in Eq. (20). By making use of the relation $\mathbb{I} = P^{(0)} + P^{(1)} + P^{(2)}$, we find that the Hamiltonian

$$H_{\mathrm{J2-J0}}^{(k=4)} = \sum_i \cos\theta_{2,0} P_i^{(2)} - \sin\theta_{2,0} P_i^{(0)} \tag{23}$$

is related to the Hamiltonian of Eq. (20),

$$H_{\mathrm{J2-J1}}^{(k=4)} = \sum_i \cos\theta_{2,1} P_i^{(2)} - \sin\theta_{2,1} P_i^{(1)}, \tag{24}$$

via

$$\tan\theta_{2,1} = -\frac{\tan\theta_{2,0}}{1+\tan\theta_{2,0}}, \tag{25}$$

up to an unimportant shift in energy.

The ground-state energy as a function of the angle $\theta_{2,0}$ is given in Fig. 15 for a chain of size $L = 18$. The kinks in the ground-state energy indicate that there are two first-order phase transitions. These first-order phase transitions mark the boundaries of the gapped phase located at $-\pi/2 < \theta_{2,0} < 0$ in the new angle variable $\theta_{2,0}$ ($0 < \theta_{2,1} < 3\pi/4$ in terms of the original variable $\theta_{2,1}$; see phase diagram in Fig. 12).

To identify the location of the continuous transition between the other gapped phase and the neighboring gapless phases, we plot the first and second derivatives of the ground-state energy per site. From these derivatives, it can be concluded that these transitions are roughly located at $\theta_{2,0} = \pi/2$ and $\theta_{2,0} = \pi$. In terms of the original variable $\theta_{2,1}$, these locations correspond to $\theta_{2,1} = -\pi/4$ and $\theta_{2,1} = \pi$. This conclusion is corroborated by Fig. 16, in which we plot the ground-state energy in the gapped phase surrounding the angle $\theta_{2,1} = 3\pi/2$, i.e., $\theta_{2,0} = 3\pi/4$ for system sizes ranging from $L = 8$ to $L = 20$.

In order to locate the phase boundaries, we also considered the structure of the orbifold CFTs describing the gapless phases (we refer to Appendix E 5 for more details on the orbifold CFTs). We know that throughout the critical region, two fields with scaling dimension $h + \bar{h} = 1/8$ and two fields

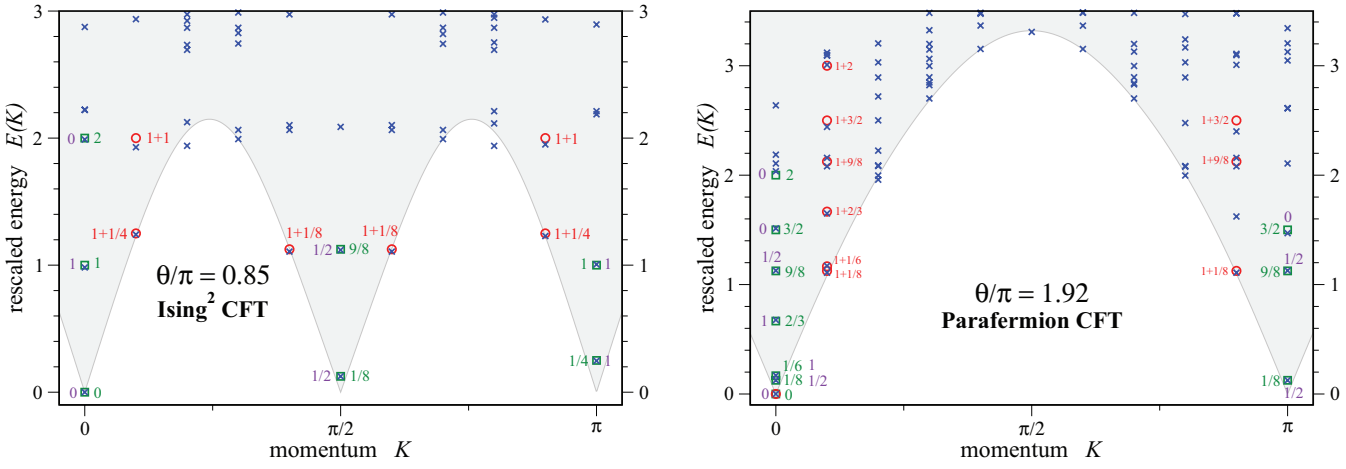

FIG. 14. (Color online) The su(2)$_4$ chain: HIS. Energy spectra at various points in the gapless phases of the phase diagram displayed in Fig. 12(c). The energy spectra have been rescaled to match the CFT prediction given in Eq. (15). Green squares indicate the location of the primary fields; red circles indicate the descendant fields. The topological symmetry sector is indicated by the violet index. Data shown are for system size $L = 20$.

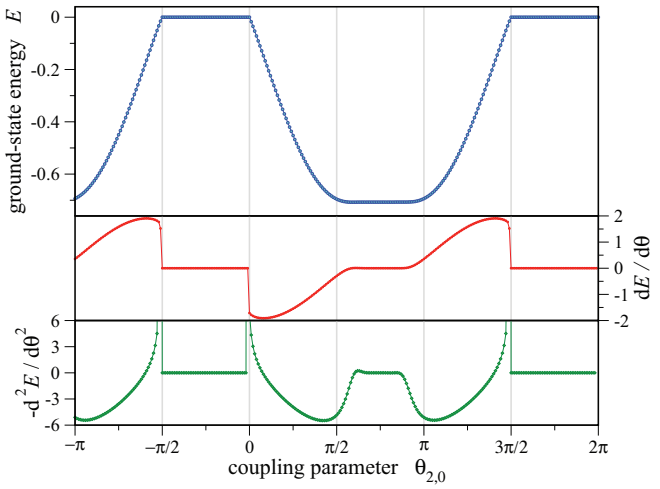

FIG. 15. (Color online) The ground-state energy per site (top panel) and its first and second derivative (middle and bottom panels, respectively) of the IS su(2)$_4$ chain. Data shown are for system size $L = 18$.

with scaling dimension $h + \bar{h} = 9/8$ must appear. In addition, there are several fields with scaling dimensions $\lambda^2/(2p)$ ($\lambda = 1, \ldots, p-1$) for some value of p. Depending on the sector (IS or HIS), and depending on the critical region, these fields appear at different momenta, as detailed in Table II. This table also includes our numerical results for the topological symmetry sectors of the various fields.

The structure of the critical theories describing the critical region allows us to numerically determine the value of p as a function of the angle $\theta_{2,0}$. Moreover, in doing so, we gain insight into the locations of the phase boundaries. We proceed as follows. We first shift the spectrum such that the ground state has energy zero, and we rescale the spectrum such that the two degenerate lowest fields with topological eigenvalue $y = 0$ have energy $1/8$. Since these fields are always among the low-lying fields, finite size effects are insignificant. After shifting and rescaling the energy, we focus on the two states corresponding to the fields with scaling dimensions $1/(2p)$ and $4/(2p)$. By equating the numerical energies to the p-dependent predictions from the CFT, we obtain a numerical estimate of p as a function of the interaction angle. We note one has to be watchful of level crossings when using this procedure.

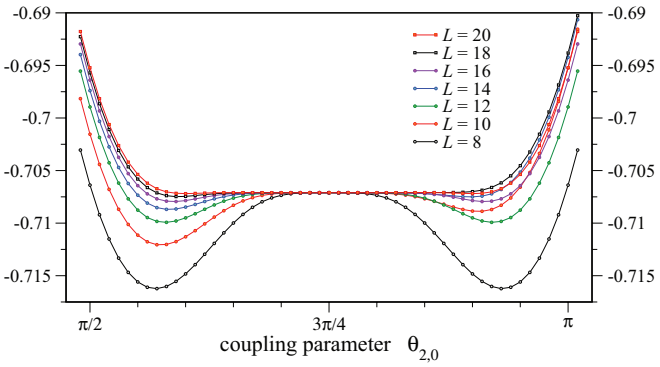

FIG. 16. (Color online) The ground-state energy per site of the IS su(2)$_4$ chain for system sizes $L = 8, \ldots, 20$, in steps of two.

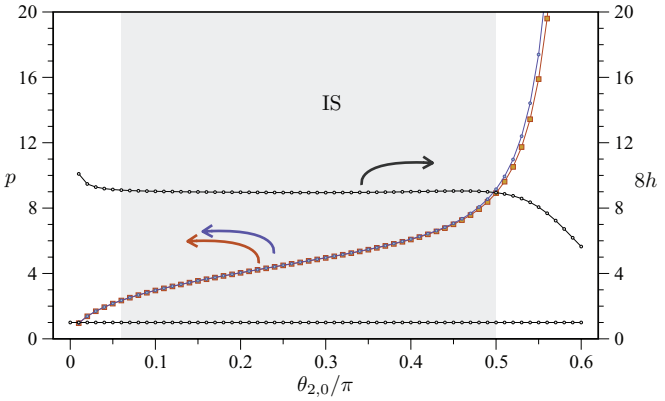

FIG. 17. (Color online) Numerical estimate (system size $L = 20$) of parameter p from the eigenenergies that are associated with operators with scaling dimensions $1/2p$ (red squares) and $4/2p$ (blue dots) in the IS gapless phase with twist operators at $k = 0$ and $k = \pi$. The parameter p is about 1 at $\theta_{2,0} = 0$ and grows to about 9 at $\theta_{2,0} = \pi/2$. For angles $\theta_{2,0} > \pi/2$, the estimates of p obtained from the two operators start to deviate. The black dots correspond the scaling dimension of the fields with dimensions $h = 1/8$ and $h = 9/8$ multiplied by eight, as obtained from exact diagonalization. The shaded region indicates the range of $\theta_{2,0}$ for which the latter dimension lies between $8.9 < 8h < 9.1$.

In Figs. 17 and 18, we display the numerically obtained values for p as a function of the angle for system size $L = 20$. In these figures, we also show the energy of the state corresponding to the field with scaling dimension $9/8$. The range of angles $\theta_{2,0}$ over which the field with scaling dimension $9/8$ is constant is shaded in Fig. 17: The shaded region includes all angles for which the energy associated with the field multiplied by eight takes values between 8.9 and 9.1. It is immediately apparent that the two independent numerical estimates of p agree very well in the range $0 < \theta_{2,0} < \pi/2$. This applies to both IS and HIS. In addition, the energy of the

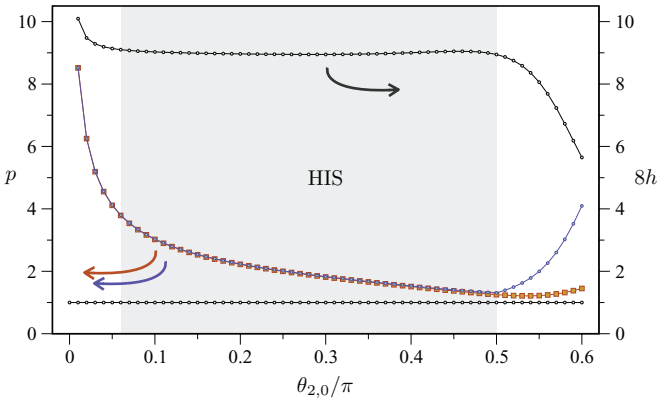

FIG. 18. (Color online) Numerical estimate (system size $L = 20$) of parameter p from the eigenenergies that are associated with operators with scaling dimensions $1/2p$ (red squares) and $4/2p$ (blue dots) in the HIS gapless phase. The black dots correspond to the scaling dimension of the fields with dimensions $h = 1/8$ and $h = 9/8$ multiplied by eight, as obtained from exact diagonalization. The shaded region indicates the range of $\theta_{2,0}$ for which the latter dimension lies between $8.9 < 8h < 9.1$.

state corresponding to the field with scaling dimension 9/8 agrees very well with the prediction over this range. Thus, our numerical data is consistent with the picture that the Z_2 critical region extends over the range $0 \leqslant \theta_{2,0} \leqslant \pi/2$, giving way at $\theta_{2,0} = \pi/2$ to the gapped phase with a Z_2 sublattice structure.

We do not include similar Figures for the Z_4 critical region, but note that they show very similar behavior. This leads to the location of the boundaries of this critical region being $\theta_{2,0} = \pi$ and $\theta_{2,0} = 3\pi/2$, the latter being the location of the first order transition.

We also studied the various values of p which are realized in the su(2)$_4$ spin-1 model. The region close to the first-order transitions is most suitable for identifying the various orbifold models because of drastic changes in the spectrum in this region. Since the Z_2 orbifold CFTs appear in opposite order in the IS and HISs, respectively, both the low- and the high-p orbifold CFTs are observed near the first-order phase transitions at $\theta_{2,0} = 0$. In the IS, we identified the $p = 1$ orbifold CFT (see Fig. 13), which suggests that the gapless phases in the IS su(2)$_4$ chain include the orbifold CFTs starting at the lowest integer value $p = 1$. In contrast, in the HIS, we were able to match the spectrum for the $p = 2$ CFT, but we did not find evidence that the $p = 1$ model exists in the phase diagram. Moreover, we found that the values of p in the HIS increase quite rapidly when decreasing $\theta_{2,0}$ to zero. We were able to identify the orbifold CFTS up to $p = 9$. The reason is that the abundance of low-lying (primary) fields in the high-p orbifold theories requires large system sizes to identify these CFTs with sufficient accuracy.

Further insight into the critical phases can be gained by considering the topological sectors of the various operators in the spectra for the integer values of p (see Table II). All orbifold CFTs (i.e., all p) include a marginal operator with conformal dimension $h = 2$. This marginal operator has momentum $K = 0$ and topological quantum number y_0; i.e., it has the same quantum numbers as the ground state. It is this marginal operator which causes the continuously varying critical behavior within the gapless phase. With increasing p, the number of fields whose scaling dimensions are smaller than two increases. However, these fields are not relevant because their topological and/or momentum quantum numbers differ from those of the ground state. The lowest-p orbifold CFT for which there exists an additional marginal operator with the same quantum numbers as the ground state is $p = 9$. For general p, this operator has scaling dimension $h + \bar{h} = 36/(2p)$ (see Table II). The existence of an additional relevant operator for $p > 9$ (as $36/2p$ surpasses two for $p > 9$) suggests that the range of p values which are realized in our model is $p = 1,2,\ldots,9$. Moreover, if the marginal operator which first appears for $p = 9$ is indeed the operator which is driving the phase transition, it is not surprising that the location of the continuous phase transition is hard to determine.

In conclusion, we provide evidence that the orbifold CFTs with $p = 2,3,\ldots,9$ are realized in both IS and HIS of the su(2)$_4$ spin-1 anyon chain, while the $p = 1$ orbifold CFT appears only in the IS. We note that the su(2)$_4$ anyonic spin-1 chain has some similarities with the one-dimensional quantum Ashkin-Teller model.[43] The one-dimensional quantum Ashkin-Teller model, which is an anisotropic version of the two-dimensional Ashkin-Teller model,[44] also has a line of critical points on its self-dual line, realizing the orbifold CFTs with $p = 1,2,3,4$, in addition to two gapped phases, one of which has a Z_2 sublattice structure.

VI. ANYONIC SU(2)$_k$ SPIN-$\frac{1}{2}$ CHAINS

In this section, we discuss the results of our study of the su(2)$_k$ spin-$\frac{1}{2}$ anyonic spin chains for $k = 2,4,5$. The case $k = 3$ is the original "golden chain" model, which marked the beginning of the study of anyonic quantum spin chains.[15] In the latter publication, it was established numerically that for both antiferromagnetic as well as ferromagnetic interactions, the system is critical and that the system can be described by the tricritical Ising model and the Z_3 parafermion CFT (three-state Potts model criticality), respectively.[15]

In addition, it was shown that the model can be mapped onto an exactly solvable model, namely, a particular "restricted solid-on-solid" (RSOS) model.[15] This mapping is applicable to arbitrary k, and thus the critical behavior of the spin-$\frac{1}{2}$ anyonic chains is described by the k-critical Ising model for AFM interactions and Z_k parafermions for FM interactions.[15]

Finally, it was conjectured in Ref. 15 that the criticality of these spin-$\frac{1}{2}$ anyonic chains is not merely due to a fine tuning of parameters, but is, in fact, protected by a nonlocal, topological symmetry of the model. This implies that the model remains gapless if a perturbation which preserves both the spatial and the topological symmetry is added to the model. This property is essential for the nucleation of a new topological liquid as a result of interactions between anyons.[16]

In this section, we consider the topological symmetry properties of the su(2)$_k$ spin-$\frac{1}{2}$ chains and explain why the criticality is topologically protected for all finite k. Explicit Hamiltonians are given in Appendix C 2.

The numerically obtained spectra for both AFM and FM interactions are given in Figs. 19, 20, and 21 for $k = 2$, $k = 4$, and $k = 5$, respectively. The spectra were obtained by exact diagonalization of the Hamiltonian, followed by shifting and rescaling of the spectrum in order to match the CFT predictions.

The numerical results confirm that the spin-$\frac{1}{2}$ su(2)$_k$ chains are described by the k-critical Ising model for AFM interactions and the Z_k-parafermion CFT for FM interactions. Details of these CFTs are given in Appendixes E 1 and E 4.

In the remainder of this section, we discuss the assignment of topological symmetry sectors to the states in the energy spectra, as indicated in Figs. 19, 20, and 21. The topological symmetry sectors were obtained by acting with the operator Y on the eigenstates. Because Y commutes with both the Hamiltonian and the momentum operator, and because most states are nondegenerate, it follows that the eigenstates of the Hamiltonian (in the momentum representation) are also eigenstates of the topological operator Y.

We begin the analysis with a general observation. A topological symmetry sector is assigned to each state in the spectrum. Moreover, each state is associated with a field in the CFT describing the critical behavior of the chain. These conformal fields satisfy certain fusion rules, which, generally, are different from the fusion rules of the anyons themselves (typically, the number of conformal fields differs from the number of types of anyons). As a result, the topological

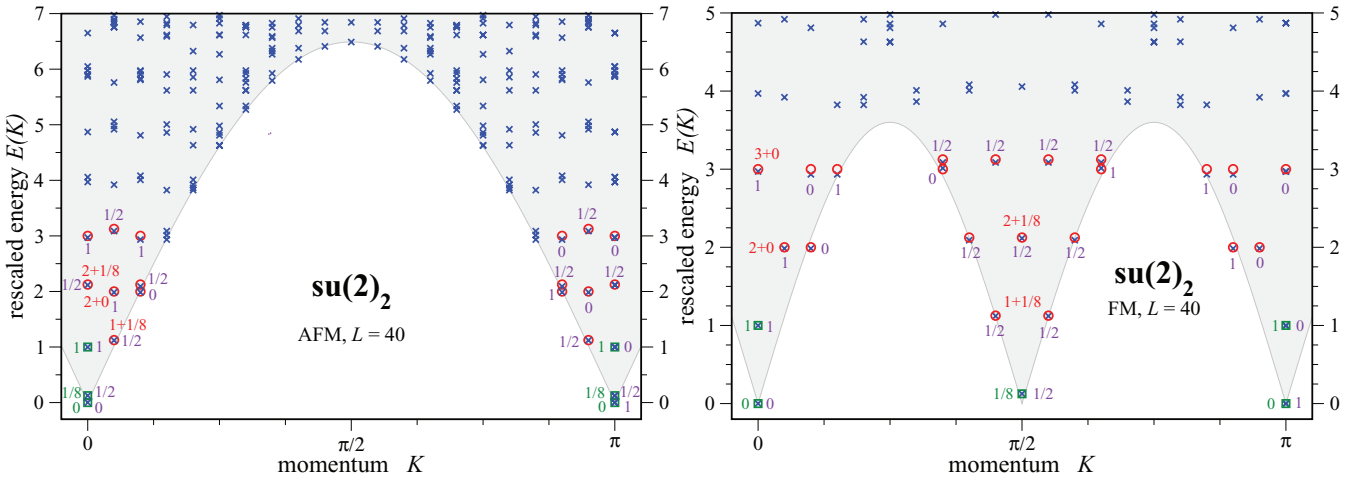

FIG. 19. (Color online) The su(2)$_2$ spin-$\frac{1}{2}$ chain. Energy spectra have been rescaled to match the CFT prediction given in Eq. (15). Green squares indicate the location of the primary fields; red circles specify the descendant fields. The topological symmetry sector is indicated by the violet index. Data shown are for system size $L = 40$.

symmetry sectors must be associated with the conformal fields in a manner that both the su(2)$_k$ fusion rules of the anyons and the fusion rules of the conformal fields are satisfied. For the case of the su(2)$_k$ spin-$\frac{1}{2}$ anyonic chain, this constraint is obeyed for the following reason: The relevant critical theories are so-called coset theories, which contain a su(2)$_k$ theory and other theories such as u(1). This implies that the fields in the critical theory inherit su(2)$_k$ topological symmetry labels; thus, the topological symmetry sectors can be assigned in a consistent manner.

A. The ferromagnetic case

The ferromagnetic su(2)$_k$ spin-$\frac{1}{2}$ anyon chain is described by the coset theory $su(2)_k/u(1)_{2k}$ (details can be found in Appendix E 4). The fields in this CFT carry two labels, a su(2)$_k$ label l and an u(1) label m, where $l = 0,1,\ldots,k$, $m = 0,1,\ldots,2k-1$, and $l+m = 0 \bmod 2$. Under fusion of two fields with labels (l_1,m_1) and (l_2,m_2), the labels m_1 and m_2 are added modulo $2k$, while the labels l_1 and l_2 satisfy the fusion rules of su(2)$_k$. Thus, the fields (l,m) can be assigned a topological label l, and this assignment automatically obeys the correct fusion rules.

The momentum quantum numbers of the fields cannot be predicted from the CFT itself. Different realizations of a particular CFT may vary in the assignment of momenta to conformal fields. For example, the su(2)$_2$ spin-$\frac{1}{2}$ chain is described by the Ising CFT for both AFM and FM interactions, but the states corresponding to the σ or $j = 1/2$ field occur at different momenta, as illustrated in Fig. 19.

We first consider the case of k even. The Hilbert space is given by labelings of the the fusion chain as displayed in Fig. 1, where, in the case of the spin-$\frac{1}{2}$ anyon chain, the "incoming" labels are spin-$\frac{1}{2}$ anyons. As a consequence, the labels x_i alternate between integer and half-integer values. Thus, there are two decoupled "sectors": In one sector, the

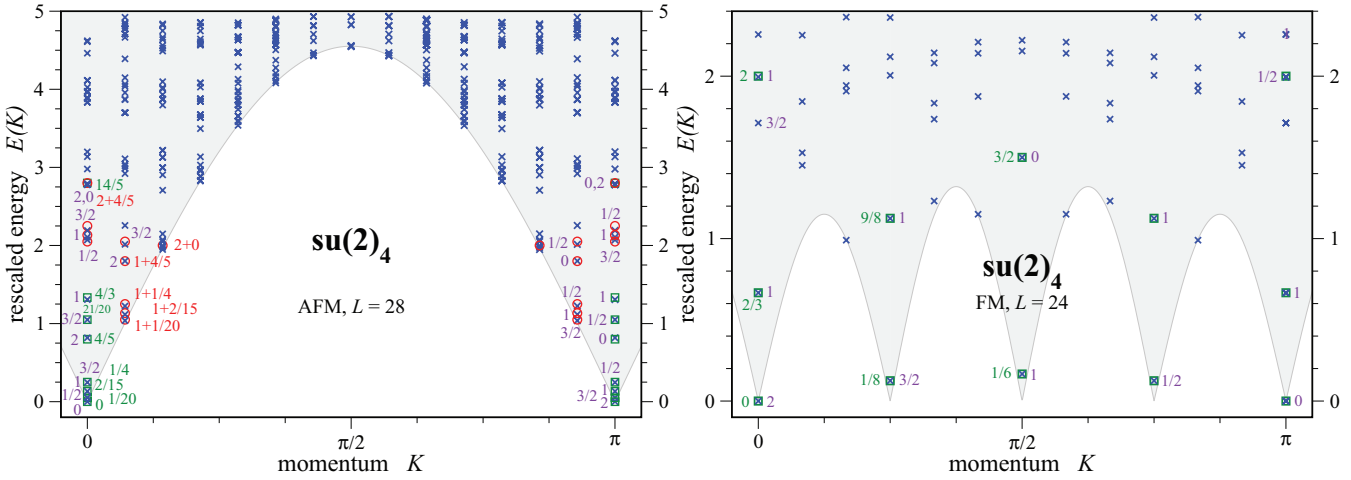

FIG. 20. (Color online) The su(2)$_4$ spin-$\frac{1}{2}$ chain. Energy spectra have been rescaled to match the CFT prediction given in Eq. (15). Green squares indicate the location of the primary fields; red circles specify the descendant fields. The topological symmetry sector is indicated by the violet index. Data shown are for system size $L = 28$ and $L = 24$.

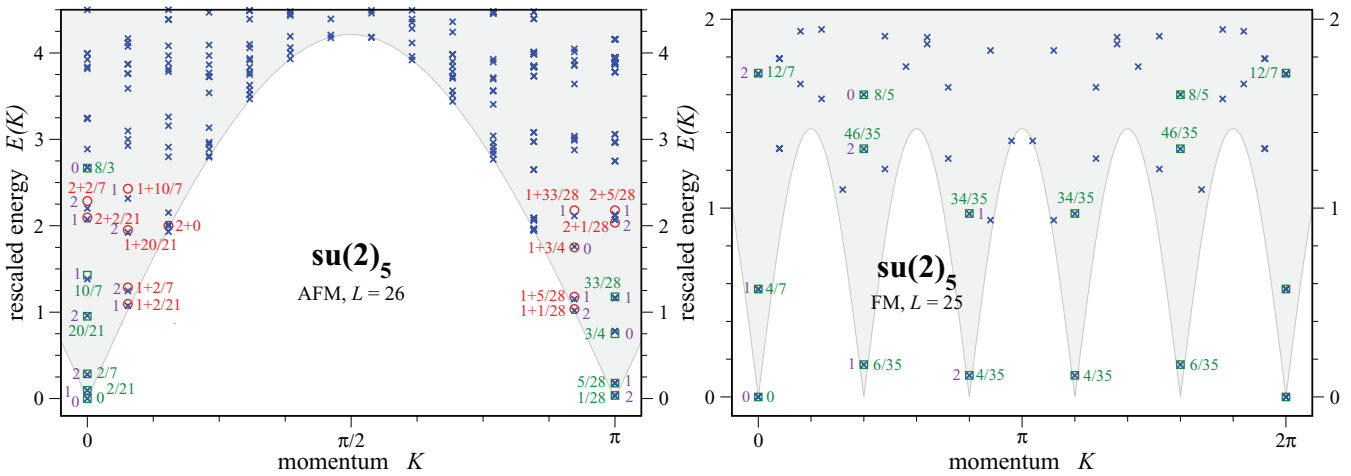

FIG. 21. (Color online) The $su(2)_5$ spin-$\frac{1}{2}$ chain. Energy spectra have been rescaled to match the CFT prediction given in Eq. (15). Green squares indicate the location of the primary fields; red circles indicate the descendant fields. The topological symmetry sector is indicated by the violet index. Data shown are for system size $L = 26$ and $L = 25$, respectively.

labels of the odd sites correspond to integer-spin anyons, while in the other sector, the odd sites correspond to half-integer-spin anyons. Because of this, each field in the CFT will appear twice in the spectrum, once at momentum K and once at momentum $K + \pi$.

As discussed above, for the case of even k, the topological sector y of a field labeled by (l,m) is determined by l, namely, $y = l/2$. Our numerical results show that the momenta of the fields are either given by $K(m) = \frac{m\pi}{k}$, or by $K(m) = \pi + \frac{m\pi}{k}$, as can be seen in the right hand side panel of Fig. 20. The scaling dimensions of the Z_4 parafermion CFT describing that spectrum are given in Table V. To establish that the FM spin-$\frac{1}{2}$ chain is stable under perturbations preserve both spatial and topological symmetry, we need to show that there are no relevant operators with the same momentum and topological quantum numbers as the ground state.

In the case of odd k, anyon spins j are automorph to anyon spins $k/2 - j$ (see Appendix A), and therefore the labels of the conformal fields are given by (l,m) where both l and m are even. The topological sectors are given by $l/2$, and the momenta of the fields are given by $K(m) = \frac{m\pi}{k}$.

From the above-discussed relations between field labels (l,m) and the quantum numbers (topological sectors and momenta), it becomes apparent that each momentum and each topological sector appears at most once. This implies that the critical behavior is indeed stable to perturbations which preserve both spatial and topological symmetry.

TABLE V. Scaling dimensions in the Z_4 parafermion model. The labels corresponding to the positions marked by 'x' do not correspond to primary fields.

	m : 0	1	2	3	4	5	6	7
l: 0	0	x	$\frac{3}{2}$	x	2	x	$\frac{3}{2}$	x
1	x	$\frac{1}{8}$	x	$\frac{9}{8}$	x	$\frac{9}{8}$	x	$\frac{1}{8}$
2	$\frac{2}{3}$	x	$\frac{1}{6}$	x	$\frac{2}{3}$	x	$\frac{1}{6}$	x
3	x	$\frac{9}{8}$	x	$\frac{1}{8}$	x	$\frac{1}{8}$	x	$\frac{9}{8}$
4	2	x	$\frac{3}{2}$	x	0	x	$\frac{3}{2}$	x

B. The antiferromagnetic case

In this section, we show that the criticality of the antiferromagnetic $su(2)_k$ spin-$\frac{1}{2}$ chain is stable under perturbations that do not break the symmetries of the model. The model is described by the k-critical Ising model, which can be formulated in terms of a coset-model $su(2)_1 \times su(2)_{k-1}/su(2)_k$ (some details of this coset model can be found in Appendix E 1). The conformal fields in this CFT are labeled by (r,s), where the r label $(1 \leqslant r \leqslant k)$ is associated with $su(2)_{k-1}$, while s $(1 \leqslant s \leqslant k+1)$ is associated with $su(2)_k$. There is also a label associated with $su(2)_1$; however, this label is fixed by the constraint $t = r + s \bmod 2$.

The topological sectors are given by $(s-1)/2$. Since s is the conformal label associated with the denominator $su(2)_k$ of the coset, the fusion rules of the coset CFT are consistent with the fusion rules associated with the topological sectors.

In the case of even k, all fields appear twice in the spectrum, (once at momentum K and once at $K + \pi$) as a result of the "doubling" of the Hilbert space. Our numerical calculations yield the following. The topological sector of each field is determined by s, namely, $y = (s-1)/2$. The momentum of a field labeled by (r,s) is given by either $K = (r + s \bmod 2)\pi$ or by $K = (r + s + 1 \bmod 2)\pi$; the system size determines which one of the two possibilities occurs (we verified this behavior for $k = 2,4$). The scaling dimensions of the tetra-critical Ising model, describing the critical behavior in the case $k = 4$, can be found in Table VI.

For odd k, the association of field labels (r,s) with topological and momentum sectors coincides with that for even k. However, only odd values of s appear, due to the above-mentioned automorphism of anyon spins. These results were verified for $k = 3$ in Ref. 15, and for $k = 5$ in this study (see Fig. 21).

To confirm that the criticality of the AFM spin-$\frac{1}{2}$ chains is stable under perturbations which preserve the spatial and

TABLE VI. Scaling dimensions for the tetracritical Ising model.

	s : 1	2	3	4	5
r: 1	0	$\frac{1}{4}$	$\frac{4}{3}$	$\frac{13}{4}$	6
2	$\frac{4}{5}$	$\frac{1}{20}$	$\frac{2}{15}$	$\frac{21}{20}$	$\frac{14}{5}$
3	$\frac{14}{5}$	$\frac{21}{20}$	$\frac{2}{15}$	$\frac{1}{20}$	$\frac{4}{5}$
4	6	$\frac{13}{4}$	$\frac{4}{3}$	$\frac{1}{4}$	0

topological symmetries of the model, we have to analyze the scaling dimensions of the fields which have the same topological quantum number as the ground state. The ground state has label $s = 1$ (i.e., topological sector $y = 0$). The scaling dimensions of the fields with label $s = 1$ are given by $2h = [r^2(k+2) - 2(k+1)r + k]/[2(k+1)]$, which for $r \geqslant 1$ increases monotonically. The most relevant field in the same momentum sector as the ground state thus carries the labels $(r,s) = (3,1)$, and has scaling dimension $2h = 2 + \frac{4}{k+1}$, which is irrelevant for k finite, and becomes marginal in the limit $k \to \infty$. Again, we conclude that the AFM spin-$\frac{1}{2}$ chains are stable with respect to perturbations which preserve both topological and translational symmetry.

When breaking the spatial symmetry of the model by dimerizing the system, the most relevant field has labels $(r,s) = (2,1)$ and thus a scaling dimension $2h = (k+4)/[2(k+1)]$ that is relevant for all k. Therefore, a perturbation which breaks translational symmetry may open up a gap.

VII. DISCUSSION

The anyonic analogs of the SU(2) Heisenberg spin-1 model have a rich structure, as can be seen from the phase diagrams of the ordinary bilinear-biquadratic spin-1 model, the generic *even* $k \geqslant 6$ anyonic model, the generic *odd* $k \geqslant 5$ anyonic model, and the special case $k = 4$ (displayed side by side in Fig. 22).

The distinct nature of the phase diagram for $k = 4$ originates in the symmetry of the fusion rules of the su(2)$_k$ theory under the exchange $j \leftrightarrow \frac{k}{2} - j$, which, for $k = 4$, maps $j = 1$ onto itself. It is also the lowest value of k for which a generic fusion rule $1 \times 1 = 0 + 1 + 2$ applies (compare with $k = 3$, where $1 \times 1 = 0 + 1$), thus making it possible to define an anyonic spin-1 model. Moreover, the central charge of the defining su(2)$_4$ algebra is an integer ($c = 2$), and the quantum dimensions of the su(2)$_4$ anyons are all integers or square roots of integers (we discuss the various anyon models in more detail in Appendix A). We note that fusion models with such quantum dimensions typically do not permit "universal quantum computation," a property which requires a "fine tuning" of the braid properties.[45,46] Models analogous to the case $k = 4$ have been studied from the integrability point of view.[47,48]

Upon increasing the level k, the su(2)$_k$ anyon model increasingly resembles the ordinary SU(2) spin algebra. In terms of the quantum group language, the limit $k \to \infty$ corresponds to $q \to 1$, where $q = e^{\pi i/(k+2)}$. For $q = 1$, the quantum group reduces to the ordinary SU(2) algebra. One would therefore intuitively expect that the phase diagram of the generic k case has the same structure as the phase diagram of the SU(2) bilinear-biquadratic spin-1 chain. The numerics presented in the paper shows that this is indeed the case for both even and odd k, with one notable exception: For even k, we find a gapped dimerized phase that is separated from the Haldane gapped phase by an extended critical region; in contrast, for odd k, we observe only an extended critical region but no dimerized phase. The fact that the anyonic spin-1 models behave differently for even and odd k is very interesting in its own right.

In the following, we discuss some of the differences between the cases of odd k versus even k. It is instructive to consider the model for the lowest (generic) value of even k, i.e., $k = 6$. From the symmetry of the fusion rules under the exchange $j \leftrightarrow \frac{k}{2} - j$ it follows that $j = 1$ and $j = 2$ are exchanged. This implies a "symmetry" in the phase diagram of the $k = 6$ model under exchange of the projectors $P^{(1)}$ and $P^{(2)}$. The parametrization chosen in this paper, $H = \sum_i \cos\theta_{2,1} P_i^{(2)} - \sin\theta_{2,1} P^{(1)}$, renders the phase diagram symmetric in the line through the points $\theta_{2,1} = 3\pi/4$ and $\theta_{2,1} = 7\pi/4$. It is important to realize that this "symmetry" only applies to the values of the energies which appear in the spectra, but not to the momenta and the degeneracies of the energy levels. In particular, the gapped dimerized phase is the "mirror phase" of the gapped Haldane phase. We also note that the same mechanism resulted in a symmetric phase diagram for $k = 4$, if plotted in terms of the projectors $P^{(0)}$ and $P^{(2)}$.

For even $k = 6$, there is an extended critical region between these two gapped phases; however, we were not able to determine its precise critical behavior. For $k = 8$, the extent of this critical region is smaller, and it is therefore not

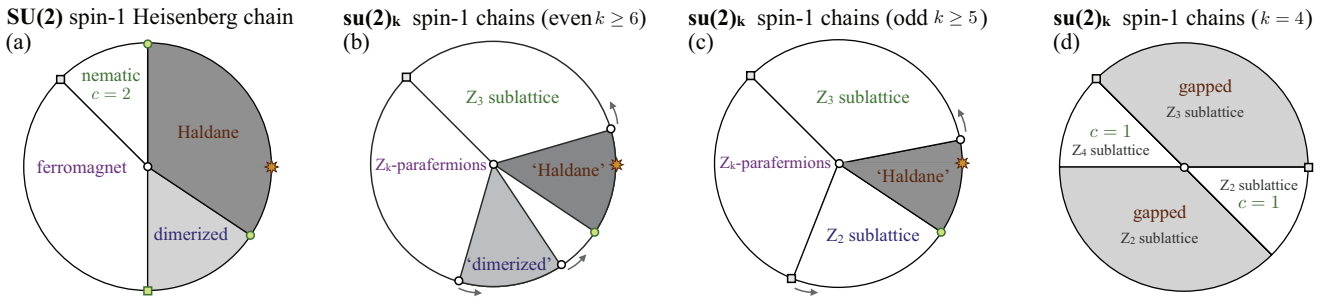

FIG. 22. (Color online) Phase diagrams of the various spin-1 models considered in the paper: (a) the bilinear-biquadratic spin-1 Heisenberg chain, (b) the generic even $k \geqslant 6$ anyonic spin-1 chain, (c) the generic odd $k \geqslant 5$ anyonic spin-1 chain, (d) the special case $k = 4$.

inconceivable that for very large even k, this critical region will shrink to a single critical point separating the two gapped phases, as is the case for the SU(2) spin-1 bilinear-biquadratic model.

As indicated by the above terminology, the gapped phase around the angle $\theta_{2,1} = 0$ is the anyonic analog of the Haldane gapped phase.[2] The ground states at $\theta_{2,1} = 0$ can be obtained exactly, and they are the anyonic analogues of the AKLT state.[21] In Sec. III E4, we studied this "AKLT" point of our anyonic models with open boundary conditions. We obtained edge states similar to the ones observed in the SU(2) case. In the case of periodic boundary conditions, we find a $k+1$-fold degenerate ground state (one for each topological sector), occurring at momentum $K = 0$. Although the Haldane phases of the SU(2) and anyonic models share many properties, they differ in their degeneracy for periodic boundary conditions. Therefore, it is interesting to investigate in which way the underlying quantum group symmetry changes the classification of gapped phases in one-dimensional spin systems.[4]

The dimerized gapped phase of the anyon model exhibits exactly the same values of the energy levels as the gapped Haldane phase, as pointed out above. Nevertheless, this gapped phase is of a different nature. At $\theta_{2,1} = 3\pi/2$, there is a (unique) zero-energy state at momentum $K = \pi$; i.e., the phase is dimerized, like the corresponding phase in the SU(2) spin-1 model. In addition, there is a set of degenerate zero-energy ground states at momentum $K = 0$, where the number of states depends on k.

Almost two decades ago, Koo and Saleur[40] considered a spin-1 type loop model that was based on the "fused Potts model." The underlying algebra of their model is the Birman-Murakami-Wenzl (BMW) algebra, which replaces the Temperley-Lieb[49] algebra that appears in the study of the Potts model in its loop representation. For details on the BMW algebra, we refer to Ref. 50. The Koo-Saleur model contains a *continuous* parameter Q, which is closely related to the discrete level k in the anyon models we consider (see below). More specifically, the model Koo and Saleur considered is

$$H_{\mathrm{KS}} = \sum_i (Q-1)(\sin\omega - \cos\omega) P_i^{(0)} - (Q-2)\cos\omega P^{(1)}. \tag{26}$$

The projectors $P^{(0)}$ and $P^{(1)}$ project two neighboring spin-1 loops onto the spin-0 and spin-1 channels, respectively (see Ref. 50 for explicit expressions of these projectors in terms of the BMW algebra). The number of Potts states Q is related to the quantum dimension of the spin-$\frac{1}{2}$ anyons $d_{1/2}$ (or the parameter d appearing in the Temperley-Lieb algebra) via $Q = d_{1/2}^2 = 4\cos[\pi/(k+2)]^2$, and thus $Q = 1,2,3,4$ corresponds to $k = 1,2,4,\infty$. In particular, the case $Q = 4$ corresponds to the ordinary SU(2) spin-1 chain. We note that the anyonic chains can only be defined for integer $k \geqslant 4$, and recall that we parametrized the anyonic spin-1 model as $H = \sum_i \cos(\theta_{2,1}) P_i^{(2)} - \sin(\theta_{2,1}) P^{(1)}$. By making use of the relation $\mathbf{1} = P^{(0)} + P^{(1)} + P^{(2)}$, one finds the following relation between the parameters of the models:

$$\begin{aligned} \cos\theta_{2,1} &= -(Q-1)(\sin\omega - \cos\omega), \\ \sin\theta_{2,1} &= -\cos\omega + (Q-1)\sin\omega. \end{aligned} \tag{27}$$

Despite the similarities between the model of Koo and Saleur and our anyonic model, they behave rather differently. The phase boundaries between the various phases observed in the Koo-Saleur model depend smoothly on the continuous parameter Q, while the phase diagrams of the anyonic spin-1 models depend on whether k is even or odd. In addition, the Koo-Saleur model displays nonunitary critical behavior, while the critical behavior of the anyon models is described by unitary CFTs. The explanation for this difference in behavior should be sought in the representations used in the two models. In the Koo-Saleur model, a representation which essentially behaves like a SU(2) representation is used (which makes it possible to define the model as a function of the continuous parameter). In the anyonic version, the truncated $\mathrm{su}(2)_k$ representations play a central role. For a related discussion in the general context of loop models, we refer to Refs. 51 and 52.

These observations suggest that a deeper investigation into the differences and similarities of the two models is warranted, especially because the Koo-Saleur model exhibits various integrable points.[40] One of the integrable points identified in Ref. 40 corresponds to the supersymmetric critical point forming the boundary of the Haldane phase. The location of this integrable point, in terms of the parameters used in this paper, is $\tan\theta_{2,1} = -\frac{1}{2}\frac{d_1+1}{d_1}$, where $d_1 = 1 + 2\cos[2\pi/(k+2)]$ (see Ref. 53). For $k \geqslant 4$, this location depends only weakly on k; namely, for $k = 4$, one obtains $\theta_{2,1} = -\arctan(3/4) \approx -0.2048\pi$, while in the limit $k \to \infty$, one obtains $\theta_{2,1} = -\arctan(2/3) \approx -0.1872\pi$. The location of the critical end point of the Haldane phase we obtained in this paper are consistent with the location of this integrable point.

To solve the anyonic spin-1 chain at this integrable point, one approach is to map the model to a fused RSOS model, as studied in Refs. 23 and 54 (see also Refs. 55 and 56). This subject will be described in a separate publication.[53]

ACKNOWLEDGMENTS

We acknowledge insightful discussions with P. Fendley, P. Finch, J. Nissinen, and H. Saleur. We thank the Aspen Center for Theoretical Physics, where parts of this paper were written, for hospitality and support under Grant No. NSF 1066293. A.W.W.L. was supported, in part, by NSF Grant No. DMR-0706140. C.G. was supported, in part, by Grant No. NSERC-163953. S.T. was supported, in part, by Grant No. SFB TR 12 of the DFG.

APPENDIX A: $\mathrm{SU}(2)_k$ ANYONS

In this Appendix, we briefly review of the properties of $\mathrm{su}(2)_k$ anyons—the building blocks of the anyonic chains considered in this paper—for arbitrary level $k \geqslant 2$. We explicitly discuss the levels $k = 2, \ldots, 7$. For a general discussion of anyon models, see, e.g., Refs. 14, 19, and 20.

The anyons of the $\mathrm{su}(2)_k$ theories are closely related to ordinary SU(2) spin degrees of freedom; thus, we label the anyons by their "generalized angular momenta," or simply "spin" value $j = 0, \frac{1}{2}, 1, \ldots, \frac{k}{2}$. We note that in the $\mathrm{su}(2)_k$ theory, there is a maximum allowed value of the "spin," namely, $k/2$, a feature not present for ordinary SU(2) spins.

Ordinary spins can be combined using tensor products. In general, combining two spins gives rise to several different spins. An analogous phenomenon occurs if we combine two anyons of the $su(2)_k$ theory. In the following, we assume that k is fixed, but arbitrary; i.e., the anyons combined belong to the same theory. The rules for combining two anyons—also denoted as "fusion rules"—are closely related to the SU(2) tensor products, namely,

$$j \times j' = \sum_{j''=|j-j'|}^{\min(j+j',k-j-j')} j''. \tag{A1}$$

The only difference to the case of ordinary SU(2) spins is the cutoff in the upper limit of the sum in Eq. (A1). The cutoff is the result of the finite number of types of anyons in the $su(2)_k$ theories. The fusion rules in Eq. (A1) are associative.

The fusion rules can be represented in terms of the fusion matrices N_j which, in the case of $su(2)_k$ anyons, have entries (the so-called fusion coefficients) $N_{j,j'}^{j''} = 1$ if and only if the fusion of labels j and j' gives rise to the label j'' and zero otherwise. In general, fusion coefficients bigger than one are possible, but they do not appear in the context of this paper.

Fusion is commutative and associative; i.e., fusing several anyons in different order gives rise to the same result. This implies that the fusion matrices N_j commute and that they can be diagonalized simultaneously. Diagonalizing the fusion matrices yields the quantum dimensions d_j,

$$N_j\, \mathbf{d} = d_j\, \mathbf{d}, \tag{A2}$$

where $\mathbf{d}$ is a vector whose components are the quantum dimensions d_j. The total quantum dimension $\mathcal{D}$ is defined as

$$\mathcal{D} = \sqrt{\sum_j d_j^2}. \tag{A3}$$

For $su(2)_k$ anyons, the quantum dimensions are given by

$$\begin{aligned} &d_0 = 1, \quad d_{1/2} = 2\cos\left(\frac{\pi}{k+2}\right), \\ &d_j = d_{1/2} d_{j-1/2} - d_{j-1}, \quad j \geqslant 1. \end{aligned} \tag{A4}$$

Explicitly, one obtains

$$d_j = \sin\left(\frac{(2j+1)\pi}{k+2}\right) \Big/ \sin\left(\frac{\pi}{k+2}\right), \tag{A5}$$

where we note that the dimensions d_j depend on the level k, which we have suppressed in the notation.

The matrix which diagonalizes the fusion rules is called the modular S matrix. Its entries for the $su(2)_k$ theories are given by

$$S_{j,j'}(k) = \sqrt{\frac{2}{k+2}} \sin\left(\frac{(2j+1)(2j'+1)\pi}{k+2}\right). \tag{A6}$$

For odd k, there exists an automorphism relating anyons with spin j to anyons with spin $\frac{k}{2} - j$. The automorphism thus relates integer and half-integer spins, reducing the study of odd-k anyon systems to only integer (or only half-integer) anyon spins (it also means that there are only $k/2$ distinct anyon types for odd k). In this paper, we consider anyons with integer spin when studying odd-k systems.

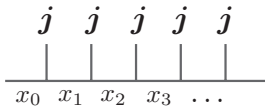

FIG. 23. Basis (fusion diagram) of a chain of spin-j anyons [$j = 1/2$ in the case of the $su(2)_k$ spin-$\frac{1}{2}$ chain, discussed in Sec. VI, and $j = 1$ in the case of the $su(2)_k$ spin-1 chain, discussed in Sec. III].

The Hilbert space of a multianyon system is nonlocal, and it can be represented by a a trivalent graph with each line segment representing an anyonic degree of freedom. Such a graph is called a fusion diagram. The labeling of the segments has to be such that the fusion rules are obeyed at all the vertices. In Fig. 23, we display the fusion diagram that defines the Hilbert space of the models studied in this paper.

Each distinct labeling of the fusion diagram defines a basis state $|\psi\rangle = |x_0, x_2, \ldots, x_{L-1}\rangle$. We define the basis states $|\psi\rangle$ to be orthogonal; i.e., the inner product of two basis states is one if the labels of the two states are identical, and zero otherwise. The number of basis states in a chain of spin-j anyons of length L grows asymptotically as d_j^L, where d_j is the quantum dimension of the anyon of type j. It is important to note that d_j generally is not an integer, as would be the case for ordinary SU(2) spins. This means that it is not possible to associate a local Hilbert space with each anyon, and that the total Hilbert space is not a simple tensor product of local Hilbert spaces. It also implies that there are no "internal s_z quantum numbers" in anyonic Hilbert spaces. The reason behind all these features is that the fusion rules enforce nonlocal constraints on the possible labelings of the fusion diagrams.

In order to define Hamiltonians acting on anyonic Hilbert spaces, the anyonic analog to the $6j$ symbols for ordinary spin degrees of freedom has to be considered. The anyonic version of the $6j$ symbols is the so-called F transformation, which relates the two different ways three anyon spins, j_1, j_2, j_3, can fuse into a fourth anyon spin j_4. The F matrix can be defined as a result of the associativity of the fusion rules, depicted in Fig. 24. In the case of $su(2)_k$, the F matrices are uniquely determined by a consistency relation, namely, the pentagon equation, and by imposing unitarity. A useful expression (for general k) can be found in Ref. 57, and is given in Appendix B.

A further basis transformation of interest is the so-called S transformation which relates the "flux" of anyon spin i through a loop of anyon spin l to the case without an anyon loop, as depicted in Fig. 25. The matrix elements of this transformation are the elements of the modular S matrix.[14,19]

In the following, we give matrix representations of some of the above-discussed properties of a model of $su(2)_k$ anyons. The upper indices in round brackets denote the level k.

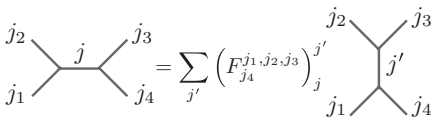

FIG. 24. The associativity of the fusion rules.

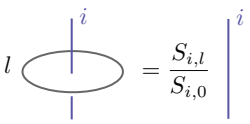

FIG. 25. (Color online) The relation between the flux of anyon spin i through a loop of anyon spin l to the case without the anyon loop l.

Level $k = 2$: Ising anyons. This class of anyons comprises the spin-0 anyon, the Ising anyon (spin-$\frac{1}{2}$) with non-Abelian braiding properties, and the fermion (spin-1). The nontrivial fusion rules are given by

$$\tfrac{1}{2} \times \tfrac{1}{2} = 0 + 1, \quad \tfrac{1}{2} \times 1 = \tfrac{1}{2}, \quad 1 \times 1 = 0. \tag{A7}$$

The corresponding quantum dimensions are given by

$$d_0^{(2)} = d_1^{(2)} = 1, \quad d_{\frac{1}{2}}^{(2)} = \sqrt{2}, \tag{A8}$$

and the S matrix takes the explicit form (the entries are ordered according to ascending value of the anyon spins)

$$S^{(2)} = \frac{1}{2}\begin{pmatrix} 1 & \sqrt{2} & 1 \\ \sqrt{2} & 0 & -\sqrt{2} \\ 1 & -\sqrt{2} & 1 \end{pmatrix}. \tag{A9}$$

Level $k = 3$: Fibonacci anyons. This class of non-Abelian anyons exhibits only two distinct particles, with spins 0 and 1 (the Fibonacci anyon), respectively (the spins $\frac{1}{2}$ and $\frac{3}{2}$ are automorph to spins 1 and 0, respectively). Thus, there is only one nontrivial fusion rule,

$$1 \times 1 = 0 + 1, \tag{A10}$$

and the quantum dimensions are given by

$$d_0^{(3)} = 1, \quad d_1^{(3)} = (1 + \sqrt{5})/2. \tag{A11}$$

Using the notation $\phi = (1 + \sqrt{5})/2$, the S matrix reads

$$S^{(3)} = \frac{1}{\sqrt{2+\phi}}\begin{pmatrix} 1 & \phi \\ \phi & -1 \end{pmatrix}. \tag{A12}$$

Level $k = 4$. The $k = 4$ anyon model contains five anyon spins, namely, $j = 0, \frac{1}{2}, 1, \frac{3}{2}, 2$. The fusion rules are given by

$\times$	$\frac{1}{2}$	1	$\frac{3}{2}$	2
$\frac{1}{2}$	$0+1$	$\frac{1}{2}+\frac{3}{2}$	$1+2$	$\frac{3}{2}$
1		$0+1+2$	$\frac{1}{2}+\frac{3}{2}$	$1\cdot$
$\frac{3}{2}$			$0+1$	$\frac{1}{2}$
2				0

(A13)

The (nontrivial) quantum dimensions can be obtained from Eq. (A4):

$$d_0^{(4)} = d_2^{(4)} = 1, \quad d_{\frac{1}{2}}^{(4)} = d_{\frac{3}{2}}^{(4)} = \sqrt{3}, \quad d_1^{(4)} = 2. \tag{A14}$$

Finally, the S matrix takes the form

$$S^{(4)} = \frac{1}{2\sqrt{3}}\begin{pmatrix} 1 & \sqrt{3} & 2 & \sqrt{3} & 1 \\ \sqrt{3} & \sqrt{3} & 0 & -\sqrt{3} & -\sqrt{3} \\ 2 & 0 & -2 & 0 & 2 \\ \sqrt{3} & -\sqrt{3} & 0 & \sqrt{3} & -\sqrt{3} \\ 1 & -\sqrt{3} & 2 & -\sqrt{3} & 1 \end{pmatrix}. \tag{A15}$$

Level $k = 5$. This class of non-Abelian anyons gives rise to three distinct anyon particles with spins 0, 1, and 2 (which are automorph to the spins $\frac{5}{2}$, $\frac{3}{2}$, and $\frac{1}{2}$, respectively). The nontrivial fusion rules are given by

$$1 \times 1 = 0 + 1 + 2, \quad 1 \times 2 = 1 + 2, \quad 2 \times 2 = 0 + 1.$$

The quantum dimensions take the following values:

$$\begin{aligned} &d_0^{(5)} = 1, \quad d_1^{(5)} = \left(d_2^{(5)}\right)^2 - 1 = 1 + 2\cos(2\pi/7), \\ &d_2^{(5)} = 2\cos(\pi/7). \end{aligned} \tag{A17}$$

The S matrix of the su(2)$_5$ theory is given by

$$S = \frac{1}{\mathcal{D}^{(5)}}\begin{pmatrix} 1 & d_1^{(5)} & d_2^{(5)} \\ d_1^{(5)} & -d_2^{(5)} & 1 \\ d_2^{(5)} & 1 & -d_1^{(5)} \end{pmatrix}, \tag{A18}$$

where $\mathcal{D}^{(5)}$ denotes the total quantum dimension $\mathcal{D}^{(5)} = \sqrt{1 + (d_1^{(5)})^2 + (d_2^{(5)})^2}$ of the su(2)$_5$ theory (restricted to the integer "spins").

Level $k = 6$. The anyon model with $k = 6$ has seven anyons labeled by $j = 0, \frac{1}{2}, 1, \frac{3}{2}, 2, \frac{5}{2}, 3$. The fusion rules read

$\times$	$\frac{1}{2}$	1	$\frac{3}{2}$	2	$\frac{5}{2}$	3
$\frac{1}{2}$	$0+1$	$\frac{1}{2}+\frac{3}{2}$	$1+2$	$\frac{3}{2}+\frac{5}{2}$	$2+3$	$\frac{5}{2}$
1		$0+1+2$	$\frac{1}{2}+\frac{3}{2}+\frac{5}{2}$	$1+2+3$	$\frac{3}{2}+\frac{5}{2}$	2
$\frac{3}{2}$			$0+1+2+3$	$\frac{1}{2}+\frac{3}{2}+\frac{5}{2}$	$1+2$	$\frac{3}{2}$
2				$0+1+2$	$\frac{1}{2}+\frac{3}{2}$	1
$\frac{5}{2}$					$0+1$	$\frac{1}{2}$
3						$0.$

(A19)

The quantum dimensions can be obtained from Eq. (A4),

$$\begin{aligned} &d_0^{(6)} = d_3^{(6)} = 1, \quad d_{\frac{1}{2}}^{(6)} = d_{\frac{5}{2}}^{(4)} = \sqrt{2+\sqrt{2}}, \\ &d_1^{(6)} = d_2^{(6)} = 1 + \sqrt{2}, \quad d_{\frac{3}{2}}^{(6)} = \sqrt{2}\sqrt{2+\sqrt{2}}. \end{aligned} \tag{A20}$$

The entries of the S matrix are given by $S_{i,j} = \sqrt{\frac{2}{k+2}}\sin(\frac{(2i+1)(2j+1)\pi}{(k+2)})$, for $i, j = 0, 1/2, 1, \ldots, k/2$, with $k = 6$.

Level $k = 7$. Finally, we provide some details of the $k = 7$ model, which contains four distinct anyons with spins 0, 1, 2, and 3. The fusion rules are

$\times$	1	2	3
1	$0+1+2$	$1+2+3$	$2+3$
2		$0+1+2+3$	$1+2$
3			$0+1$

(A21)

and the quantum dimensions are given by

$$\begin{aligned} &d_0^{(7)} = 1, \quad d_1^{(7)} = 1 + 2\cos(2\pi/9), \\ &d_2^{(7)} = 1 + 2\cos(\pi/9), \quad d_3^{(7)} = 2\cos(\pi/9). \end{aligned} \tag{A22}$$

The entries of the S matrix are given by $S_{i,j} = \sqrt{\frac{4}{k+2}}\sin(\frac{(2i+1)(2j+1)\pi}{(k+2)})$, for $i,j = 0,1,\ldots,(k-1)/2$, with $k = 7$.

APPENDIX B: F MATRICES OF THE SU(2)$_k$ THEORIES

In this section, we give an explicit expression for the F symbols, following Ref. 57. We begin with some preliminary notation. The q numbers are defined as $\lfloor n\rfloor = \sum_{i=1}^{n} q^{\frac{n+1}{2}-i} = \frac{q^{\frac{n}{2}}-q^{-\frac{n}{2}}}{q^{\frac{1}{2}}-q^{-\frac{1}{2}}}$. The q factorials are defined as $\lfloor n\rfloor! = \lfloor n\rfloor\lfloor n-1\rfloor\cdots\lfloor 1\rfloor$, for integer $n > 0$, and $\lfloor 0\rfloor! = 1$. The labels of the anyons $a,b,\ldots$ take the values $0,1/2,1,\ldots$. The quantum dimensions are $d_j = \lfloor 2j+1\rfloor = \sin(\frac{(2j+1)\pi}{k+2})/\sin(\frac{\pi}{k+2}) = d_{k/2-j}$. Moreover, we define

$$\Delta(a,b,c) = \sqrt{\frac{\lfloor a+b-c\rfloor!\lfloor a-b+c\rfloor!\lfloor -a+b+c\rfloor!}{\lfloor a+b+c+1\rfloor!}}, \tag{B1}$$

where $a \leqslant b+c$, $b \leqslant a+c$, $c \leqslant a+b$, and $a+b+c = 0 \bmod 1$. Using the above introduced notation, the F symbols can be written as[57]

$$\begin{aligned}\left(F_d^{abc}\right)_f^e = {} & (-1)^{a+b+c+d}\Delta(a,b,e)\Delta(c,d,e)\Delta(b,c,f)\Delta(a,d,f)\sqrt{\lfloor 2e+1\rfloor}\sqrt{\lfloor 2f+1\rfloor} \\ & \times {\sum_n}' \frac{(-1)^n\lfloor n+1\rfloor!}{\lfloor a+b+c+d-n\rfloor!\lfloor a+c+e+f-n\rfloor!\lfloor b+d+e+f-n\rfloor!} \\ & \times \frac{1}{\lfloor n-a-b-e\rfloor!\lfloor n-c-d-e\rfloor!\lfloor n-b-c-f\rfloor!\lfloor n-a-d-f\rfloor!},\end{aligned} \tag{B2}$$

where the sum over n runs over (non-negative) integers such that

$$\begin{aligned}&\max(a+b+e,c+d+e,b+c+f,a+d+f) \\ &\quad \leqslant n \leqslant \min(a+b+c+d,a+c+e+f,b+d+e+f),\end{aligned}$$

which guarantees that the arguments of the q factorials are non-negative integers.

APPENDIX C: MICROSCOPIC MODELS

1. Basis and Hamiltonian

We consider a chain of spin-j anyons, using the basis displayed in Fig. 23. We fix the spin-j anyon to be either a spin-$\frac{1}{2}$ anyon or a spin-1 anyon; however, the Hamiltonian defined below can be generalized to any value $j \in \{0,1/2,\ldots,k/2\}$. Throughout most of this paper, we apply periodic boundary conditions, i.e., $x_L = x_0$, where L denotes the number of anyonic quasiparticles in the chain.

We consider interactions between nearest-neighboring spin-j anyons. In the case of $j = 1/2$ [the "su(2)$_k$ spin-$\frac{1}{2}$ chain"], two neighboring spin-$\frac{1}{2}$ anyons may fuse into a spin-0 or a spin-1 anyon. In contrast, for the case of $j = 1$ [the "su(2)$_k$ spin-1 chain"], two neighboring spin-1 anyons may fuse into a spin-0, a spin-1, or a spin-2 anyon (for $k \geqslant 4$). In order to obtain the fusion product of two nearest-neighbor spin-j anyons in the basis shown in Fig. 23, an F transformation has to be performed, as illustrated in Fig. 26. Consequently, the

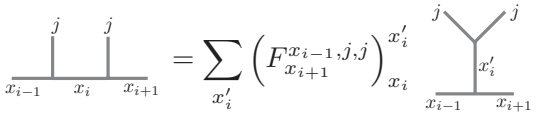

FIG. 26. Basis transformation used to obtain the fusion product of two neighboring spin-j anyons.

projector onto a particular fusion channel l is composed of two F transformations. This projector, denoted by $P_i^{(l)}$, penalizes the fusion of anyons at positions i and $i+1$ into an l-anyon, and it is defined as follows:

$$\begin{aligned}P_i^{(l)}&|x_0,\ldots,x_{i-1},x_i,x_{i+1},\ldots,x_{L-1}\rangle \\ &= \sum_{x_i'} \left(F^{x_{i-1},j,j}_{x_{i+1}}\right)^{l}_{x_i}\left(F^{x_{i-1},j,j}_{x_{i+1}}\right)^{l}_{x_i'} \\ &\quad \times |x_0,\ldots,x_{i-1},x_i',x_{i+1},\ldots,x_{L-1}\rangle.\end{aligned} \tag{C1}$$

We note that this definition utilizes that $F = F^{-1}$ for su(2)$_k$. The explicit form of the local projectors for the systems studied in this paper is given in Appendix B. The Hamiltonians discussed in the following section are composed of the sum of the local projection operators $P_i^{(l)}$ onto the fusion product l of two nearest-neighbor spin-j anyons

2. Hamiltonian of the su(2)$_k$ spin-$\frac{1}{2}$ chain

The Hamiltonian of the su(2)$_k$ spin-$\frac{1}{2}$ chain is given by

$$H = J\sum_i P_i^{(0)}, \tag{C2}$$

where the projector $P_i^{(0)}$ is defined in Eq. (C1) (note that $l = 0$ and $j = \frac{1}{2}$), and the coupling constant takes the values $J = \pm 1$. In analogy to the "ordinary" Heisenberg spin-$\frac{1}{2}$ chain, we denote the case $J = -1$ in Hamiltonian (C2) as antiferromagnetic (AFM) coupling while $J = 1$ is ferromagnetic (FM) coupling.

In the following, we present matrix representations of the Hamiltonians of the spin-$\frac{1}{2}$ anyon chains for $k = 2,3,4,5$. The matrix formulation for the su(2)$_3$ spin-$\frac{1}{2}$ chain was first introduced in Ref. 15 (see also Ref. 58). Local basis elements are labeled by x_i, where $x_i \in \{0,1/2,1,\ldots,k/2\}$. The order

of anyon spins in the matrix representation is ascending. We also introduce the operators n_i^j acting on local state $|x_i\rangle$: $n_i^j|x_i\rangle = e|x_i\rangle$ where the eigenvalue $e = 1$ if the local basis element $x_i = j$ and $e = 0$ otherwise.

From the definition of the summands of the Hamiltonian [Eq. (C1)], it is apparent that the matrix representation of the projector P_i^0 depends on the basis elements x_{i-1}, x_i, and x_{i+1}. In particular, nontrivial contributions to P_i^0 exist only for certain values of x_{i-1} and x_{i+1}, and thus each contribution to the projector will be proportional to $n_{i-1}^j n_{i+1}^{j'}$, for some values of j and j'. By specifying both j and j', the possible values of x_i are fixed by the fusion rules. If there is only one value x_i can take (for given j and j'), we omit the identity operator that is applied to basis element $|x_i\rangle$. If there is more than one possible value of x_i, we specify the matrix assigning the correct energies.

In the case of even-k spin-$\frac{1}{2}$ chains, the fusion rules Eq. (A7) impose that the values of the local basis elements x_i alternate between integer and half-integer values. For the odd-k spin chains (both spin-$\frac{1}{2}$ and spin-1 chains), we only consider the integer anyon spin subspace (recall the automorphism that applies to odd k anyons, see Appendix A). For the even-k spin-1 chains, the Hilbert space splits into two disjoint sectors, the IS (all x_i take integer values) and the HIS (all x_i assume half-integer values).

a. su(2)$_2$ spin-$\frac{1}{2}$ chain

The Hamiltonian Eq. (C2) takes a rather simple form in the case of su(2)$_2$, namely,

$$H^{(k=2)} = J\sum_i n_{i-1}^0 n_{i+1}^0 + n_{i-1}^1 n_{i+1}^1 + + \frac{1}{2} n_{i-1}^{1/2} n_{i+1}^{1/2} \begin{pmatrix} 1 & -1 \\ -1 & 1 \end{pmatrix}_i . \tag{C3}$$

b. su(2)$_3$ spin-$\frac{1}{2}$ chain

The Hamiltonian for the $k = 3$ spin-$\frac{1}{2}$ chain is given by

$$H^{(k=3)} = J\sum_i n_{i-1}^0 n_{i+1}^0 + \frac{1}{d^2} n_{i-1}^1 n_{i+1}^1 \begin{pmatrix} 1 & -\sqrt{d} \\ -\sqrt{d} & d \end{pmatrix}_i , \tag{C4}$$

where $d = d_1 = (1+\sqrt{5})/2$.

c. su(2)$_4$ spin-$\frac{1}{2}$ chain

In the case $k = 4$, the local basis elements alternate between integer spin, $x_i \in \{0,1,2\}$ and half integer spin, $x_{i+1} \in \{1/2,3/2\}$. The Hamiltonian takes the following form:

$$\begin{aligned} H^{(k=4)} = J\sum_i & n_{i-1}^0 n_{i+1}^0 + n_{i-1}^2 n_{i+1}^2 + \frac{1}{2} n_{i-1}^1 n_{i+1}^1 \begin{pmatrix} 1 & -1 \\ -1 & 1 \end{pmatrix}_i \\ & + \frac{1}{3} n_{i-1}^{1/2} n_{i+1}^{1/2} \begin{pmatrix} 1 & -\sqrt{2} \\ -\sqrt{2} & 2 \end{pmatrix}_i \\ & + \frac{1}{3} n_{i-1}^{3/2} n_{i+1}^{3/2} \begin{pmatrix} 2 & -\sqrt{2} \\ -\sqrt{2} & 1 \end{pmatrix}_i . \end{aligned} \tag{C5}$$

d. su(2)$_5$ spin-$\frac{1}{2}$ chain

Using the notation $d_1 = 1 + 2\cos(2\pi/7)$ and $d_2 = 2\cos(\pi/7)$, the Hamiltonian reads

$$\begin{aligned} H^{(k=5)} = & J\sum_i n_{i-1}^0 n_{i+1}^0 + \frac{1}{d_1 d_2} n_{i-1}^1 n_{i+1}^1 \begin{pmatrix} d_1 & -\sqrt{d_1 d_2} \\ -\sqrt{d_1 d_2} & d_2 \end{pmatrix}_i \\ & + \frac{1}{d_2^2} n_{i-1}^2 n_{i+1}^2 \begin{pmatrix} 1 & -\sqrt{d_1} \\ -\sqrt{d_1} & d_1 \end{pmatrix}_i . \end{aligned} \tag{C6}$$

3. Hamiltonian of the su(2)$_k$ spin-1 chain

We define the Hamiltonian of the su(2)$_k$ spin-1 chain as follows:

$$H = J_1 \sum_i P_i^{(1)} + J_2 \sum_i P_i^{(2)} . \tag{C7}$$

The projectors $P_i^{(1)}$ and $P_i^{(2)}$ are defined in Eq. (C1), where $l = 1$ and $l = 2$, respectively. This Hamiltonian is the su(2)$_k$ anyonic equivalent of the bilinear-biquadratic spin-1 chain. Throughout the paper, we parametrize the Hamiltonian by the angle θ as follows: $J_1 = -\sin(\theta_{2,1})$, $J_2 = \cos(\theta_{2,1})$.

The Hamiltonian Eq. (C7) is defined for levels $k \geqslant 4$, in which case the fusion of two spin-1 anyons may result in a spin-0, a spin-1, or a spin-2 anyon (for level $k = 3$, spins $\frac{1}{2}$ and 1 are automorph, i.e., the spin-1 chain is equivalent to the spin-$\frac{1}{2}$ chain; moreover, the fusion rules imply $1 \times 1 = 0 + 1$. For $k = 2$, the fusion of two spin-1 particles is trivial, $1 \times 1 = 0$).

a. The su(2)$_4$ spin-1 chain

We now present a matrix representation of the Hamiltonian of the su(2)$_4$ spin-1 chain, using the same notation as in the previous section. In the IS, the projectors onto the different channels can be written as follows:

$$\begin{aligned} P_{i,\mathrm{IS}}^{(0)} = & n_{i-1}^0 n_{i+1}^0 + n_{i-1}^2 n_{i+1}^2 + \frac{1}{4} n_{i-1}^1 n_{i+1}^1 \\ & \times \begin{pmatrix} 1 & -\sqrt{2} & 1 \\ -\sqrt{2} & 2 & -\sqrt{2} \\ 1 & -\sqrt{2} & 1 \end{pmatrix}_i , \end{aligned} \tag{C8}$$

$$\begin{aligned} P_{i,\mathrm{IS}}^{(1)} = & n_{i-1}^0 n_{i+1}^1 + n_{i-1}^1 n_{i+1}^0 + n_{i-1}^1 n_{i+1}^2 + n_{i-1}^2 n_{i+1}^1 \\ & + \frac{1}{2} n_{i-1}^1 n_{i+1}^1 \begin{pmatrix} 1 & 0 & -1 \\ 0 & 0 & 0 \\ -1 & 0 & 1 \end{pmatrix}_i , \end{aligned} \tag{C9}$$

$$\begin{aligned} P_{i,\mathrm{IS}}^{(2)} = & n_{i-1}^0 n_{i+1}^2 + n_{i-1}^2 n_{i+1}^0 \\ & + \frac{1}{4} n_{i-1}^1 n_{i+1}^1 \begin{pmatrix} 1 & \sqrt{2} & 1 \\ \sqrt{2} & 2 & \sqrt{2} \\ 1 & \sqrt{2} & 1 \end{pmatrix}_i . \end{aligned} \tag{C10}$$

In the HIS, we can write the projectors as follows:

$$P^{(0)}_{i,\mathrm{HIS}} = \frac{1}{2}\left(n^{1/2}_{i-1}n^{1/2}_{i+1} + n^{3/2}_{i-1}n^{3/2}_{i+1}\right)\begin{pmatrix} 1 & -1 \\ -1 & 1 \end{pmatrix}_i, \tag{C11}$$

$$P^{(1)}_{i,\mathrm{HIS}} = \frac{1}{2}\left(n^{1/2}_{i-1}n^{1/2}_{i+1} + n^{3/2}_{i-1}n^{3/2}_{i+1}\right)\begin{pmatrix} 1 & 1 \\ 1 & 1 \end{pmatrix}_i + \frac{1}{2}\left(n^{1/2}_{i-1}n^{3/2}_{i+1} + n^{3/2}_{i-1}n^{1/2}_{i+1}\right)\begin{pmatrix} 1 & -1 \\ -1 & 1 \end{pmatrix}_i, \tag{C12}$$

$$P^{(2)}_{i,\mathrm{HIS}} = \frac{1}{2}\left(n^{1/2}_{i-1}n^{3/2}_{i+1} + n^{3/2}_{i-1}n^{1/2}_{i+1}\right)\begin{pmatrix} 1 & 1 \\ 1 & 1 \end{pmatrix}_i. \tag{C13}$$

b. The su(2)$_5$ spin-1 chain

Using notation $d_1 = 1 + 2\cos(2\pi/7)$ and $d_2 = 2\cos(\pi/7)$, the projectors are given by

$$P^{(1)}_i = n^0_{i-1}n^1_{i+1} + n^1_{i-1}n^0_{i+1} + \frac{1}{d_1^4}n^1_{i-1}n^1_{i+1}\begin{pmatrix} d_1^3 & -d_1^{3/2} & -d_1^2 d_2^{3/2} \\ -d_1^{3/2} & 1 & \sqrt{d_1}d_2^{3/2} \\ -d_1^2 d_2^{3/2} & \sqrt{d_1}d_2^{3/2} & d_1 d_2^3 \end{pmatrix}_i + \frac{d_2}{d_1^2}\left(n^1_{i-1}n^2_{i+1} + n^2_{i-1}n^1_{i+1}\right)\begin{pmatrix} d_2 & -\sqrt{d_2} \\ -\sqrt{d_2} & 1 \end{pmatrix}_i + \frac{1}{d_1 d_2}n^2_{i-1}n^2_{i+1}\begin{pmatrix} d_2 & \sqrt{d_1 d_2} \\ \sqrt{d_1 d_2} & d_1 \end{pmatrix}_i, \tag{C14}$$

$$P^{(2)}_i = n^0_{i-1}n^2_{i+1} + n^2_{i-1}n^0_{i+1} + \frac{1}{d_1^4}n^1_{i-1}n^1_{i+1}\begin{pmatrix} d_1^2 d_2 & d_1^{3/2}d_2^2 & d_1 d_2^{3/2} \\ d_1^{3/2}d_2^2 & d_1 d_2^3 & \sqrt{d_1}d_2^{5/2} \\ d_1 d_2^{3/2} & \sqrt{d_1}d_2^{5/2} & d_2^2 \end{pmatrix}_i + \frac{d_2}{d_1^2}\left(n^1_{i-1}n^2_{i+1} + n^2_{i-1}n^1_{i+1}\right)\begin{pmatrix} 1 & \sqrt{d_2} \\ \sqrt{d_2} & d_2 \end{pmatrix}_i. \tag{C15}$$

c. The su(2)$_6$ spin-1 chain

In the following, we use the notation $d_{1/2} = 2\cos(\pi/8)$, $d_1 = 1 + 2\cos(\pi/4) = 1 + \sqrt{2}$ and $d_{3/2} = 2\sqrt{2}\cos(\pi/8)$. In the IS, the projectors onto the different channels can be written as follows:

$$\begin{aligned} P^{(1)}_{i,\mathrm{IS}} = {} & n^0_{i-1}n^1_{i+1} + n^1_{i-1}n^0_{i+1} + n^2_{i-1}n^3_{i+1} + n^3_{i-1}n^2_{i+1} + \frac{1}{2}\left(n^1_{i-1}n^2_{i+1} + n^2_{i-1}n^1_{i+1}\right)\begin{pmatrix} 1 & -1 \\ -1 & 1 \end{pmatrix}_i \\ & + \frac{1}{d_{1/2}d_1 d_{3/2}}n^1_{i-1}n^1_{i+1}\begin{pmatrix} d_{1/2}d_{3/2} & -\sqrt{d_{1/2}d_{3/2}} & -d_1\sqrt{d_{1/2}d_{3/2}} \\ -\sqrt{d_{1/2}d_{3/2}} & 1 & d_1 \\ -d_1\sqrt{d_{1/2}d_{3/2}} & d_1 & d_1^2 \end{pmatrix}_i \\ & + \frac{1}{d_{1/2}d_1 d_{3/2}}n^2_{i-1}n^2_{i+1}\begin{pmatrix} d_1^2 & d_1 & -d_1\sqrt{d_{1/2}d_{3/2}} \\ d_1 & 1 & -\sqrt{d_{1/2}d_{3/2}} \\ -d_1\sqrt{d_{1/2}d_{3/2}} & -\sqrt{d_{1/2}d_{3/2}} & d_{1/2}d_{3/2} \end{pmatrix}_i, \end{aligned} \tag{C16}$$

$$\begin{aligned} P^{(2)}_{i,\mathrm{IS}} = {} & n^0_{i-1}n^2_{i+1} + n^2_{i-1}n^0_{i+1} + n^1_{i-1}n^3_{i+1} + n^3_{i-1}n^1_{i+1} + \frac{1}{2}\left(n^1_{i-1}n^2_{i+1} + n^2_{i-1}n^1_{i+1}\right)\begin{pmatrix} 1 & 1 \\ 1 & 1 \end{pmatrix}_i \\ & + \frac{1}{d_{1/2}d_1 d_{3/2}}n^1_{i-1}n^1_{i+1}\begin{pmatrix} d_{1/2}d_{3/2} & d_1\sqrt{d_{1/2}d_{3/2}} & \sqrt{d_{1/2}d_{3/2}} \\ d_1\sqrt{d_{1/2}d_{3/2}} & d_1^2 & d_1 \\ \sqrt{d_{1/2}d_{3/2}} & d_1 & 1 \end{pmatrix}_i \\ & + \frac{1}{d_{1/2}d_1 d_{3/2}}n^2_{i-1}n^2_{i+1}\begin{pmatrix} 1 & d_1 & \sqrt{d_{1/2}d_{3/2}} \\ d_1 & d_1^2 & d_1\sqrt{d_{1/2}d_{3/2}} \\ \sqrt{d_{1/2}d_{3/2}} & d_1\sqrt{d_{1/2}d_{3/2}} & d_{1/2}d_{3/2} \end{pmatrix}_i. \end{aligned} \tag{C17}$$

In the HIS, the projectors onto the different channels can be written as follows:

$$P^{(1)}_{i,\mathrm{HIS}} = \frac{1}{d_1^2} n^{1/2}_{i-1} n^{1/2}_{i+1} \begin{pmatrix} d^2_{1/2} & d_{1/2}\sqrt{d_1} \\ d_{1/2}\sqrt{d_1} & d_1 \end{pmatrix}_i + \frac{1}{\sqrt{d_{1/2} d_1 d_{3/2}}} \left(n^{1/2}_{i-1} n^{3/2}_{i+1} + n^{3/2}_{i-1} n^{1/2}_{i+1}\right) \begin{pmatrix} 1 & -\sqrt{d_1} \\ -\sqrt{d_1} & d_1 \end{pmatrix}_i$$
$$+ \frac{1}{2} n^{3/2}_{i-1} n^{3/2}_{i+1} \begin{pmatrix} 1 & 0 & -1 \\ 0 & 0 & 0 \\ -1 & 0 & 1 \end{pmatrix}_i \frac{1}{\sqrt{d_{1/2} d_1 d_{3/2}}} \left(n^{3/2}_{i-1} n^{5/2}_{i+1} + n^{5/2}_{i-1} n^{3/2}_{i+1}\right) \begin{pmatrix} d_1 & -\sqrt{d_1} \\ -\sqrt{d_1} & 1 \end{pmatrix}_i$$
$$+ \frac{1}{d_1^2} n^{5/2}_{i-1} n^{5/2}_{i+1} \begin{pmatrix} d_1 & d_{1/2}\sqrt{d_1} \\ d_{1/2}\sqrt{d_1} & d^2_{1/2} \end{pmatrix}_i, \tag{C18}$$

$$P^{(2)}_{i,\mathrm{HIS}} = \frac{1}{\sqrt{d_{1/2} d_1 d_{3/2}}} \left(n^{1/2}_{i-1} n^{3/2}_{i+1} + n^{3/2}_{i-1} n^{1/2}_{i+1}\right) \begin{pmatrix} d_1 & \sqrt{d_1} \\ \sqrt{d_1} & 1 \end{pmatrix}_i + \frac{1}{d_{1/2} d_1^2 d_{3/2}} n^{3/2}_{i-1} n^{3/2}_{i+1} \begin{pmatrix} d_1^2 & d_1^{3/2} d_{3/2} & d_1^2 \\ d_1^{3/2} d_{3/2} & d^3_{1/2} d_{3/2} & d_1^{3/2} d_{3/2} \\ d_1^2 & d_1^{3/2} d_{3/2} & d_1^2 \end{pmatrix}_i$$
$$+ \frac{1}{\sqrt{d_{1/2} d_1 d_{3/2}}} \left(n^{3/2}_{i-1} n^{5/2}_{i+1} + n^{5/2}_{i-1} n^{3/2}_{i+1}\right) \begin{pmatrix} 1 & \sqrt{d_1} \\ \sqrt{d_1} & d_1 \end{pmatrix}_i. \tag{C19}$$

d. The su(2)$_7$ spin-1 chain

In the following, we use the notation $d_1 = 1 + 2\cos(2\pi/9)$, $d_2 = 1 + 2\cos(\pi/9)$, and $d_3 = 2\cos(\pi/9)$. The projector $P^{(1)}_i$ takes the form

$$P^{(1)}_i = n^0_{i-1} n^1_{i+1} + n^1_{i-1} n^0_{i+1} + n^1_{i-1} n^1_{i+1} \begin{pmatrix} \frac{1}{d_1} & -\frac{1}{\sqrt{d_1} d_2} & -\frac{d_3}{d_1\sqrt{d_2}} \\ -\frac{1}{\sqrt{d_1} d_2} & \frac{1}{d_2^2} & \frac{d_3}{\sqrt{d_1} d_2} \\ -\frac{d_3}{d_1\sqrt{d_2}} & \frac{d_3}{\sqrt{d_1} d_2} & \frac{d_3^2}{d_1 d_2} \end{pmatrix}_i + \left(n^1_{i-1} n^2_{i+1} + n^2_{i-1} n^1_{i+1}\right) \begin{pmatrix} \frac{d_3^2}{d_2^2} & -\frac{\sqrt{d_1} d_3^{3/2}}{d_2^2} \\ -\frac{\sqrt{d_1} d_3^{3/2}}{d_2^2} & \frac{d_1 d_3}{d_2^2} \end{pmatrix}_i$$
$$+ n^2_{i-1} n^2_{i+1} \begin{pmatrix} \frac{d_1^2 d_3}{d_2^3} & \frac{\sqrt{d_1} d_3}{d_2^{7/2}} & -\frac{\sqrt{d_1} d_3^{3/2}}{d_2^2} \\ \frac{\sqrt{d_1} d_3}{d_2^{7/2}} & \frac{d_3}{d_1 d_2^4} & -\frac{d_3^{3/2}}{d_1 d_2^{5/2}} \\ -\frac{\sqrt{d_1} d_3^{3/2}}{d_2^2} & -\frac{d_3^{3/2}}{d_1 d_2^{5/2}} & \frac{d_3^2}{d_1 d_2} \end{pmatrix}_i + \left(n^2_{i-1} n^3_{i+1} + n^3_{i-1} n^2_{i+1}\right) \begin{pmatrix} \frac{d_3}{d_1} & -\frac{d_3}{d_1\sqrt{d_2}} \\ -\frac{d_3}{d_1\sqrt{d_2}} & \frac{d_3}{d_1 d_2} \end{pmatrix}_i$$
$$+ n^3_{i-1} n^3_{i+1} \begin{pmatrix} \frac{1}{d_1} & \frac{\sqrt{d_2}}{d_1\sqrt{d_3}} \\ \frac{\sqrt{d_2}}{d_1\sqrt{d_3}} & \frac{d_2}{d_1 d_3} \end{pmatrix}_i. \tag{C20}$$

The projector $P^{(2)}_i$ is given by

$$P^{(2)}_i = n^0_{i-1} n^2_{i+1} + n^2_{i-1} n^0_{i+1} + n^1_{i-1} n^1_{i+1} \begin{pmatrix} \frac{d_2}{d_1^2} & \frac{d_3}{d_1^{3/2}} & \frac{d_3}{d_1^2\sqrt{d_2}} \\ \frac{d_3}{d_1^{3/2}} & \frac{d_3^2}{d_1 d_2} & \frac{d_3^2}{d_1^{3/2} d_2^{3/2}} \\ \frac{d_3}{d_1^2\sqrt{d_2}} & \frac{d_3^2}{d_1^{3/2} d_2^{3/2}} & \frac{d_3^2}{d_1^2 d_2^2} \end{pmatrix}_i + \left(n^1_{i-1} n^2_{i+1} + n^2_{i-1} n^1_{i+1}\right) \begin{pmatrix} \frac{d_1 d_3}{d_2^2} & \frac{\sqrt{d_1} d_3^{3/2}}{d_2^2} \\ \frac{\sqrt{d_1} d_3^{3/2}}{d_2^2} & \frac{d_3^2}{d_2^2} \end{pmatrix}_i$$
$$+ n^1_{i-1} n^3_{i+1} + n^3_{i-1} n^1_{i+1} + n^2_{i-1} n^2_{i+1} \begin{pmatrix} \frac{d_3^2}{d_2^3} & \frac{d_3^3}{\sqrt{d_1} d_2^{5/2}} & \frac{d_3^{3/2}}{\sqrt{d_1} d_2^2} \\ \frac{d_3^3}{\sqrt{d_1} d_2^{5/2}} & \frac{d_3^4}{d_1 d_2^2} & \frac{d_3^{5/2}}{d_1 d_2^{3/2}} \\ \frac{d_3^{3/2}}{\sqrt{d_1} d_2^2} & \frac{d_3^{5/2}}{d_1 d_2^{3/2}} & \frac{d_3}{d_1 d_2} \end{pmatrix}_i + \left(n^2_{i-1} n^3_{i+1} + n^3_{i-1} n^2_{i+1}\right) \begin{pmatrix} \frac{d_3}{d_1 d_2} & \frac{d_3}{d_1\sqrt{d_2}} \\ \frac{d_3}{d_1\sqrt{d_2}} & \frac{d_3}{d_1} \end{pmatrix}_i. \tag{C21}$$

APPENDIX D: EXACT FORM OF THE AKLT STATES

In this section, we present the explicit form of the zero-energy ground states of the periodic anyonic spin-1 chains for k odd at the anyonic equivalent of the AKLT point. In the main text, we discussed the case $k = 5$.

At the AKLT point, the Hamiltonian contains only the projector onto the anyon spin-2 channel; i.e., the fusion of neighboring spin-1 anyons into a spin-2 anyon is penalized. First, we note that the fusion of anyons of types 1 and $(k-1)/2$ [the latter being the largest integer "spin" for an anyon in the su(2)$_k$ theory] results in $1 \times (k-1)/2 = (k -$

$3)/2 + (k-1)/2$. In addition, we have that $1 \times (k-3)/2 = (k-5)/2 + (k-3)/2 + (k-1)/2$. Thus, a local basis for which $x_{i-1} = x_{i+1} = (k-1)/2$ implies that $x_i = (k-3)/2$ or $x_i = (k-1)/2$. It follows that after the local basis transformation, $\tilde{x}_i$ can only take two possible values, namely, $\tilde{x}_i = 0,1$ [consider $2 \times (k-1)/2 = (k-5)/2 + (k-3)/2$, and let $\tilde{x}_i = 2$, $x_{i-1} = (k-1)/2$, then x_{i+1} could only take values $(k-5)/2$ and $(k-3)/2$ but not $(k-1)/2$]. This, in turn, means that a choice of local variables x_{i-1} and x_{i+1} does not give rise to nonzero contributions at the AKLT point as fusion of neighboring spin-1 anyons in the chain cannot result in $\tilde{x}_i = 2$. We thus obtain a zero-energy ground state of the form $|v_0\rangle = |(k-1)/2,(k-1)/2,\ldots,(k-1)/2\rangle$.

To construct the other ground states, we make use of the topological symmetry operators Y_l. These operators mutually commute, and they commute with the Hamiltonian. The state v_0 is not an eigenstate of the operators Y_l (with $l > 0$), and hence alternative zero-energy ground states of the Hamiltonian are given by $|v_l\rangle = Y_l\,|v_0\rangle$. These ground states $|v_l\rangle$ $(l > 0)$ can be obtained explicitly. The local basis states take values $x_i = p - l$ or $x_i = p - l + 1$, where $p = (k-1)/2$. The states $|v_l\rangle$ are a sum over all possible labelings of the fusion tree with these two values of x_i. We introduce the following notation: $\#l$ denotes the number of local basis states for which $x_i = l$, and $\#(l,m)$ denotes the number of local basis states for which $x_i = l$ and $x_{i+1} = m$, where we use periodic boundary conditions, $x_L = x_0$. For $l > 0$, we obtain

$$|v_l\rangle = \sum_{x_i \in \{p-l,\, p-l+1\}} f_l(\{x_i\})\,|x_0,x_1,\ldots,x_{L-1}\rangle\,. \qquad \text{(D1)}$$

The coefficients $f_l(\{x_i\})$ $(0 < l < p)$ are given by

$$f_l(\{x_i\}) = \left(\frac{d_{l+1}}{d_l d_1}\right)^{L/2} (-1)^{\#p-l+1} \left(\sqrt{\frac{d_{l-1}}{d_{l+1}}}\right)^{\#(p-l+1,\,p-l+1)} \times \left(\sqrt{d_{p-l}d_{p-l+1}}\,\frac{d_p}{d_{l+1}}\right)^{\#(p-l+1,\,p-l)}.$$

For $l = p$, this results in

$$f_p(\{x_i\}) = \left(\frac{d_p}{d_{p-1}}\right)^{L/2} \left(-\frac{d_{p-1}}{d_p\sqrt{d_1}}\right)^{\#1}.$$

We denoted the ground states by $|v_l\rangle$ for the following reason. In Sec. II, we explained that the operators Y_l can be thought of as fusing an anyon with "spin" l into the chain, effectively changing the "overall fusion channel," or flux thought the chain. If we take a state $|v_{j_2}\rangle$ and act on it with the operator Y_{j_1}, we find that $Y_{j_1}|v_{j_2}\rangle = \sum_{j_3 \in j_1 \times j_2} |v_{j_3}\rangle$, where the sum is over those j_3 which appear in the fusion $j_1 \times j_2$. Thus, the ground states of the AKLT anyonic spin chain form a "representation" of the fusion algebra of $\mathrm{su}(2)_k$. This implies that eigenstates of the topological operators Y_l can be constructed because the modular S matrix diagonalizes the fusion rules. In particular, orthogonal (not normalized) ground states at the AKLT point are written as $|\psi_{\mathrm{AKLT,i}}\rangle = \sum_{j=0}^{(k-1)/2} S_{i,j}|v_j\rangle$, where $S_{i,j}$ is the modular S matrix for $\mathrm{su}(2)_k$, and the sum is over integer values.

TABLE VII. Modular invariants of the Virasoro minimal models. For a given pair of indices, $(p,p') = (m+1,m)$ and n integer, only the fields with indices (r,s) as specified in the third column appear ($1 \leqslant r < p'$, $1 \leqslant s < p$). Some fields have multiplicity two, as indicated in column four.

p, p'	(A,D)	(r,s)	Multiplicity 2
$p' = 2(2n+1)$	$(D_{p'/2+1}, A_{p-1})$	r odd	$r = p' - r$
$p = 2(2n+1)$	$(A_{p'-1}, D_{p/2+1})$	s odd	$s = p - s$

APPENDIX E: CONFORMAL FIELD THEORIES OF INTEREST

In this appendix we summarize the most important aspects of the CFTs relevant to this paper. In the following, "primary fields" refers to Virasoro primary fields. Detailed discussions of CFTs can be found in Refs. 59 and 60.

1. Virasoro minimal models

The unitary minimal models,[60] which can also be described in terms of the coset $\frac{\mathrm{su}(2)_1 \times \mathrm{su}(2)_{k-1}}{\mathrm{su}(2)_k}$, have a central charge $c = 1 - \frac{6}{(k+1)(k+2)}$ $(k \geqslant 2)$. The primary fields are labeled by integers r and s, where $1 \leqslant r \leqslant k$ and $1 \leqslant s \leqslant k+1$. Their conformal dimensions are given by

$$h_{r,s} = \frac{[r(k+2) - (k+1)s]^2 - 1}{4(k+1)(k+2)}. \qquad \text{(E1)}$$

Typically, the minimal models are labeled by a parameter $m = k+1$.

Apart from the so-called diagonal models, there exist modular invariants that give rise to CFTs with a different field content.[34,35] More information on these modular invariants can be found in Table VII.

2. $\mathcal{N} = 1$ superconformal minimal models

The $\mathcal{N} = 1$ superconformal minimal models[38] are described by the coset

$$\frac{\mathrm{su}(2)_2 \times \mathrm{su}(2)_{k-2}}{\mathrm{su}(2)_k}$$

and have central charge $c = \frac{3}{2} - \frac{12}{k(k+2)}$. The primary fields have conformal dimension

$$h_{(r,s)} = \frac{[r(k+2) - sk]^2 - 4}{8k(k+2)} + \frac{1}{32}[1 - (-1)^{r-s}], \qquad \text{(E2)}$$

where $1 \leqslant r \leqslant k-1$ and $1 \leqslant s \leqslant k+1$. The fields with $r+s$ even, i.e., the fields in the Neveu-Schwarz sector, have a super partner, whose conformal dimensions are given by

$$h'_{(r,s)} = h_{(r,s)} + 1/2 + \delta_{r+s,2} \quad \text{for } r+s \text{ even}. \qquad \text{(E3)}$$

3. S_3 minimal models

The class of S_3 symmetric minimal models[36,37] are described by the coset theory

$$\frac{\mathrm{su}(2)_4 \times \mathrm{su}(2)_{k-4}}{\mathrm{su}(2)_k},$$

and have central charge

$$c = 2 - \frac{24}{(k-2)(k+2)}. \tag{E4}$$

There are two main sets of primary fields. The first set has conformal weights,

$$h_{(r,s)} = \frac{[r(k+2) - s(k-2)]^2 - 16}{16(k-2)(k+2)} + \frac{1 - \cos^4[\pi(r-s)/4]}{12}. \tag{E5}$$

The second set has scaling dimensions

$$h'_{(r,s)} = h_{(r,s)} + \frac{1 + \sin^2[\pi(r-s)/4]}{3} + \delta_{r,1}\delta_{s,1} + \delta_{r,1}\delta_{s,2} + 2\delta_{r,2}\delta_{s,1}, \tag{E6}$$

where for both sets $1 \leqslant r \leqslant k-3$ and $1 \leqslant s \leqslant k+1$. There are additional (Virasoro) primary fields, with scaling dimensions differing by integers from the scaling dimensions listed above. These additional primary fields are not relevant to this work.

4. The Z_k parafermion CFT

The Z_k parafermions[32] can be described in terms of the coset

$$\frac{\mathrm{su}(2)_k}{u(1)_{2k}},$$

where $\mathrm{u}(1)_{2k}$ denotes the $c = 1$ boson, compactified on a circle of radius $R = \sqrt{2k}$. The central charge is given by $c = \frac{2(k-1)}{k+2}$, and the conformal dimensions of the primary fields are given by

$$h_{(l,m)} = \frac{l(l+2)}{4(k+2)} - \frac{m^2}{4k}. \tag{E7}$$

Here, the indices run over values $l = 0,1,\ldots,k$ and $m = -l+2, -l+4, \ldots, l$.

5. The $\mathbb{Z}_2$ orbifold theories

We briefly discuss the $\mathbb{Z}_2$ orbifold of the compactified boson at squared radius $R^2 = 2p$. For a detailed account, we refer to Ref. 42. The number of primary fields is given $p+7$, where $p = 1,2,\ldots$. For $p = 1$, the CFT is Abelian, and it is equivalent to a the compactified boson theory with eight primary fields. In general, the following fields are present:

(i) the identity field $\mathbf{1}$, with scaling dimension $h_{\mathbf{1}} = 0$ and quantum dimension $d_{\mathbf{1}} = 1$;

(ii) the field Θ, with dimension $h_\Theta = 1$ and quantum dimension $d_\Theta = 1$;

(iii) two "degenerate" fields Φ^1 and Φ^2, with scaling dimension $h_\Phi = \frac{p}{4}$ and quantum dimension $d_\Phi = 1$;

(iv) the twist fields σ^1, σ^2 and τ^1, τ^2, with scaling dimensions $h_\sigma = \frac{1}{16}$ and $h_\tau = \frac{9}{16}$ and quantum dimensions $d_\sigma = d_\tau = \sqrt{p}$;

(v) the fields ϕ_λ, with $\lambda = 1,2,\ldots,p-1$, with scaling dimensions $h_\lambda = \frac{\lambda^2}{4p}$ and quantum dimensions $d_\lambda = 2$.

a. The S matrix

To verify that the assignment of the topological symmetry sectors of states of the critical $\mathrm{su}(2)_4$ spin-1 anyonic chains are compatible with the fusion rules of the orbifold CFTs describing the critical behavior, we need the fusion rules of the orbifold CFTs. We do not give these fusions rules explicitly here, but specify the modular S matrix. The fusion rules can be obtained from the modular S matrix by means of the Verlinde formula.[61]

The modular S matrix can be written in a compact way as follows. In the basis $(\mathbf{1},\Theta,\Phi^i,\sigma^i,\tau^i,\phi_\lambda)$ for the rows and $(\mathbf{1},\Theta,\Phi^j,\sigma^j,\tau^j,\phi_\mu)$ for the columns, where $i,j = 1,2$ and $\lambda,\mu = 1,2,\ldots,p-1$, the modular S matrix is given by

$$S = \frac{1}{\sqrt{8p}} \begin{pmatrix} 1 & 1 & 1 & \sqrt{p} & \sqrt{p} & 2 \\ 1 & 1 & 1 & -\sqrt{p} & -\sqrt{p} & 2 \\ 1 & 1 & (-1)^p & b_{i,j} & b_{i,j} & (-1)^\mu 2 \\ \sqrt{p} & -\sqrt{p} & b_{i,j} & a_{i,j} & -a_{i,j} & 0 \\ \sqrt{p} & -\sqrt{p} & b_{i,j} & -a_{i,j} & a_{i,j} & 0 \\ 2 & 2 & (-1)^\lambda 2 & 0 & 0 & c_{\lambda,\mu} \end{pmatrix}. \tag{E8}$$

Here, the matrices a,b,c have the elements

$$a_{i,j} = \sqrt{p/2}[1 + (2\delta_{i,j} - 1)]e^{-\pi i p/2},$$
$$b_{i,j} = (-1)^{p+\delta_{i,j}}\sqrt{p}e^{\pi i p/2},$$
$$c_{\lambda,\mu} = 4\cos(\pi\lambda\mu/p).$$

We note that we used a simplified notation in the above definition: For the matrix elements that do not depend i or j, the particular element does not depend on i and j.

[1] I. Affleck, J. Phys.: Condens. Matter **1**, 3047 (1989).

[2] F. D. M. Haldane, Phys. Lett. A **93**, 464 (1983); Phys. Rev. Lett. **50**, 1153 (1983).

[3] F. Pollmann, E. Berg, A. M. Turner, and M. Oshikawa, Phys. Rev. B **85**, 075125 (2012); F. Pollmann, A. M. Turner, E. Berg, and M. Oshikawa, *ibid.* **81**, 064439 (2010).

[4] X. Chen, Z.-C. Gu, and X.-G. Wen, Phys. Rev. B **83**, 035107 (2011).

[5] M. Z. Hasan and C. L. Kane, Rev. Mod. Phys. **82**, 3045 (2010); X.-L. Qi and S.-C. Zhang, *ibid.* **83**, 1057 (2011).

[6] See, e.g., M. Hase, I. Terasaki, and K. Uchinokura, Phys. Rev. Lett. **70**, 3651 (1993).

[7] See, e.g., C. Blumenstein, J. Schäfer, S. Mietke, S. Meyer, A. Dollinger, M. Lochner, X. Y. Cui, L. Patthey, R. Matzdorf, and R. Claessen, Nat. Phys. **7**, 776 (2011).

[8] See, e.g., H. Schwager, J. I. Cirac, and G. Giedke, Phys. Rev. A **87**, 022110 (2013).

[9] G. Moore and N. Read, Nucl. Phys. B **360**, 362 (1991).

[10] N. Read and D. Green, Phys. Rev. B **61**, 10267 (2000).

[11] L. Fu and C. L. Kane, Phys. Rev. Lett. **100**, 096407 (2008).

[12]J. D. Sau, R. M. Lutchyn, S. Tewari, and S. DasSarma, Phys. Rev. Lett. **104**, 040502 (2010); J. Alicea, Phys. Rev. B **81**, 125318 (2010).
[13]J. Chaloupka, G. Jackeli, and G. Khaliullin, Phys. Rev. Lett. **105**, 027204 (2010); H. C. Jiang, Z. C. Gu, X. L. Qi, and S. Trebst, Phys. Rev. B **83**, 245104 (2011); Y. Singh, S. Manni, J. Reuther, T. Berlijn, R. Thomale, W. Ku, S. Trebst, and P. Gegenwart, Phys. Rev. Lett. **108**, 127203 (2012).
[14]A. Y. Kitaev, Ann. Phys. **321**, 2 (2006).
[15]A. Feiguin, S. Trebst, A. W. W. Ludwig, M. Troyer, A. Kitaev, Z. Wang, and M. H. Freedman, Phys. Rev. Lett. **98**, 160409 (2007).
[16]C. Gils, E. Ardonne, S. Trebst, A. W. W. Ludwig, M. Troyer, and Z. Wang, Phys. Rev. Lett. **103**, 070401 (2009).
[17]S. Trebst, E. Ardonne, A. Feiguin, D. A. Huse, A. W. W. Ludwig, and M. Troyer, Phys. Rev. Lett. **101**, 050401 (2008).
[18]A. W. W. Ludwig, D. Poilblanc, S. Trebst, and M. Troyer, New J. Phys. **13**, 045014 (2011).
[19]Z. Wang, *Topological Quantum Computation, Regional Conference Series in Mathematics*, Vol. 112 (American Mathematical Society, Providence, RI, 2010).
[20]P. H. Bonderson, Ph.D. thesis, California Institute of Technology, 2007.
[21]I. Affleck, T. Kennedy, E. H. Lieb, and H. Tasaki, Phys. Rev. Lett. **59**, 799 (1987); Commun. Math. Phys. **115**, 477 (1988).
[22]M. N. Barber and M. T. Batchelor, Phys. Rev. B **40**, 4621 (1989); A. Klümper, Europhys. Lett. **9**, 815 (1989); Y. Xian, Phys. Lett. A **183**, 437 (1993).
[23]E. Date *et al.*, Nucl. Phys. B **290**, 231 (1987).
[24]A. Lauchli, G. Schmid, and S. Trebst, Phys. Rev. B **74**, 144426 (2006).
[25]G. Fáth and J. Sólyom, Phys. Rev. B **44**, 11836 (1991).
[26]C. K. Lai, J. Math. Phys. **15**, 1675 (1974); B. Sutherland, Phys. Rev. B **12**, 3795 (1975).
[27]G. V. Uimin, Pis'ma Zh. Eksp. Teor. Fix. **12**, 332 (1970) [JETP Lett. **12**, 225 (1970)].
[28]A. V. Chubukov, Phys. Rev. B **43**, 3337 (1991).
[29]G. Fáth and J. Sólyom, Phys. Rev. B **51**, 3620 (1995).
[30]T. Grover and T. Senthil, Phys. Rev. Lett. **98**, 247202 (2007).
[31]J. L. Cardy, J. Phys. A **17**, L385 (1984).
[32]A. B. Zamolodchikov and V. A. Fateev, Sov. Phys. JETP **62**, 215 (1985).
[33]J. L. Cardy, Nucl. Phys. B **270**, 186 (1986).
[34]A. Cappelli, C. Itzykson, and J.-B. Zuber, Nucl. Phys. B **280**, 445 (1987).
[35]A. Cappelli, C. Itzykson, and J.-B. Zuber, Comm. Math. Phys. **13**, 1 (1987).
[36]V. A. Fateev and A. B. Zamolodchikov, Nucl. Phys. B **280**, 644 (1987).
[37]A. B. Zamolodchikov and V. A. Fateev, Theor. Math. Phys. **71**, 451 (1987).
[38]D. Friedan, Z. Qiu, and S. Shenker, Phys. Lett. B **151**, 37 (1984).
[39]S. R. White and D. A. Huse, Phys. Rev. B **48**, 3844 (1993).
[40]W. M. Koo and H. Saleur, Int. J. Mod. Phys. A **8**, 5165 (1993).
[41]P. Ginsparg, Nucl. Phys. B **295**, 153 (1988).
[42]R. Dijkgraaf, C. Vafa, E. Verlinde, and H. Verlinde, Commun. Math. Phys. **123**, 485 (1989).
[43]M. Kohmoto, M. den Nijs, and L. P. Kadanoff, Phys. Rev. B **24**, 5229 (1981).
[44]J. Ashkin and E. Teller, Phys. Rev. **64**, 178 (1943).
[45]M. H. Freedman, M. J. Larsen, and Z. Wang, Commun. Math. Phys. **227**, 605 (2002).
[46]M. H. Freedman, M. J. Larsen, and Z. Wang, Commun. Math. Phys. **228**, 117 (2002).
[47]P. E. Finch, J. Phys. A **46**, 055305 (2013).
[48]V. A. Verbus, L. Martina, and A. P. Protogenov, Theor. Math. Phys. **167**, 843 (2011).
[49]H. N. Temperley and E. H. Lieb, Proc. R. Soc. London A **322**, 251 (1971).
[50]P. Fendley and V. Krushkal, Adv. Theor. Math. Phys. **14**, 507 (2010).
[51]P. Fendley and N. Read, J. Phys. A **35**, 10675 (2002).
[52]P. Fendley, J. Phys. A **39**, 15445 (2006).
[53]J. Nissinen and E. Ardonne (unpublished).
[54]E. Date, M. Jimbo, T. Miwa, and M. Okado, Lett. Math. Phys. **12**, 209 (1986).
[55]V. Pasquier, Commun. Math. Phys. **118**, 355 (1988).
[56]D. Gepner, arXiv:hep-th/9211100.
[57]A. N. Kirillov and N. Y. Reshetikhin, in *Infinite Dimensional Lie Algebras and Groups, Proceedings of the Conference Held at CIRM, Luminy, Marseille*, edited by V. G. Kac (World Scientific, Singapore, 1988), p. 285.
[58]S. Trebst, M. Troyer, Z. Wang, and A. W. W. Ludwig, Prog. Theor. Phys. Supp. **176**, 384 (2008).
[59]P. Di Francesco, P. Mathieu, and D. Sénéchal, *Conformal Field Theory* (Springer, New York, 1999).
[60]A. A. Belavin, A. M. Polyakov, and A. B. Zamolodchikov, Nucl. Phys. B **241**, 333 (1984).
[61]E. Verlinde, Nucl. Phys. B **300**, 360 (1988).